ELECTRONIC MODEL OF TURBINE GENERATOR INCLUDING REHEATERS, GOVERNOR AND SHAFT TORSIONAL SYSTEM

by

Pierre R. Legault, B.Eng. (McGill University)

A thesis submitted to the Faculty of Graduate Studies and Research in partial fulfilment of the requirements for the degree of

Master of Engineering

Department of Electrical Engineering
McGill University
Montreal, Canada

AN ELECTRONIC MODEL OF TURBINE-GENERATOR,

INCLUDING REHEATERS, GOVERNORS AND SHAFT TORSIONAL SYSTEM

Electrical Pierre R. Legault, B. Eng. M. Eng.

ABSTRACT

An analog simulator for the turbine-generator shaft assembly has been developed. The simulator consists of the following electronic modules:

1) Inertia-Shaft Modules
    1) Turbine Section
    2) Generator Unit
2) Exciter Module
3) Steam Distribution Modules
4) Speed-Governor Module

These modules offer flexibility of simulating a variety of turbine-reheat configurations. The design of the modules has been proven by frequency domain test of individual modules, and their combination as a system. This simulator has been developed as an addition to the existing electronic simulator of generators and power systems at the Institut de Recherche de l'Hydro-Quebec.

AN ELECTRONIC MODEL OF TURBINE-GENERATOR,

INCLUDING REHEATERS, GOVERNORS AND SHAFT TORSIONAL SYSTEM

Electrical Pierre R. Legault, B.Eng. M.Eng.

RESUME

Un simulateur analogique pour l'assemblage axial d'un turbo-générateur a été développé. Ce simulateur est composé des modules électroniques suivants:

1) des modules d'inerties axiales pour
   i) une section de turbine
   ii) un générateur
2) un module d'excitateur
3) un module de distribution de vapeur
4) un module de régulateur de vitesse

Ces modules offrent la possibilité de simuler une variété de configurations pour turbines avec resurchauffage. La validité des modules a été demontré par une série de tests dans le domaine de fréquences, pour chaqu'un des modules individuellement, ainsi que pour (un systeme particulier au complet). Ce simulateur a été developpé pour augmenter les (capacités) existances d'un simulateur électronique de générateurs et de réseaux de puissance.

TABLE OF CONTENTS

		Page
ABSTRACT		i
RESUME		ii
LIST OF FIGURES		vii
LIST OF PRINCIPAL SYMBOLS		xiii
ACKNOWLEDGEMENTS		xv
CHAPTER		
1	INTRODUCTION	1
	SUBJECT OF THESIS	4
	MATHEMATICAL MODELS	4
2	DYNAMIC MODELS OF STEAM TURBINE AND TORSIONAL SHAFT SYSTEM	5
	2.1 Steam-Turbine Torsional Shaft System	6
	2.2 Model of Turbine-Generator Shaft Assembly: Schematic and Mathematical Description	9
	2.3 Model for the Steam Distribution System: Schematic and Mathematical Description	11
	2.3.1 Single Shaft System	13
	2.3.2 Two-Shaft System	18
	2.4 Torque from Steam Power	21
	2.5 Model for Speed-Governor System: Schematic and Mathematical Description	21

Page

2.6 Integration of models a complete system model representation 25

3 ELECTRONIC MODULES 29

3.1 Torsional Shaft System 30

3.2 Inertia-Shaft Modules:

1) Turbine Section

2) Generator Unit 32

3.2.1 Module Parameters 37

3.2.2 Module Inputs 38

3.2.3 Module Outputs 39

3.3 Exciter Modules 39

3.3.1 Module Parameters 42

3.3.2 Module Inputs 42

3.3.3 Module Outputs 42

3.4 Steam Distribution Module 43

3.4.1 Module Parameters 43

3.4.2 Module Inputs 46

3.4.3 Module Outputs 46

3.4.4 Steam Distribution Power Fractioning Unit 46

3.5 Speed-Governor Module 49

3.5.1 Module Parameters 53

3.5.2 Module Inputs 53

		Page
	3.5.3 Module Outputs	53
	3.5.4 Control Setting	
	1) Reference Angular Velocity	
	2) Reference Power	54
	3.6 Steam System Configurations ...	54
	3.7 Fast-Valving Simulation, Boiler Dynamics Representation and Governor Dead Band.............	55
4	**PERFORMANCE OF MODULES**	64
	4.1 Performance Criteria	66
	4.2 Module Testing and Results	66
	4.2.1 Test results for the inertia module: Turbine sections	67
	4.2.2 Test results for the inertia modules: Generator Unit	69
	4.2.3 Test results for the inertia modules: exciter unit	70
	4.2.4 Test results for the steam distribution modules ...	72

Page

4.2.5 Test results for the speed-governor module... 72

4.2.6 Test results on range of operation of given variables 78

4.3 Inertia Shaft Assembly System.. 78

4.3.1 Mathematical Predictions 83

4.3.2 Test Results 84

4.4 Complete System Testing and Results 84

4.4.1 Mathematical Predictions 89

4.4.2 Test Results 90

4.5 Evaluation of System Performance 97

5 CONCLUSION 98

REFERENCES 100

APPENDIX

I PER UNIT SYSTEM OF EQUATIONS............ 112

II BASIC ELECTRONIC COMPONENTS AND CONFIGURATIONS................................ 117

III SPEED-GOVERNING SYSTEM: MATHEMATICAL MODEL 124

LIST OF FIGURES

Figures		Page
2-1	Block Diagram of a Steam-Turbine System	7
2-2	Block Diagram of a turbine-generator Shaft Assembly	10
2-3	Block Diagram for the General Model of a Turbine's Steam System	12
2-4	Block Diagram for the Model of a one-Shaft turbine's steam as recommended in the IEEE Committee Report	14
2-5	A Typical i^{th} Node of the model for a one-Shaft Turbine's Steam System	16
2-6	Block Diagram for the Model of a one-Shaft Turbine's steam system with intermediate thermal Powers..	17
2-7a'	Block Diagram for the Power Division at the i^{th} Node for a two-Shaft System	19
2-7b	Block Diagram for the Total Power Division at the i^{th} Node	19
2-7c	Block Diagram for the Total Power output at the i^{th} Node with a fractioning Module	20

Figures | Page

Figures		Page
2-8	Block Diagram for an electronic analog Divider	22
2-9	Block Diagram for the General Model for a Speed-Governor System.	24
2-10	Block Diagram for an integrated System Model	26
3-1	Block Diagram for a Torsional Shaft System	31
3-2	Mimic Diagram for an Inertia-Shaft Module: Turbine Section	33
3-3	Wiring Diagram for an Inertia-Shaft Module: Turbine Section	34
3-4	Mimic Diagram for an Inertia-Shaft Module: Generator Unit	35
3-5	Wiring Diagram for an Inertia-Shaft Module: Generator Unit	36
3-6	Mimic Diagram for an Exciter Module	40
3-7	Wiring Diagram for an exciter Module	41
3-8	Mimic Diagram for a steam Power Distribution Module	44
3-9	Wiring Diagram for a steam Distribution Module	45
3-10	Mimic Diagram for the Fractioning Module	47

Figures | Page

Figures		Page
3-11	Wiring Diagram for the Fractioning Module	48
3-12	Mimic Diagram for the Speed-Governor Module	50
3-13	Wiring Diagram for the Speed-Governor Module (1)	51
3-14	Wiring Diagram for the Speed-Governor Module (2)	52
3-15	Diagram Reproduced from IEEE Committee Report [14], fig. 6 and fig. 7	56
3-16	Block Diagram for a one-Shaft System Configuration	57
3-17	Block Diagram for a four turbine section one-Shaft system Configuration	58
3-18	Block Diagram for a two-Shaft system Configuration	59
3-19	Typical turbine Power Decay curves	61
3-20	Wiring Diagram for the addition of Boiler Dynamics	62
4-1	Magnitude of the frequency response of the Inertia Modules: Turbine sections	68
4-2	Magnitude of the frequency response of the Inertia Modules: Generator Units	71

Figures		Page
4-3	Magnitude of the frequency response of the exciter modules	73
4-4	Magnitude of the frequency response of the steam distribution modules..	74
4-5	Magnitude of the frequency response of the Speed-Governor Modules: Module # 1	76
4-6	Magnitude of the frequency response of the Speed-Governor Modules: Module # 2	77
4-7	Magnitude of the frequency response of variable $2H_i$ over a range of operation	79
4-8	Magnitude of the frequency response of variable $K_{i,i+1}$ over a range of operation	80
4-9	Block Diagram for Inertia-Shaft Assembly system	81
4-10	Modules interconnection for implementation of Inertia-Shaft Assembly system	82
4-11	Magnitude of the frequency response of the Torque $[K_{1,2}(\theta_1-\theta_2)/T_e]$ between the VHP-IP sections of the Inertia-Shaft Assembly	85

Figures		Page
4-12	Magnitude of the frequency response of the torque $[K_{2,3}(\theta_2-\theta_3)]$ between the IP-GEN sections of the inertia shaft assembly	86
4-13	Magnitude of the frequency response of the torque $[K_{3,4}(\theta_3-\theta_4)]$ between the GEN-EXC sections of the inertia shaft assembly	87
4-14	Block diagram of a complete turbine-generator system, with steam distribution system and speed-governor system	88
4-15	Magnitude of the frequency response of the torque $[K_{1,2}(\theta_1-\theta_2)]$ between the VHP-IP inertia shaft sections of the complete system	91
4-16	Phase of the frequency response of the torque $[K_{1,2}(\theta_1-\theta_2)]$ between the VHP-IP inertia shaft sections of the complete system	92
4-17	Magnitude of the frequency response of the torque $[K_{2,3}(\theta_2-\theta_3)]$ between the IP-GEN inertia shaft sections of the complete system	93

Figures		Page
4-18	Phase of the frequency response of the torque $[K_{2,3}(\theta_2-\theta_3)]$ between the IP-GEN inertia shaft sections of the complete system	94
4-19	Magnitude of the frequency response of the torque $[K_{3,4}(\theta_3-\theta_4)]$ between the GEN-EXC inertia shaft sections of the complete system	95
II-1	Operational Amplifier Symbol........	118
II-2	Operational Amplifier Pin Connection Diagram............................	118
II-3	Wiring Diagram for Addition Operation	119
II-4	Wiring Diagram for Substraction Operation............................	119
II-5	Wiring Diagram for Integration Operation..................................	119
II-6	Wiring Diagram for Variable Constant $(R_v \leq 1)$............................	120
II-7	Wiring Diagram for Variable Constant Operation $(R_v \geq 1)$..................	120
II-8	Divider Symbol......................	121
II-9	Divider Pin Connection Diagram......	121
II-10	Divider Circuit Implementation......	122
II-11	Multiplier Symbol..................	123

LIST OF PRINCIPAL SYMBOLS

D_{ii}	Self Damping Constant
$D_{i,j}$	Mutual Damping Constant
$K_{i,j}$	Torsional Spring Constant
T_e	Electrical Torque Applied at the Generator
F_{VHP}	Very High Pressure Turbine Power Fraction
F_{HP}	High Pressure Turbine Power Fraction
F_{IP}	Intermediate Pressure Turbine Power Fraction
F_{LP}	Low Pressure Turbine Power Fraction
T_{CH}	Steam Chest Time Constant
T_{RH}	Reheat Time Constant
T_{CO}	Crossover Time Constant
K	Total Effective Speed-Governor System Gain Constant
T_1, T_2, T_3	Speed-Governor System Time Constants
$T_4 - T_7$	General Model Time Constant
$\dot{P}_{UP}, \dot{P}_{DOWN}$	Limits on Rate of Change of Power Imposed by Control Valve Rate Limits
P_{MAX}, P_{MIN}	Power Limits Imposed by Valve or Gate Travel
P_o	Reference Mechanical Power
ω_o	Reference Angular Velocity

Operators

All equations in this thesis are formulated in the S-domain. In the formulation of these equations, the variables are expressed in a short form [i.e. X_i instead of $X_i(S)$], but it is understood that these are functions of frequency. The variables expressed in that form are the following:

θ_i [instead of $\theta_i(S)$]	Angular Displacement
ω_i [instead of $\omega_i(S)$]	Angular Velocity
P_i [instead of $P_i(S)$]	Steam Power
P_{GV} [instead of $P_{GV}(S)$]	Power a Gate or Valve Outlet

ACKNOWLEDGEMENT

The work reported through this thesis has been sponsored and supported financially by the Institut de recherche de l'Hydro-Quebec (IREQ). The author wishes to sincerely thank his supervisor Dr. B. T. Ooi, who provided encouragement and active assistance throughout the course of this research, and his co-supervisor, Dr. H. L. Nakra, who has provided the topic of this research work, as well as guidance and valuable contributions during the progress of this work.

In a very special way, the author acknowledges his sincere appreciation to Dr. P. C. Krishnaya and Dr. R. Pronovost, who have accepted, through IREQ, to support this research work. He is also indebted to Guy Jeanson, technician at IREQ, for his valued assistance in the field of electronic.

The excellent typing skills of Ms Susan St Denis is gratefully acknowledge.

CHAPTER 1

INTRODUCTION

Predictions of power system behaviour presuppose the availability of mathematical models. The early efforts have begun by modelling the loads [1-4], the synchronous generator [5-9], the exciter system [10-11] and the governor system [12-14]. For the transient stability studies, this proved to be adequate. Recently there have been occasions to consider reaching further upstream for a more detailed model of the prime mover source. In the hydro-station, this consists of more detailed model of penstock, the surge tanks, etc. In fossil fuels system, this consists of the modelling of the turbines, reheaters, boilers, superheaters, etc. The shaft failures at the "Navajo Project" [15] arising from subsynchronous resonance interacting with torsional resonance at the turbine system has also focussed on the need for more detailed description of the torsional shaft dynamics.

These mathematical models pose difficulties for the following reasons:

a) High dimensionality

b) Non-linearities

The solutions have been pursued by two different methods:

1) Numerical integration using digital computers [16,17].

2) Using analog simulation[18-20].

To date, there has been no clear cut advantages of digital method over analog method. There are those who believe that with the diminishing cost in digital hardware, the digital simulation method will ultimately prove to be the winning choice. But these advocates may have not accounted for the cost in software development. Many research group, notably General Electric Corporate Research and Development [18], the Department of Electrical Eng., Purdue, Lafayette [19,20], and the Institut de recherche de l'Hydro-Quebec (IREQ) [21,22], continue to believe in analog simulation. Admittedly, the cost of analog hardware has reached its plateau many years ago now. The preference for analog simulation stems chiefly from the "plug-in" convenience of analog modules, in contrast to tedious rewrites of software programs. The other reason for this preference is the possibility of long runs at low cost, for real-time simulation.

In the domain of analog simulation, one finds two schools of thoughts:

1) There are those who work with standard analog computer hardware, such as integrators, multipliers, adders, etc. [18-20].

2) Those who work with dedicated simulators [21,22].

As expected, the first approach has flexibility and generality to deal with a large variety of problems. In fact, Lipo [18] and Krauss [19,20] have treated a range of problems from reluctance motor simulation to wind turbine generators. The second approach is justified when the research subject is orientated to a specific class of problems. Thus, in IREQ, it is found justifiable to build an electronic micro machine [21,22] which simulate Park's equations of the synchronous generator. This is used in conjunction with the transient network analyser (T.N.A.) and the high voltage direct current (H.V.D.C.) simulator.

The work of this thesis is orientated towards the second approach. In fact, its goal is to augment the simulation capability of IREQ's existing installations in the following ways:

a) The ability to simulate multi-inertia generator shaft as is typical of thermal stations where the generator shaft is coupled to the HP, IP, and LP turbine stages.

b) The ability to simulate the turbine heater and reheater stages.

c) The ability to simulate the governor feedback control loop.

Subject of Thesis

With these objectives in mind, the aim of this thesis is to develop these capabilities in a number of electronic modules. These electronic modules can be combined to give a full range of flexibility normally encountered in thermal stations, such as cross compound-double reheat, or tandem compound-single reheat. These modules are built from off-the-shelf electronic components. Their performance is demonstrated through test in the following system configurations:

1) Individual operation
2) Operation as a collection of rotating masses
3) Operation in a feedback loop system

Mathematical Models

As the thesis consists of building the electronic modules from components and verifying their capabilities through tests, it relies on two papers as the source for its mathematical models. First, the state space model for torsional resonance can be found in the paper by S. Goldberg and W. R. Schmus [23]. Secondly, the representation of the steam power distribution and the speed governor system is based on the models recommended in the IEEE subsynchronous resonance task force report [14]. Other good models are also available [24-35], but these lack general acceptance. All mathematical models are formulated in the S- domain

CHAPTER 2

DYNAMIC MODELS OF STEAM TURBINE AND TORSIONAL SHAFT SYSTEM

Introduction

The objective of the work reported in this thesis is to expand the existing facilities of Hydro-Quebec's Research Institute for electronic simulation of system transient. The expansion must interface with existing installation. It must also provide for development, at a later stage not yet within the scope of this project. The point of interface consists of the signal representing the torque of the generator shaft, which is available from the existing simulation system. Future development is envisaged to be a detailed representation of the boiler system, and its output will fit into this study through the governor valves.

Within these limits lies the scope of this project, which consist of:

a) A detailed model for the steam turbine [14]

b) A detailed model of the torsional shaft system [13]

The completed facilities should enable the phenomena of torsional resonances of the shaft, bilateral negative damping [32,33], and switching transients [36] to be simulated.

2.1 Steam-Turbine Torsional Shaft System

The scope of the system under study is shown in fig. 2-1. The points of interface from the generator torque, Te, and the output of the boiler are clearly shown. Along the generator shaft are the HP,IP and LP turbine sections, which are the prime movers of the system. The steam output from the boiler is admitted to the turbine through the governor valve. The output of each turbine is usually passed through successive stages of reheating, with further power discharge through a lower pressure turbine.

The inertias of the turbine blades and the inertia of the rotors of the generators and exciters are coupled through elastic shaft, which form a torsionally resonant system. There are many different configurations of steam system. In the IEEE Committee report [14], some examples of these are given, such as:

a) Nonreheat

b) Tandem Compound, Single Reheat

c) Tandem Compound, Double Reheat

d) Cross Compound, Single Reheat

e) Cross Compound, Single Reheat

f) Cross Compound, Double Reheat

These are shown in fig. 3-15.

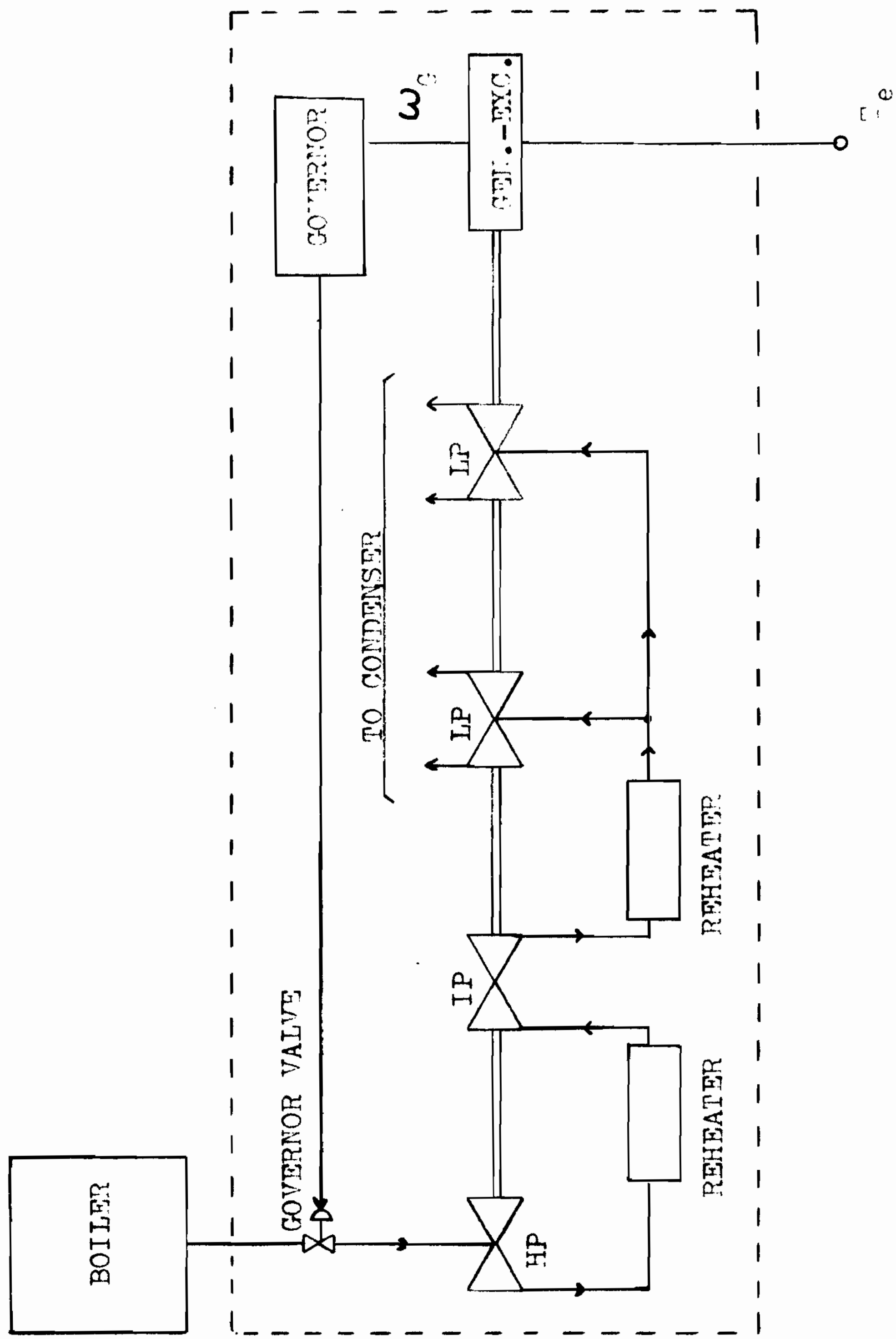

FIG 2-1   BLOCK DIAGRAM OF A STEAM-TURBINE SYSTEM

In recognizing this diversity of configurations, it is the purpose of the study to develop electronic modules which have the flexibility of being interconnected at will to simulate any conceivable configuration.

The function of the electronic model is to simulate the dynamic behavior of the system. This dynamic process is presented in the following example. As the electrical torque, Te, increases, the speed of the generator droops. The governor adjusts the governor valve opening to gradually bring back the speed of the generator to its nominal value, ωo. For the present model, it is assumed that the boiler can output any demand of steam, which is within the limits of the governor valves.

Before discussing the individual modules, it is useful to consider the typical models for each of these. Section 2.3 will discuss the steam distribution system. Section 2.5 will discuss the governor system. Section 2.6 will give the intergrated system with governor feed-back. From an understanding of their functional requirements, it will be possible to break the problem systematically into modular units.

2.2 Model of the Turbine-Generator Shaft Assembly: Schematic and Mathematical Description

Turbine-generator, for the purpose of simulation of their dynamic behaviour, are **represented by a group of** rotating inertias connected by a shaft. These inertias are connected in a specific order, and the modes in which mechanical torsional oscillations occur, depend on these various groupings.

A simplified schematic model, shown in fig. 2-2, is used to develop a formulation of a lumped-parameter model of the turbine-generator shaft assembly [14]. The mathematical formulation for the LP section of the turbine is as follows:

$$\begin{aligned}&2H_{LP}S\,\omega_{LP} + D_{LP}\omega_{LP} + D_{LP,IP}(\omega_{LP} - \omega_{IP}) + \\ &D_{LP,GEN}(\omega_{LP} - \omega_{GEN}) + K_{LP,IP}(\theta_{LP} - \theta_{IP}) + \\ &K_{LP,GEN}(\theta_{LP} - \theta_{GEN}) = 0\end{aligned} \tag{2-1}$$

The mathematical formulation for the other sections are of the same nature. For lumped-parameter representation, all inertias are represented as fixed point masses. Damping and spring coefficients are assumed constant. This model is valid for the linear region of the spring constant and shaft damping [23].

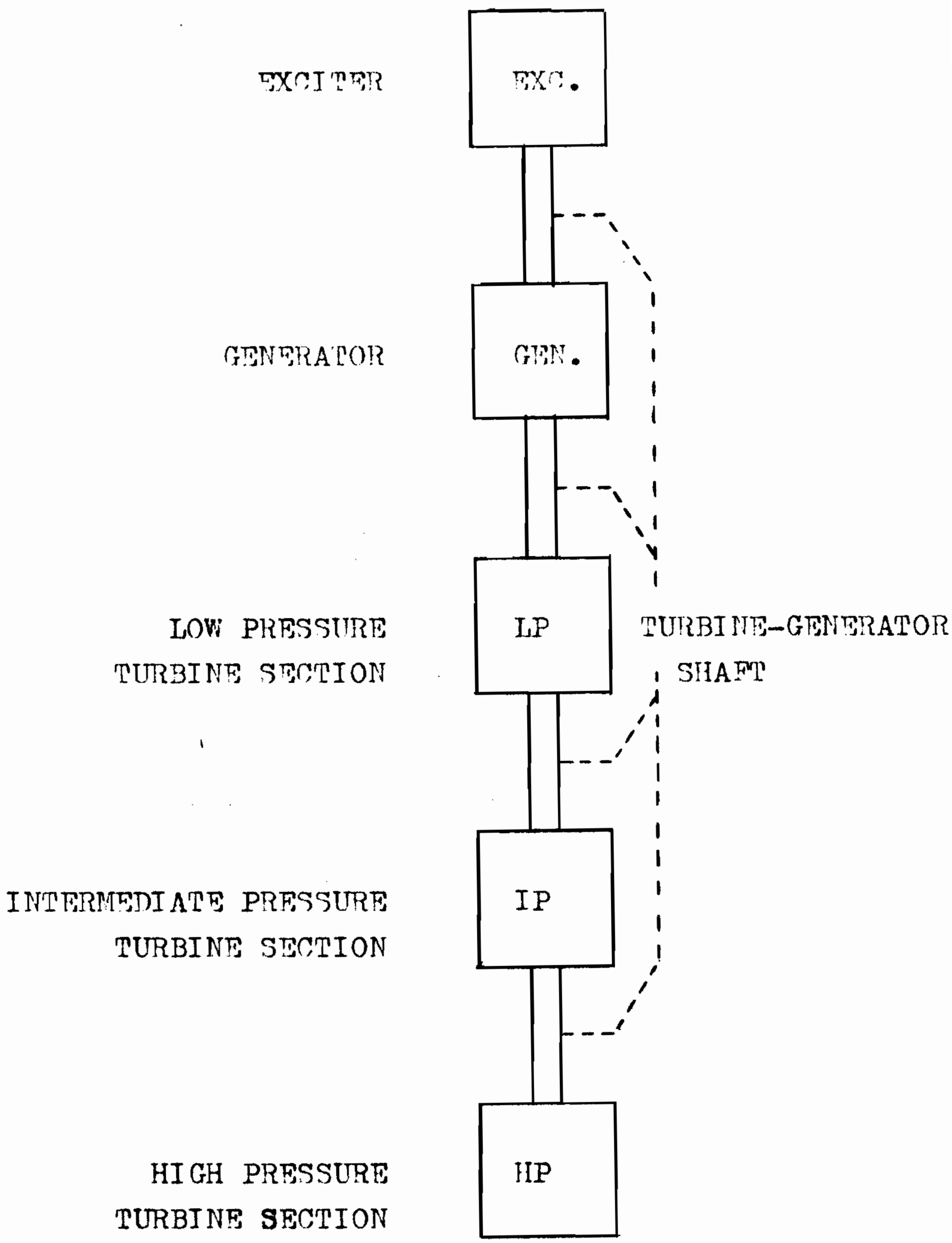

FIG. 2-2 BLOCK DIAGRAM OF A TURBINE-GENERATOR SHAFT ASSEMBLY

2.3 Model for the Steam Distribution System: Schematic and Mathematical Description

In this section and in section 2.5, linear models for the representation of steam-turbines and their governing systems are presented. These models provide adequate representation for fossil fired and pressurized water reactor nuclear units, in most stability analysis [14]. In these models, it is assumed that all turbine control is accomplished by means of governor valves.

The general model for the turbine steam systems is shown in fig. 2-3. All commonly encountered steam system configurations may be represented by this model [14].

All compound steam turbine systems utilize governor-controlled valves at the inlet to the first section of the turbine to control steam flow. The steam chest and inlet piping, reheaters and crossover piping, all introduce delays which are represented by the following time constants: T_{CH}, T_{RH} and T_{CO} respectively. The fractions, F's, represent portions of the total turbine power developed in its various sections.

Mathematically, the model in fig. 2-3 can be described by the following equations:

$$T_{CH}\, SP_1 = -P_1 + P_{GV} \qquad (2-2)$$

$$T_{RH1}\, SP_2 = -P_2 + P_1 \qquad (2-3)$$

$$T_{RH2}\, SP_3 = -P_3 + P_2 \qquad (2-4)$$

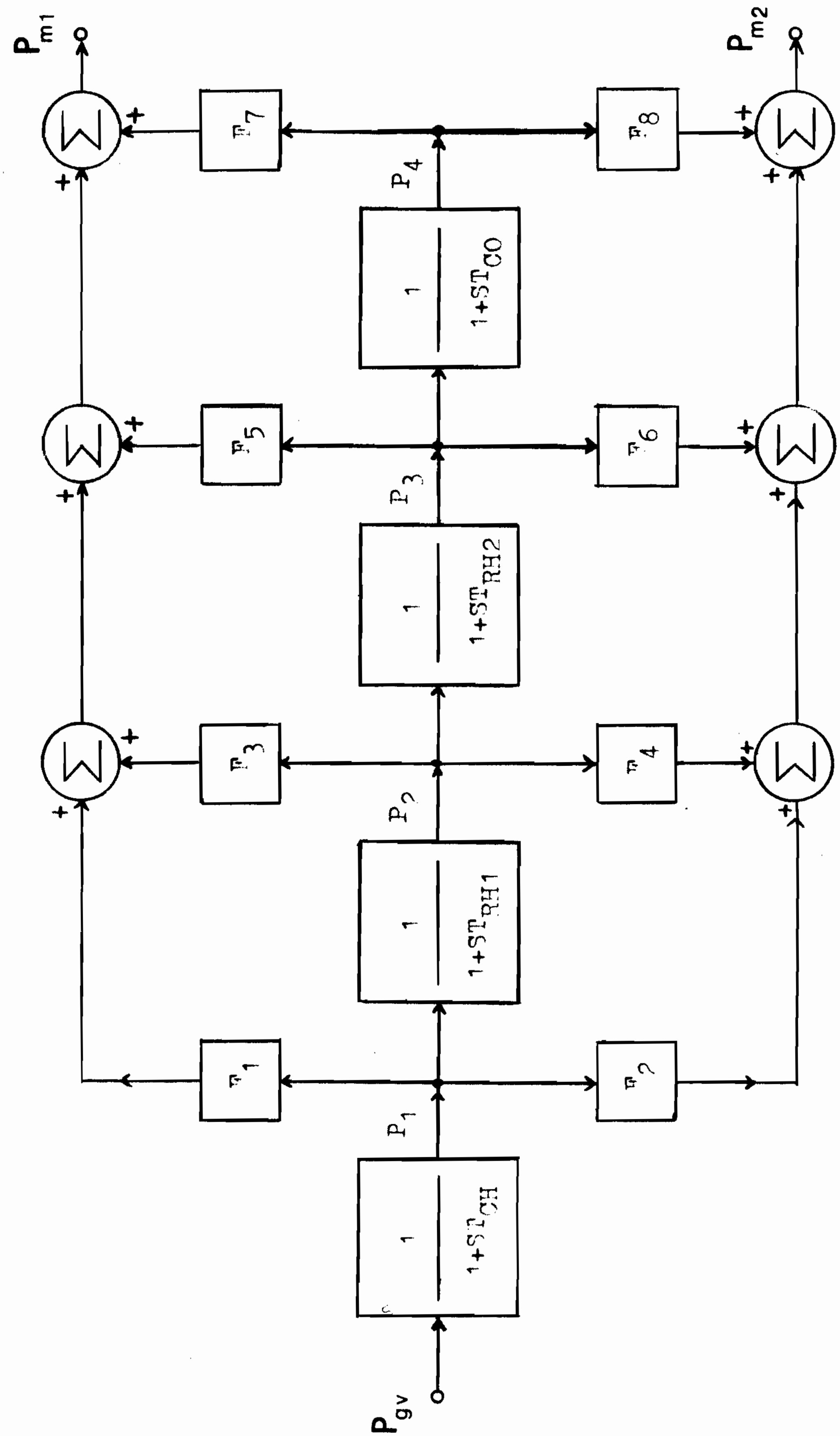

FIG. 2-3 BLOCK DIAGRAM FOR THE GENERAL MODEL OF A TURBINE'S STEAM SYSTEM

$$T_{CH}\ SP_4 = -P_4 + P_3 \qquad (2\text{-}5)$$

$$P_{M1} = (\ F_1 + F_3 + F_5 + F_7\ )\ P_{GV} \qquad (2\text{-}6)$$

$$P_{M2} = (\ F_2 + F_4 + F_6 + F_8\ )\ P_{GV} \qquad (2\text{-}7)$$

This model can easily be extended to represent more stages. The mathematical equations describing these extensions would be of the same form as equations 2-2 to 2-7.

The model of fig. 2-3 is implemented in two stages. First, the model used for a one-shaft system is discussed. Then, the required extensions for the modelling of two-shafts systems are presented.

2.3.1 Single-Shaft System

A linear model of a typical single steam turbine-reheater system recommended in the IEEE committee report is reproduced in fig. 2-4. Some care needs to be taken in translating this diagram to the electronic modules which are built to simulate the behaviour of the system.

First, it must be appreciated that physically the same mass of steam passes through all the turbines and the reheaters. As such, the fractions F_1 ,F_2 ,F_3 , etc are not the fraction of steam mass, but rather the fractions of the total power inputted to each turbine stage. The same steam mass coming out of one turbine stage is passed through a reheater where the steam picks up more thermal power, which is expended as mechanical power in the next turbine stage. The time constants T_1 , T_2 , etc convey the

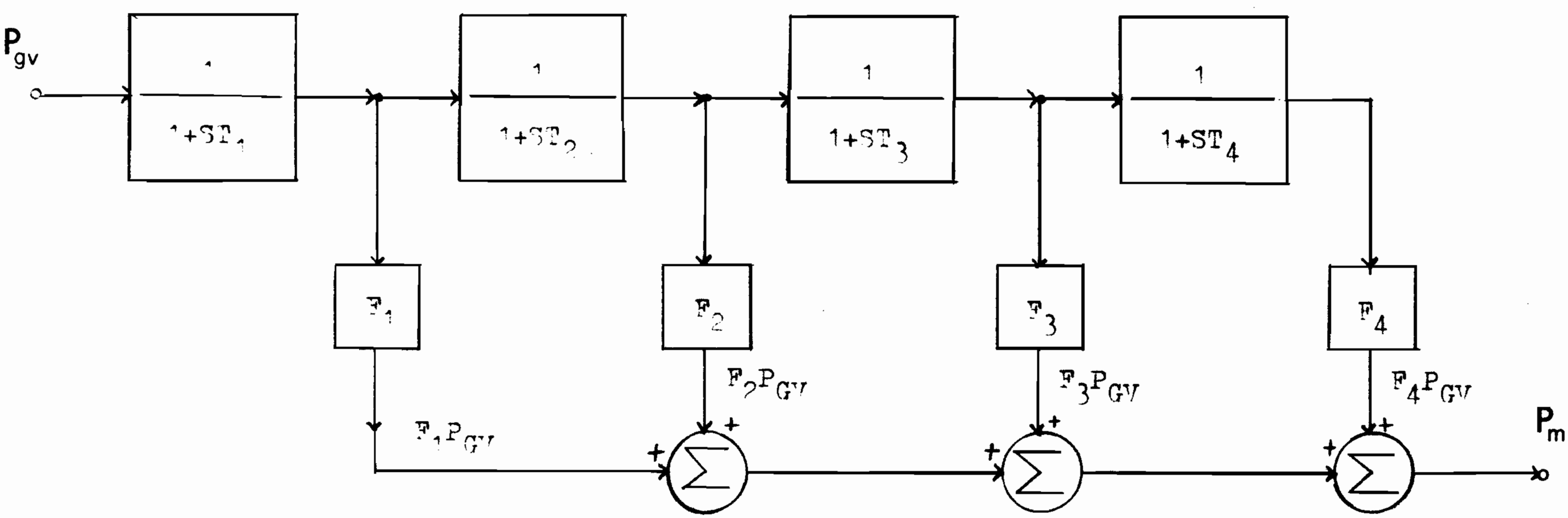

FIG. 2-4 BLOCK DIAGRAM FOR THE MODEL OF A ONE-SHAFT TURBINE'S STEAM SYSTEM AS RECOMMENDED IN THE IEEE COMMITTEE REPORT

concept of time delay in each reheat stage.

A proper interpretation of fig. 2-4 is to say that, at a typical i^{th} node as shown in fig. 2-5, the power P_i coming out of the reheater with time delay T_i is bifurcated into two parts: $G_i P_i$ which is outputted at the turbine and $(1-G_i)$ which is passed through the reheater of the next stage. The delay of this reheater is represented mathematically by the transfer function given in equation 2-8.

$$\frac{P_{i+1}(S)}{(1-G_i)\,P_i(S)} = \frac{1}{1 + ST_{i+1}} \qquad (2\text{-}8)$$

The G_i $(i=1,2,3,4)$ as designated in fig. 2-6 are the unknowns which must be calculated in order to specify correctly the parameters in the electronic modules.

On transformation, the block diagram of fig. 2-4 becomes fig. 2-6. The equivalencing is based on the steady-state power flow, where S=0 in the transfer function of equation 2-8. Under this condition, the power balance in fig. 2-4 is satisfied when:

$$P_M = (F_1 + F_2 + F_3 + F_4)\, P_{GV} \qquad (2\text{-}9)$$

As $P_M = P_{GV}$ (2-10)

$$(F_1 + F_2 + F_3 + F_4) = 1.0 \qquad (2\text{-}11)$$

But in using the block diagram of fig. 2-6, G_i is defined as the fraction of the thermal power after the i^{th} reheater which is converted into mechanical power at the turbine.

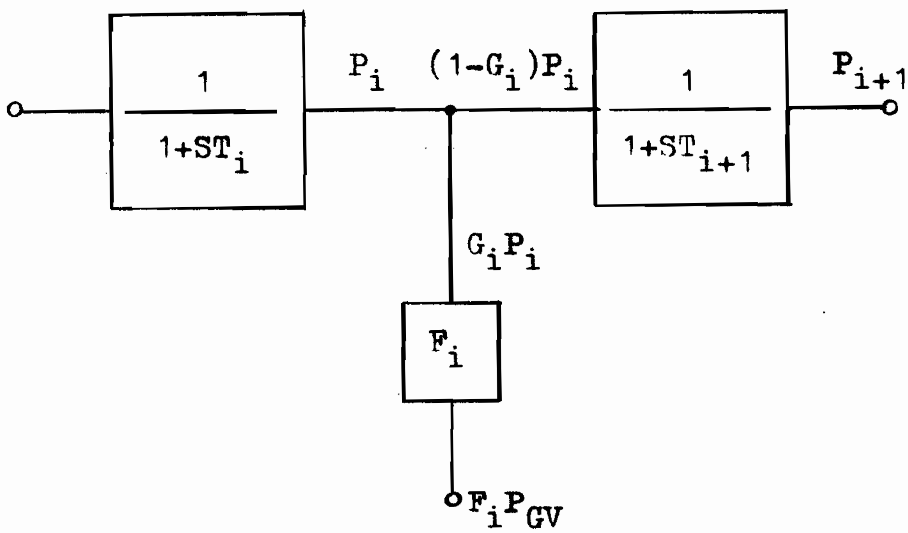

FIG. 2-5 A TYPICAL i^{th} NODE OF THE MODEL FOR A ONE-SHAFT TURBINE'S STEAM SYSTEM

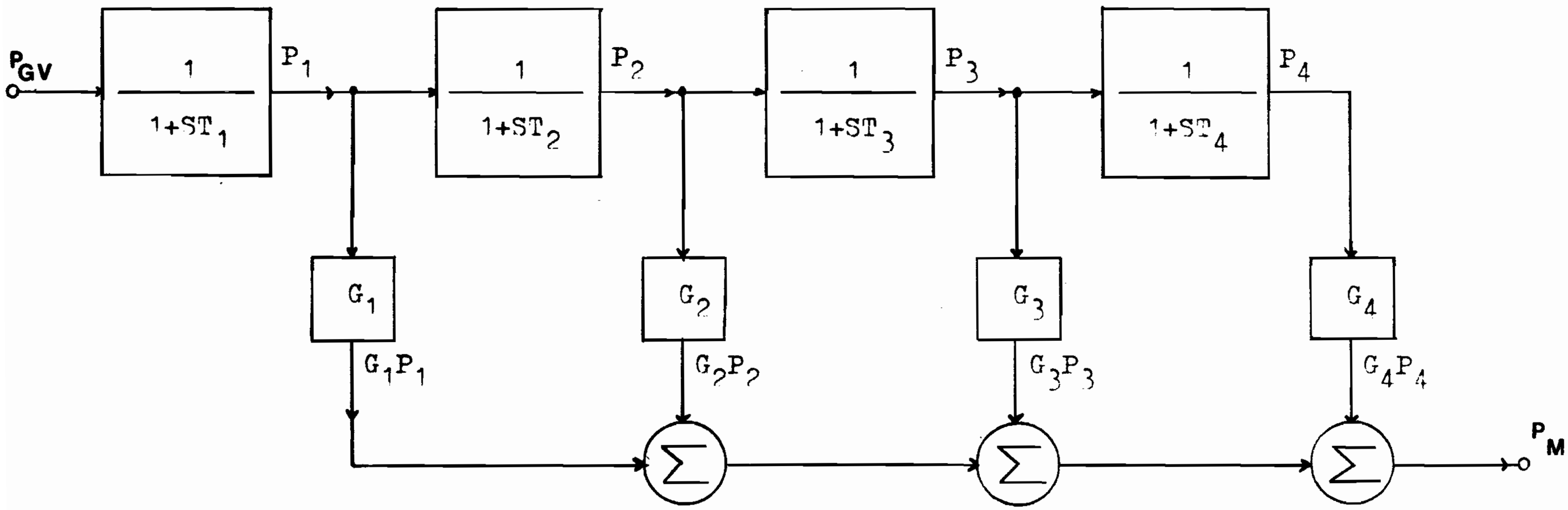

FIG. 2-6 BLOCK DIAGRAM FOR THE MODEL OF A ONE-SHAFT TURBINE'S STEAM SYSTEM WITH INTERMEDIATE THERMAL POWERS

As such, under steady state, $P_{GV} = \sum_{i=1}^{4} G_i P_i = P_M$. Each G_i is computed from a given specification of F_i $(i=1,2,3,4)$ in the following manner for the system shown in fig. 2-4 :

$$P_1 = P_{GV} \tag{2-12}$$

$$F_1 P_{GV} = G_1 P_1 \tag{2-13}$$

$$G_1 = F_1$$

$$P_2 = (1-G_1)\ P_1 = (1-F_1)\ P_{GV} \tag{2-14}$$

$$F_2 P_{GV} = G_2 P_2 = G_2\ (1-F_1)\ P_{GV} \tag{2-15}$$

$$G_2 = \frac{F_2}{1-F_1} \tag{2-16}$$

$$P_3 = (1-G_2)\ P_2 = (1-F_1-F_2)\ P_{GV} \tag{2-17}$$

$$F_3 P_{GV} = G_3 P_3 = G_3\ (1-F_1-F_2)\ P_{GV} \tag{2-18}$$

$$G_3 = \frac{F_3}{1-F_1-F_2} \tag{2-19}$$

$$P_4 = (1-G_3)\ P_3 = (1-F_1-F_2-F_3)\ P_{GV} = F_4\ P_{GV} \tag{2-20}$$

$$F_4 P_{GV} = G_4 P_4 = G_4 F_4 P_{GV} \tag{2-21}$$

$$G_4 = \frac{F_4}{F_4} = 1.0 \tag{2-22}$$

2.3.2 Two-Shaft System

Only a slight modification is necessary in order to model the system when it has two turbine shafts. Typically, the block diagram at the i^{th} reheater output is shown in fig. 2-7A , where $F_i'\ P_{GV}$ and $F_i''\ P_{GV}$ are the outputs to each of the shaft. The combined power tapped at this node is

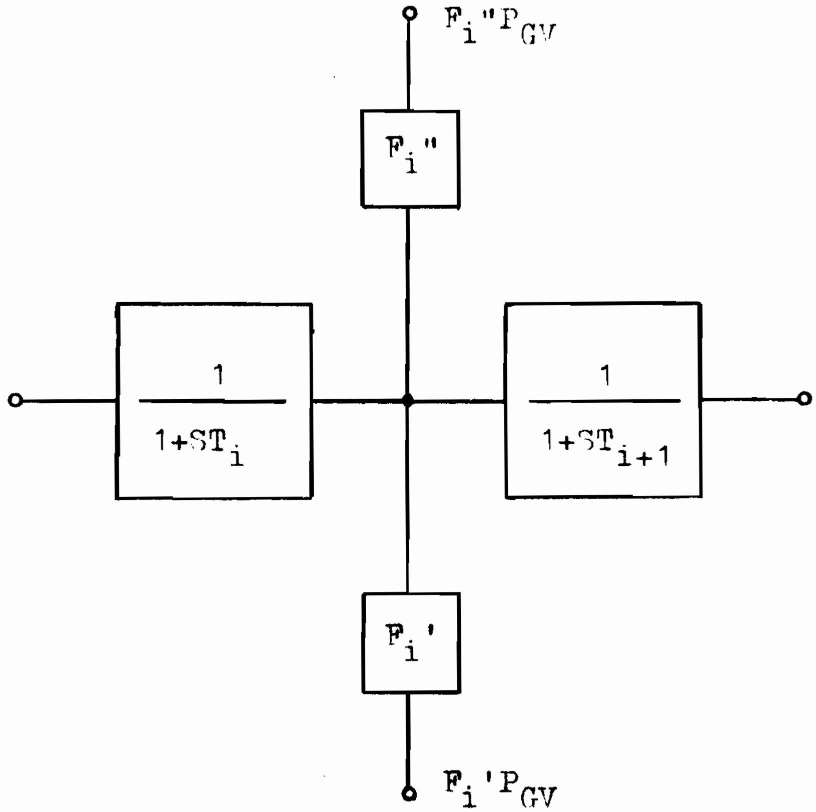

FIG. 2-7A BLOCK DIAGRAM FOR THE POWER DIVISION AT THE i^{th} NODE FOR A TWO-SHAFT SYSTEM

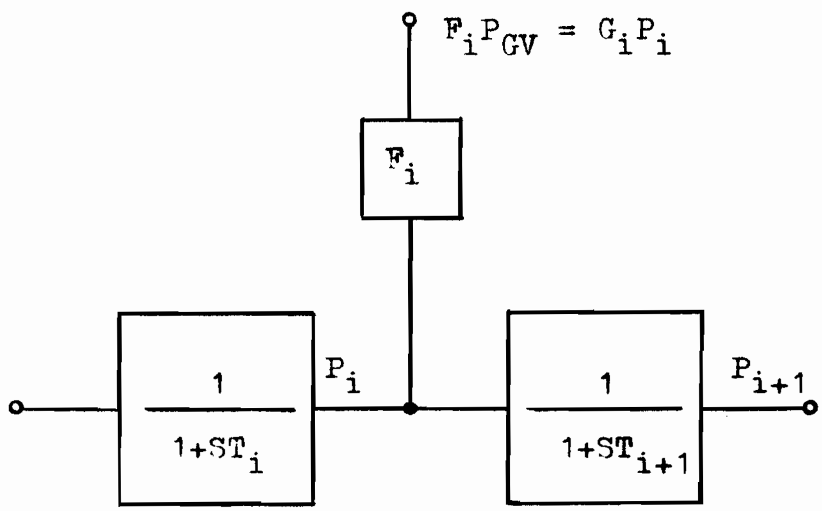

FIG. 2-7B BLOCK DIAGRAM FOR THE TOTAL POWER DIVISION AT THE i^{th} NODE

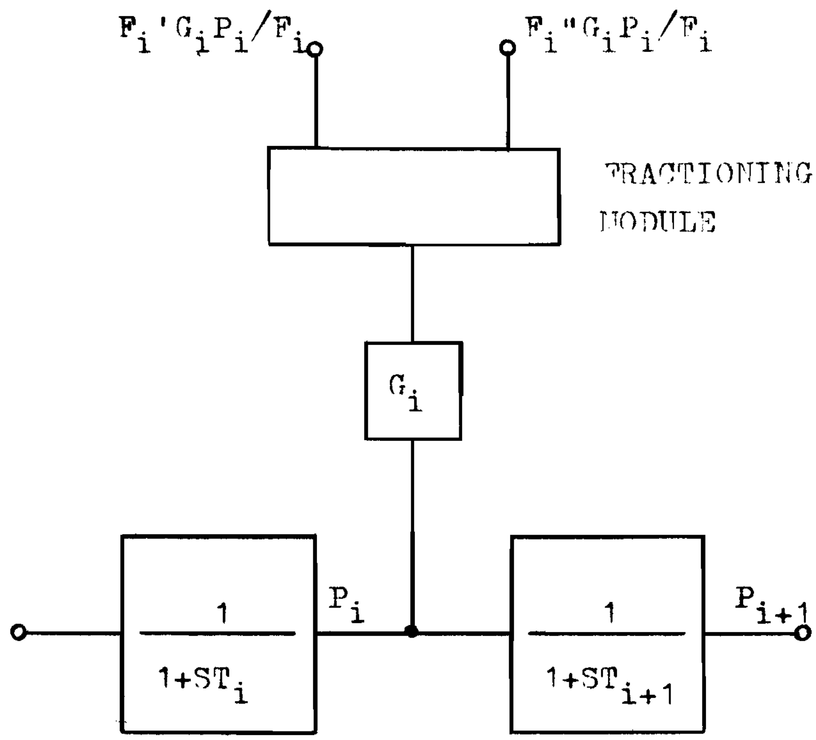

FIG. 2-7C BLOCK DIAGRAM FOR THE TOTAL POWER OUTPUT AT THE i^{th} NODE WITH A FRACTIONING MODULE

F_1P_{GV}, where $F_1=F_1'+F_1''$. Fig 2-7B is the block diagram of this combination. Using the method of equivalencing as discussed in the previous section, one can compute G_1 from F_1 . The division of power to each turbine in the fractions $F_i'G_iP_i/F_i$ and $F_i''G_iP_i/F_i$ can be implemented by a Fractioning module, which is discussed in section 3.4.4 .

2.4 Torque from Steam Power

For the steam power term to be included in the equation describing the dynamics of an inertia, it is necessary to obtain its torque contribution. The torque provided by the steam power is obtained by dividing it by the angular velocity of the inertia. All turbine sections therefore require an analog divider to determine the prime mover torque contribution. Such a divider is shown in fig. 2-8. In the modules discussed in chapter 3, this divider is incorporated in the inertia-shaft turbine section in fig. 3-2.

2.5 Model for Speed-Governor System: Schematic and Mathmatical Description

The general model for the speed-governing systems of steam turbines is shown in fig. 2-9. This is the model recommended in the IEEE committee report [14-fig. 4-A]. This model, with the proper choice of parameters, can be used

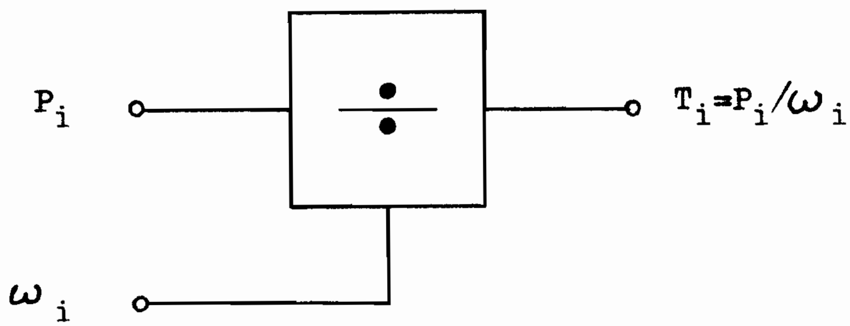

FIG. 2-8 BLOCK DIAGRAM FOR AN ELECTRONIC ANALOG DIVIDER

to represent either a mechanical-hydraulic system or an electro-hydraulic system [14]. Mathematically, the model shown in fig. 2-9 can be described by the following equations:

$$T_1 S \omega_{IS} = -\omega_{IS} + \omega_G - \omega_o \qquad (2\text{-}23)$$

$$P_{IS} = KT_2(\ {}_G - \ {}_o)/T_1 + K(1-T_2/T_1) \ {}_{IS} \qquad (2\text{-}24)$$

$$T_3 S P_{GV} = P_o - P_{IS} - P_{GV} \qquad (2\text{-}25)$$

Since the transfer function has a term of the form $(1+ST_1)/(1+ST_2)$, as shown in fig. 2-9, it requires a special technique in order to simulate it using integrators and time delays. This technique is needed because a first order state space approach is used to implement the transfer functions. The mathematical derivations for equations 2-23 to 2-25 are given in appendix # 3. Governor limit functions, shown in fig. 2-9, are the rate limits of the valve, which prevent too rapid speed deviations. Rate limits are shown at the input to the integrators representing the governor controlled valves. The first rate limits, i.e. $\dot{P}_{DOWN}$ and $\dot{P}_{UP}$, are to set the lower and upper limits on the speed of opening and closing of the valve. The second limits, ie P_{MIN} and P_{MAX}, are the position limits of the valve. The implementation of the rate limits is discussed in section 3.5 .

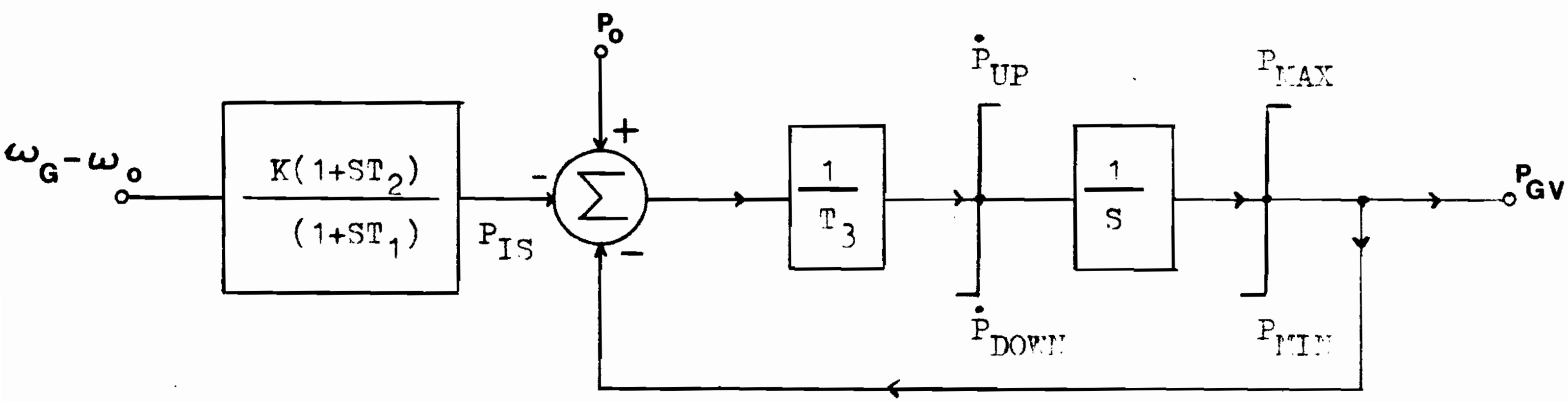

FIG. 2-9 BLOCK DIAGRAM FOR THE GENERAL MODEL FOR A SPEED-GOVERNOR SYSTEM

2.6 Integration of models into a complete system

In this section, the models presented in the previous sections are integrated into one complete system. For the purpose of illustration, a specific complete system is presented schematically in fig. 2-10. Its mathematical description is given in equations 2-26 to 2-47. As can be seen on the schematic diagram of fig. 2-10, the system takes as input a signal representing the electrical torque, T_e , at the generator. With this system simulating the dynamics of a turbine-generator system, the angular speed of the generator can be observed for transient or steady-state variation in electrical torque.

The equations describing the steam distribution system of fig. 2-10 are:

$$T_{CH} SP_{VHP} = -P_{VHP} + P_{GV} \tag{2-26}$$

$$T_{RH1} SP_{HP} = -P_{HP} + (1-G_{VHP})P_{VHP} \tag{2-27}$$

$$T_{RH2} SP_{IP} = -P_{IP} + (1-G_{HP})P_{HP} \tag{2-28}$$

$$T_{CO} SP_{LP} = -P_{LP} + (1-G_{IP})P_{IP} \tag{2-29}$$

where:

$$G_{VHP} = F_{VHP} \tag{2-30}$$

$$G_{HP} = F_{HP}/(1-F_{VHP}) \tag{2-31}$$

$$G_{IP} = F_{IP}/(1-F_{VHP}-F_{HP}) \tag{2-32}$$

$$G_{LP} = F_{LP}/(1-F_{VHP}-F_{HP}-F_{IP}) = 1.0 \tag{2-33}$$

The equations for the speed-governing system are as

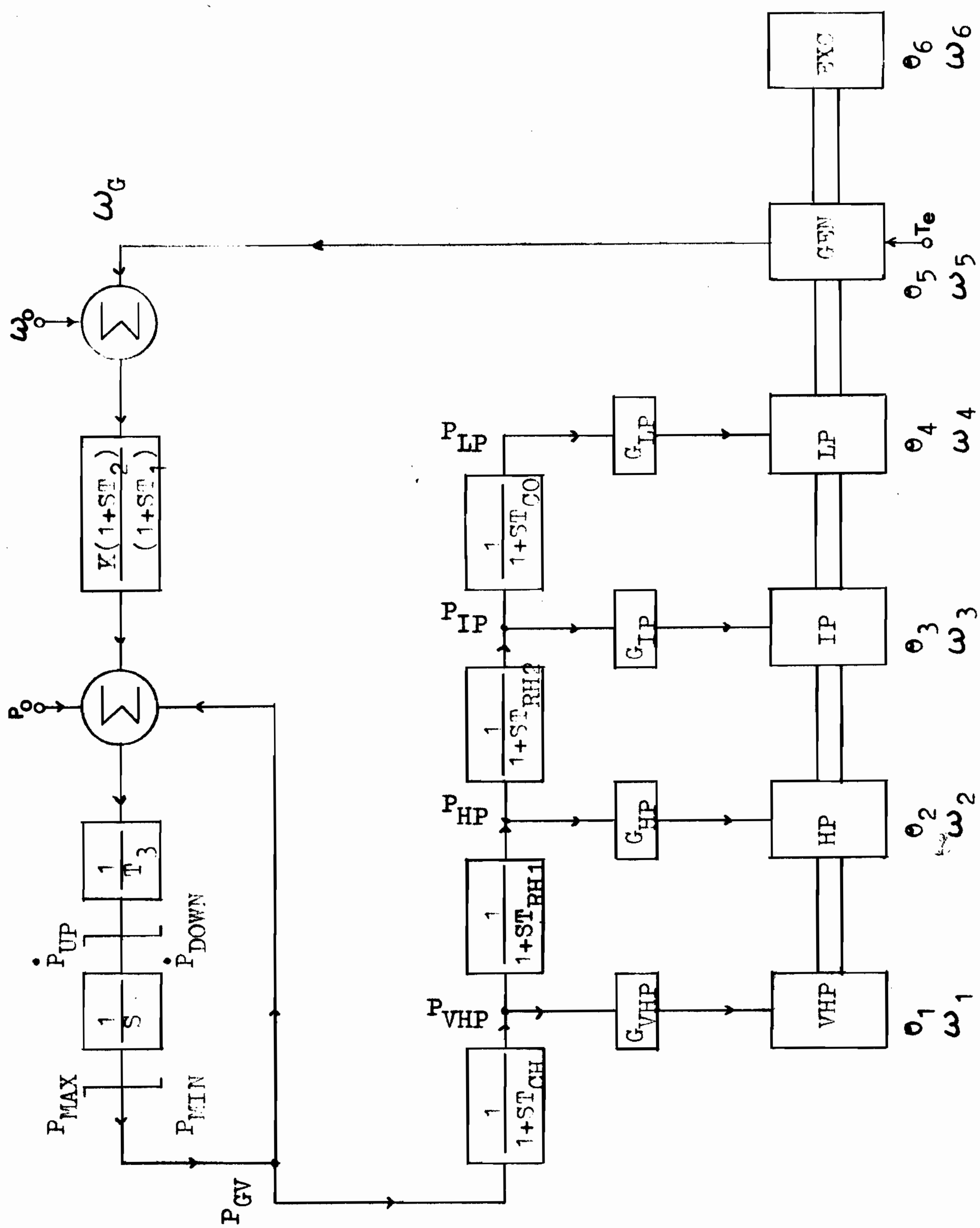

FIG. 2-10 BLOCK DIAGRAM FOR AN INTEGRATED SYSTEM MODEL

follows:

$$T_1 S\omega_{IS} = -\omega_{IS} + \omega_G - \omega_o \tag{2-34}$$

$$P_{IS} = KT_2(\omega_G - \omega_o)/T_1 + K(1-T_2/T_1)\omega_{IS} \tag{2-35}$$

$$T_3 SP_{GV} = P_o - P_{IS} - P_{GV} \tag{2-36}$$

Finally, the equations describing the dynamics of the turbine-generator shaft assembly system are:

$$S\theta_1 = \omega_1 \tag{2-37}$$

$$S\theta_2 = \omega_2 \tag{2-38}$$

$$S\theta_3 = \omega_3 \tag{2-39}$$

$$S\theta_4 = \omega_4 \tag{2-40}$$

$$S\theta_5 = \omega_5 \tag{2-41}$$

$$S\theta_6 = \omega_6 \tag{2-42}$$

$$\begin{aligned} 2H_1 S\omega_1 = {} & G_{VHP}P_{VHP}/\omega_1 - D_{1,2}(\omega_1 - \omega_2) \\ & - D_{11}\omega_1 - K_{1,2}(\theta_1 - \theta_2) \end{aligned} \tag{2-43}$$

$$\begin{aligned} 2H_2 S\omega_2 = {} & G_{HP}P_{HP}/\omega_2 - D_{22}\omega_2 - D_{2,3}(\omega_2 - \omega_3) \\ & - D_{1,2}(\omega_2 - \omega_1) - K_{2,3}(\theta_2 - \theta_3) \\ & - K_{1,2}(\theta_2 - \theta_1) \end{aligned} \tag{2-44}$$

$$\begin{aligned} 2H_3 S\omega_3 = {} & G_{IP}P_{IP}/\omega_3 - D_{33}\omega_3 - D_{3,4}(\omega_3 - \omega_4) \\ & - D_{2,3}(\omega_3 - \omega_2) - K_{3,4}(\theta_3 - \theta_4) \\ & - K_{2,3}(\theta_3 - \theta_2) \end{aligned} \tag{2-45}$$

$$\begin{aligned} 2H_4 S\omega_4 = {} & G_{LP}P_{LP}/\omega_4 - D_{44}\omega_4 - D_{4,5}(\omega_4 - \omega_5) \\ & - D_{3,4}(\omega_4 - \omega_3) - K_{4,5}(\theta_4 - \theta_5) \\ & - K_{3,4}(\theta_4 - \theta_3) \end{aligned} \tag{2-46}$$

$$2H_5 S\omega_5 = -T_e - D_{55}\omega_5 - D_{5,6}(\omega_5 - \omega_6) - D_{4,5}(\omega_5 - \omega_4) - K_{5,6}(\theta_5 - \theta_6) - K_{4,5}(\theta_5 - \theta_4) \quad (2\text{-}47)$$

$$2H_6 S\omega_6 = - D_{66}\omega_6 - D_{5,6}(\omega_6 - \omega_5) - K_{5,6}(\theta_6 - \theta_5) \quad (2\text{-}48)$$

CHAPTER 3

ELECTRONIC MODULES

INTRODUCTION

In chapter 2, the mathematical model of the typical steam turbine system, integrated with torsional shaft system, has been described. In order to achieve maximum flexibility for different possible steam system configurations, the following electronic modules have been developed:

1) Inertia-Shaft Modules (Sect.2.2)
    1) Turbine Section
    2) Generator Unit
2) Exciter Module (Sect. 2.2)
3) Steam Distribution Modules (Sect.2.3)
   Reheaters, crossover and steam chest can be represented with this modules.
4) Speed-Governor Module (Sect.2.5)

The wiring diagrams of each module, and the corresponding mimic diagrams, are presented in this chapter. The input and output points for each are shown. Provisions for the inclusion of fast valving, boiler dynamics and governor dead-band are also discussed. Finally, all equations presented in this paper are in the per unit form. A complete derivation for the per-unitization of the dynamic equations describing a specific system is presented in appendix 1.

3.1 Torsional Shaft System

Fig. 3-1 shows a typical torsional shaft system. There are two categories of inertias:

1) A mid-section inertia, i , which is connected to two neighboring inertias i+1 and i-1
2) An end inertia which is connected only to one neighbor.

In the development of the modules, it has been found that the left hand end inertia can be represented by a mid-section inertia module. Unfortunately, in the manner in which the mid-section modules have been designed, it is not possible to modify it to represent the right hand end inertia. It will be assumed that the exciter occupies the position of the right end inertia. For this reason, two modules have been developed, viz:

1) inertia-shaft modules, and
2) exciter modules

The inertia-shaft modules are either turbine sections or generator units. These two are exactly the same, except for their torque input. The generator unit has as torque input $+T_{ei}$ and the turbine section has $- G_i P_i/\omega_i$. This difference in input is expanded further in the following section.

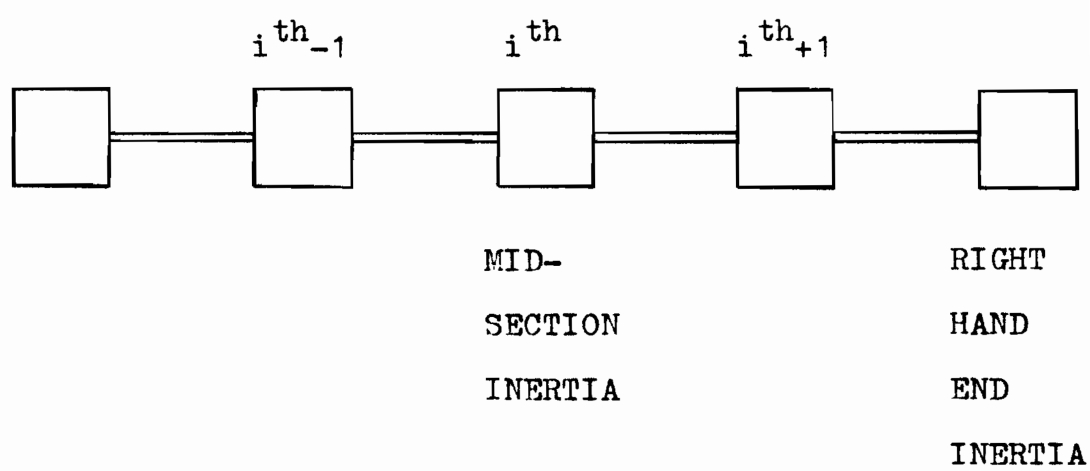

FIG. 3-1 BLOCK DIAGRAM FOR A TORSIONAL SHAFT SYSTEM

3.2 Inertia-Shaft Modules:

1) Turbine Section

2) Generator Unit

There are two types of inertia-shaft modules based on the torque unit. The torque input is the $-G_iP_i$ term in the equation 3-1 of turbine section,

$$2H_iS\omega_i - G_iP_i/\omega_i + D_{ii}\omega_i + D_{i,i+1}(\omega_i-\omega_{i+1}) + D_{i-1,i}(\omega_i-\omega_{i-1}) + K_{i,i+1}(\theta_i-\theta_{i+1}) + K_{i-1,i}(\theta_i-\theta_{i-1}) = 0 \qquad (3\text{-}1)$$

and $+T_{ei}$ term in the equation 3-2 of the generator unit.

$$2H_iS\omega_i + T_{ei} + D_{ii}\omega_i + D_{i,i+1}(\omega_i-\omega_{i+1}) + D_{i-1,i}(\omega_i-\omega_{i-1}) + K_{i,i+1}(\theta_i-\theta_{i+1}) + K_{i-1,i}(\theta_i-\theta_{i-1}) = 0 \qquad (3\text{-}2)$$

Fig. 3-3 and fig. 3-5 respectively show the electronic realization of equations 3-1 and 3-2. In these diagrams, we see that the inertia shaft modules include the terms:

$2H_iS\omega_i$, $D_{ii}\omega_i$, $D_{i+1,i}(\omega_i-\omega_{i+1})$, and $K_{i+1,i}(\theta_i-\theta_{i+1})$.

These are torque terms of the i^{th} inertia and the inter-coupling between the i^{th} and $i^{th}+1$ inertias.

The terms $D_{i,i-1}(\omega_i-\omega_{i-1})$ and $K_{i,i-1}(\theta_i-\theta_{i-1})$ are inputs to this module. These inputs are taken from the output of the $i^{th}-1$ module. When the module under consideration is a left-hand end inertia, these inputs are grounded. In the turbine section module, the input G_iP_i is

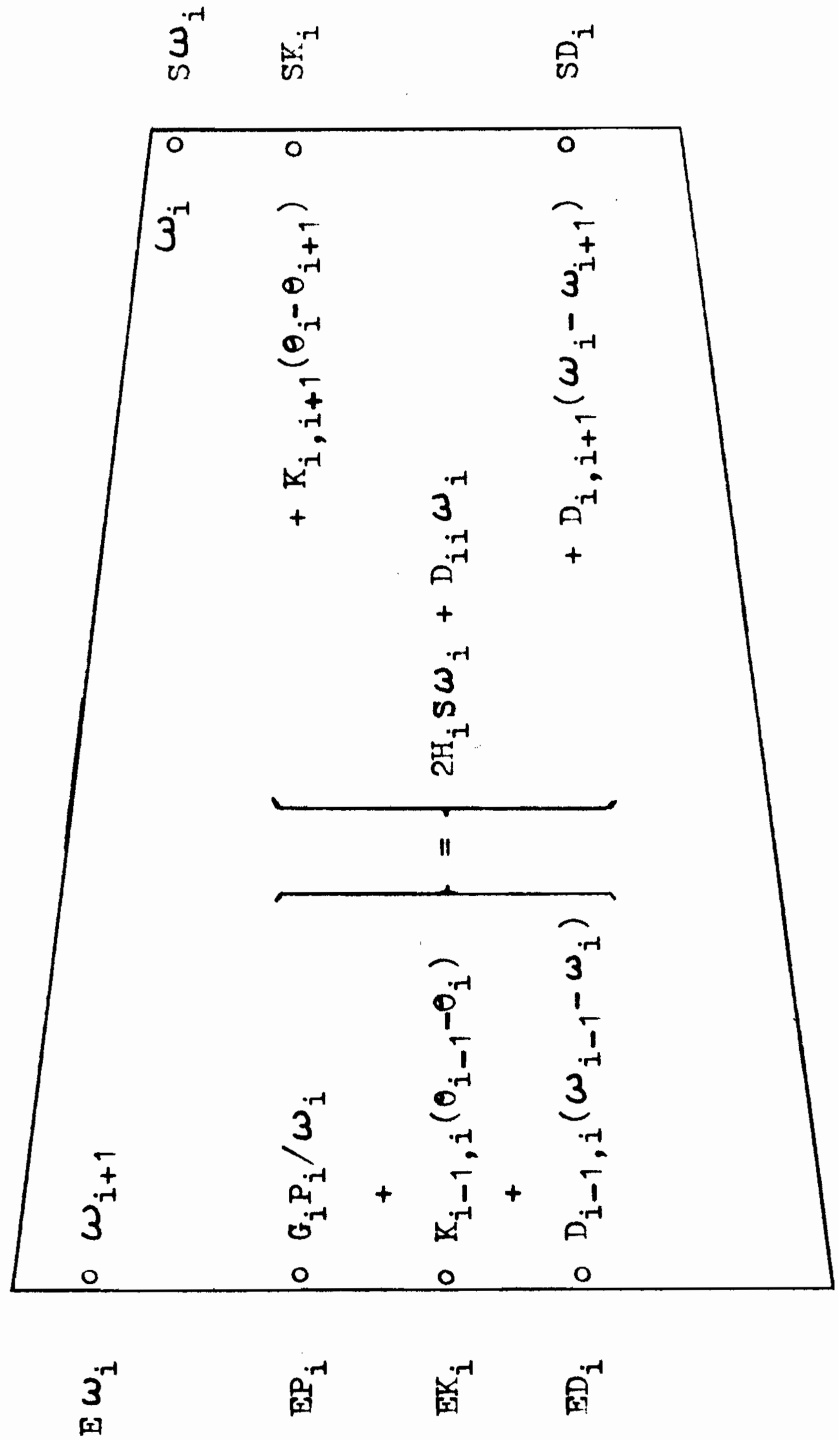

FIG. 3-2 MIMIC DIAGRAM FOR AN INERTIA-SHAFT MODULE: TURBINE SECTION

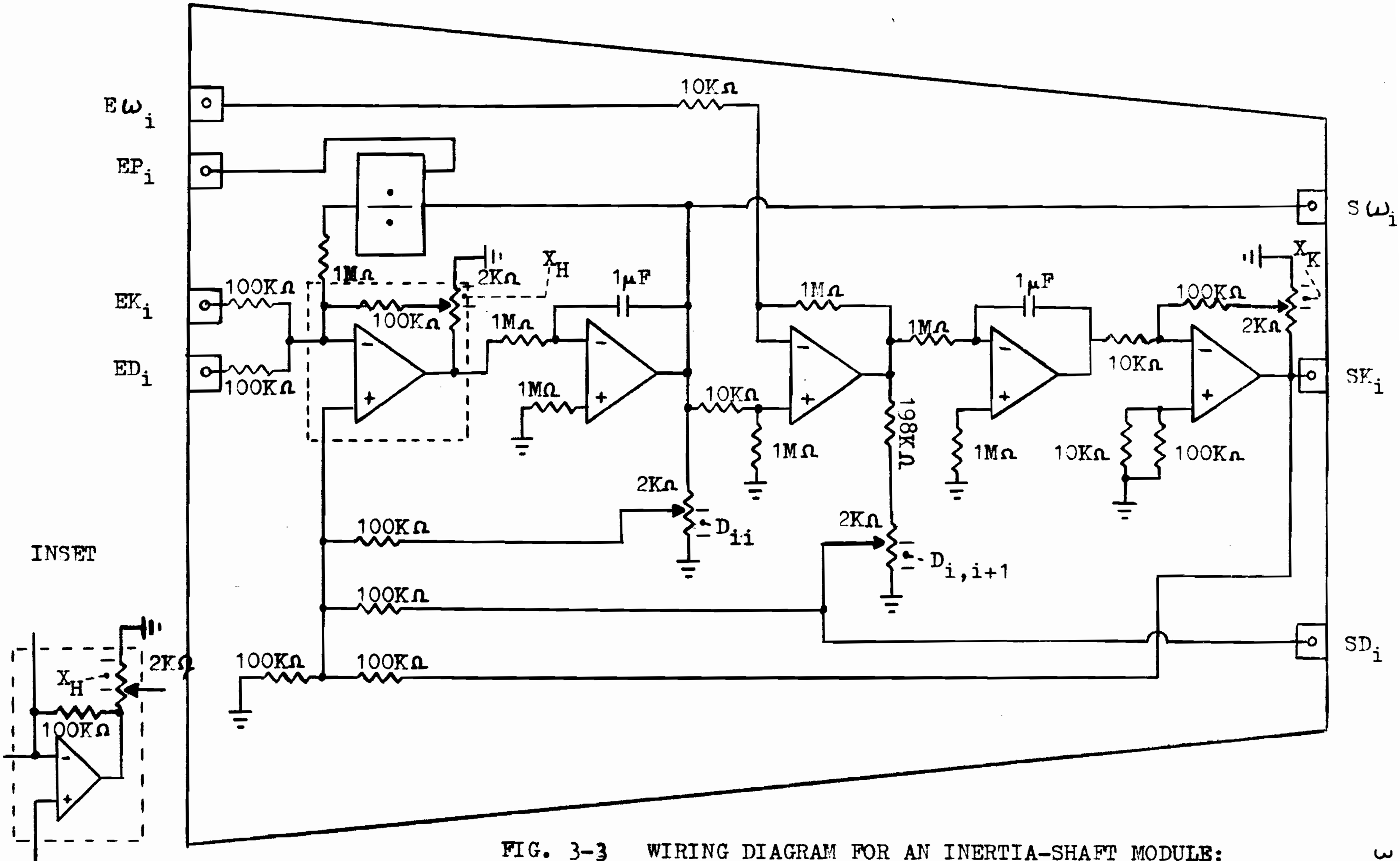

FIG. 3-3 WIRING DIAGRAM FOR AN INERTIA-SHAFT MODULE:

TURBINE SECTION

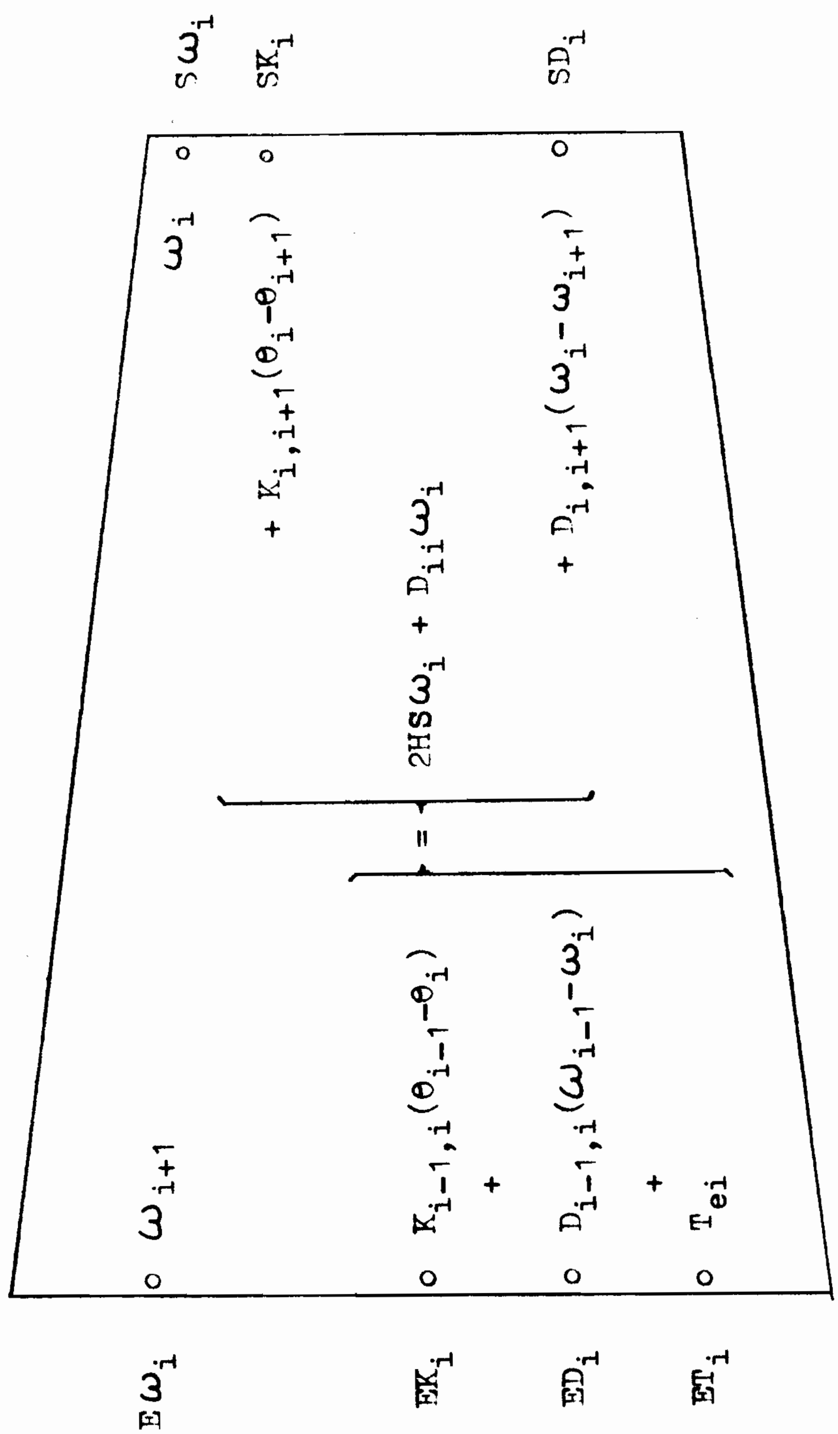

FIG. 3-4 MIMIC DIAGRAM FOR AN INERTIA-SHAFT MODULE: GENERATOR UNIT

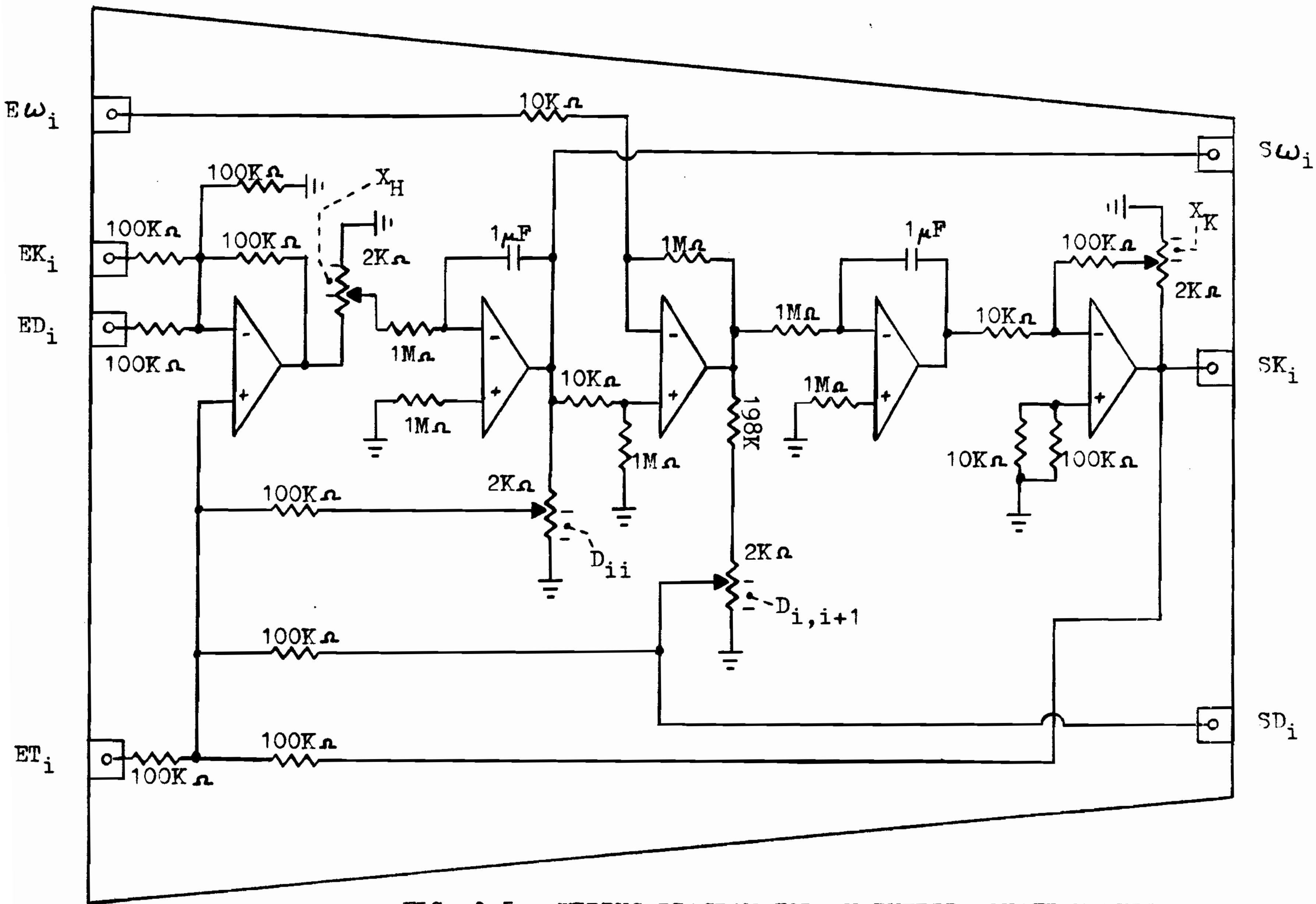

FIG. 3-5 WIRING DIAGRAM FOR AN INERTIA-SHAFT MODULE: GENERATOR UNIT

taken from the output of the corresponding steam destribution module. In the case of the generator module, the input T_{ei} (generator torque) is taken from the existing electronic micro machine simulator at IREQ.

The difference between the turbine section module and the generator unit module lies in the input terms $-G_iP_i/\omega_i$ in eq. 3-1 and $+T_{ei}$ in eq. 3-2. As implemented in fig.3-2 the output G_iP_i from the steam distribution module, is divided by the angular velocity ω_i. The negative sign in eq. 3-1 indicates that the power input is a prime mover source. In contrast, the positive sign of T_{ei} in eq. 3-2 indicates that the generator input torque is a counter torque.

Equation 3-1 is a torque equation. A divider unit is introduced to obtain the torque derived from the steam power. The torque applied to a turbine section is the steam power divided by the angular velocity of the turbine section. All the inertia shaft modules for turbine section have a divider unit.

3.2.1 Module Parameters

Four potentiometer are provided for the setting of parameter values.

$2H_i = X_H$ p.u. of 2KΩ potentiometer (for $2H_i \leq 1.0$)

$= 1/X_H$, where X_H is in p.u. of 2KΩ potentiometer (for $2H_i \geq 1.0$, see inset in fig. 3-3)

$K_{i,i+1} = 1000/X_K$, where X_K is in p.u. of $2K\Omega$ potentiometer

$D_{i,i+1}$ = p.u. of $2K\Omega$ potentiometer

D_{ii} = p.u. of $2K\Omega$ potentiometer

The potentiometers are calibrated for one thousand divisions. These must be set to the calculated values in order to implement the desired parameter values. These are shown in fig. 3-3 and fig. 3-5.

3.2.2 Module Inputs

The terminals on the left hand side of the diagram of fig. 3-2 and fig. 3-4 are the inputs to the modules. These are described, for the i^{th} module, in this section.

Terminal $E\omega_i$: "ω_{i+1}", this is the angular velocity output of the $i^{th}+1$ module

Terminal EP_i : "G_iP_i", this is the power input to the i^{th} turbine section

Terminal ET_i : "T_{ei}", this is the electrical torque on the i^{th} generator section

Terminal EK_i : "$K_{i,i-1}(\theta_i-\theta_{i-1})$", this is the shaft torque between the i^{th} and $i^{th}-1$ inertias

Terminal ED_i : "$D_{i,i-1}(\omega_i-\omega_{i-1})$", this is the mutual damping between the i^{th} and the $i^{th}-1$ inertias

3.2.3 Module Outputs

The terminals on the right hand side of the diagram of fig. 3-2 and fig. 3-4 are the outputs of the module. These are described, for the i^{th} module, in this section.

Terminal $S\omega_i$: "ω_i", this is the angular velocity output of the i^{th} module

Terminal SK_i : "$K_{i,i+1}(\theta_i-\theta_{i+1})$", this is the shaft torque between the i^{th} and the $i^{th}+1$ inertias

Terminal SD_i : "$D_{i,i+1}(\omega_i-\omega_{i+1})$", this is the mutual damping between the i^{th} and the $i^{th}+1$ inertias

3.3 Exciter Modules

The equation describing the dynamics of the exciter is:

$$2H_i S\omega_i + D_{ii}\omega_i + D_{i,i+1}(\omega_i-\omega_{i-1}) + K_{i,i-1}(\theta_i-\theta_{i-1}) = 0 \tag{3-3}$$

The electronic realization of equation 3-3 is shown in fig. 3-7. In this diagram, we can see that each exciter module include the terms $2H_i S\omega_i$ and $D_{ii}\omega_i$. These are torque terms of the i^{th} inertia. The terms $D_{i,i-1}(\omega_i-\omega_{i-1})$ and $K_{i,i-1}(\theta_i-\theta_{i-1})$ are inputs to this module. These inputs are taken from the output of the $(i-1)^{th}$ module.

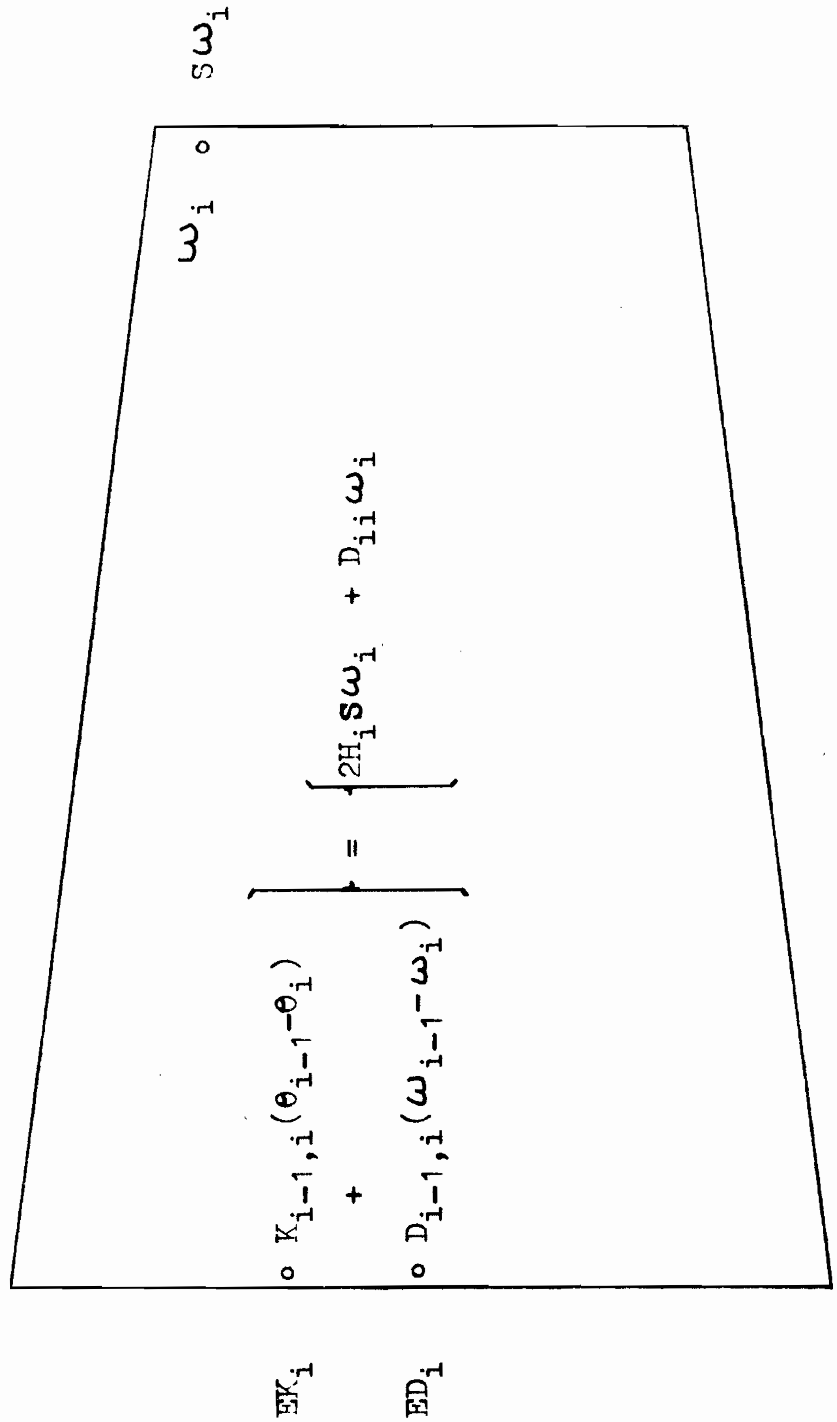

FIG. 3-6 MIMIC DIAGRAM FOR AN EXCITER MODULE

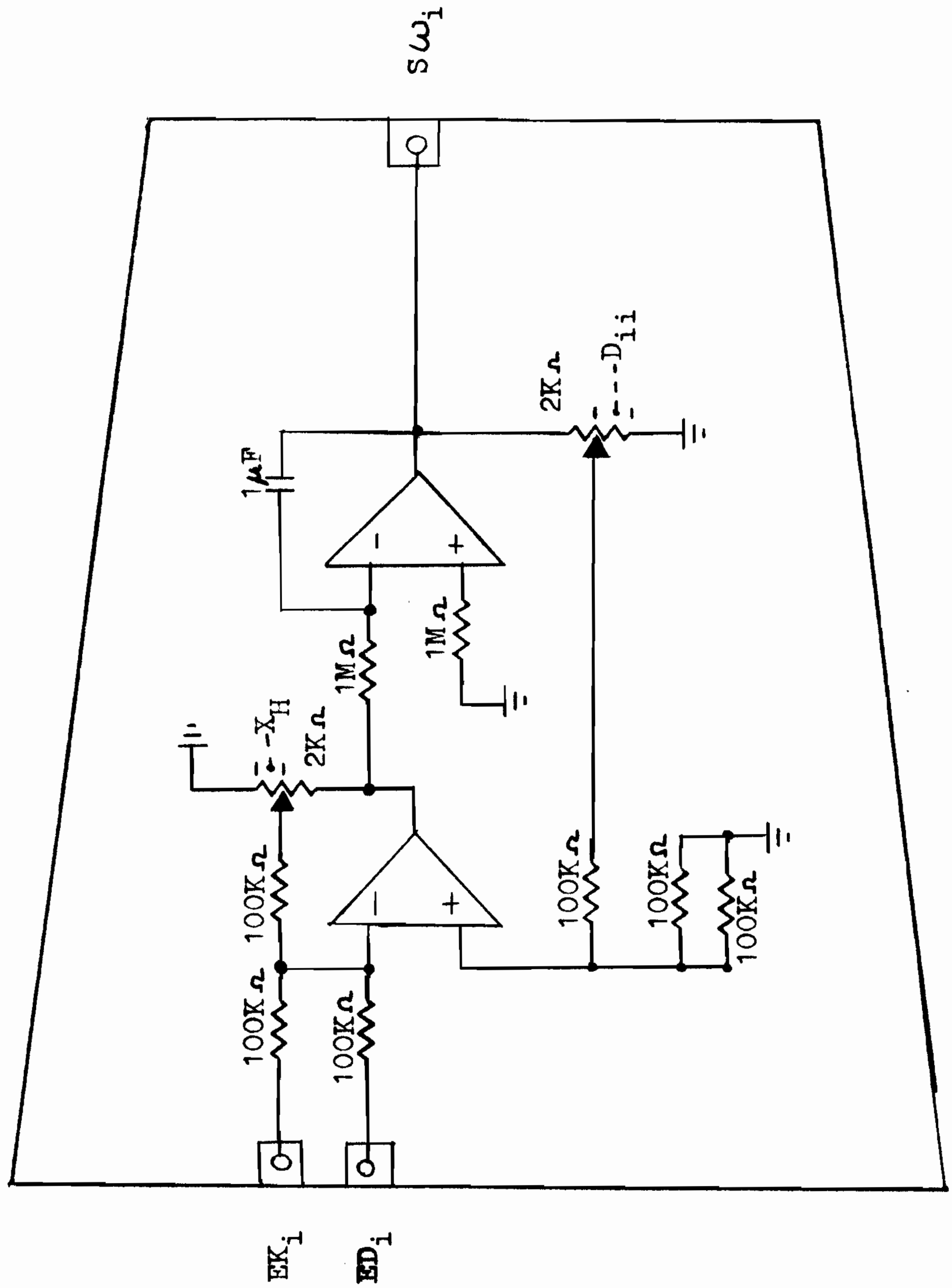

FIG. 3-7 WIRING DIAGRAM FOR THE EXCITER MODULE

3.3.1 Module Parameters

Two potentiometers are provided for the setting of parameter values.

$2H_i = X_H$ p.u. of $2K\Omega$ potentiometer (for $2H_i \leq 1.0$)

D_{ii} = p.u. of $2K\Omega$ potentiometer

These are shown in fig. 3-7.

3.3.2 Module Inputs

The terminals on the left hand side of the diagram of fig. 3-6 are the inputs to the module. These are described, for the i^{th} module, as follows:

Terminal EK_i : "$K_{i,i-1}(\theta_i-\theta_{i-1})$", This is the shaft torque between the i^{th} and the $i^{th}-1$ inertias

Terminal ED_i : "$D_{i,i-1}(\omega_i-\omega_{i-1})$", this is the mutual damping between the i^{th} and the $i^{th}-1$ inertias

3.3.3 Module Outputs

The terminal on the right hand side of the diagram of fig. 3-6 is the output of the module. It is described, for the i^{th} module, as follows:

Terminal $S\omega_i$: "ω_i", this is the angular velocity output of the i^{th} module

3.4 Steam Distribution Module

The steam distribution modules implement the time delays which the steam is subjected to as it passes through the reheaters, the crossover or steam chest piping. The modules also implement the division of the total steam power to the sections of the turbine. The equation describing the dynamics of this module is :

$$T_i SP_i = - P_i + (1-G_i)P_{i-1} \tag{3-4}$$

Fig. 3-9 shows the realization of equation 3-4. The two terms in equation 3-4 are defined as following:

T_i : time constant of the i^{th} power distribution module

P_i : power output of the i^{th} power distribution module

3.4.1 Module Parameters

Two potentiometers are provided for the setting of the parameter values.

$T_i = 1/10X_T$, where X_T is in p.u. of the 2KΩ potentiometer

$G_i = X_G$ p.u. of the 2KΩ potentiometer

These are shown in fig. 3-9.

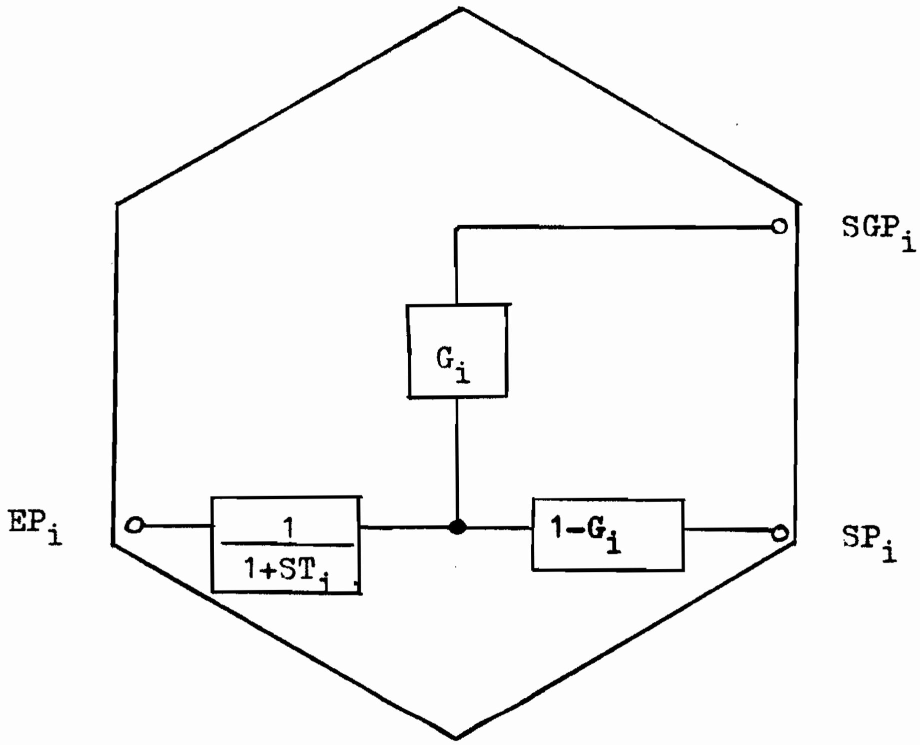

FIG. 3-8 MIMIC DIAGRAM FOR A STEAM POWER DISTRIBUTION MODULE

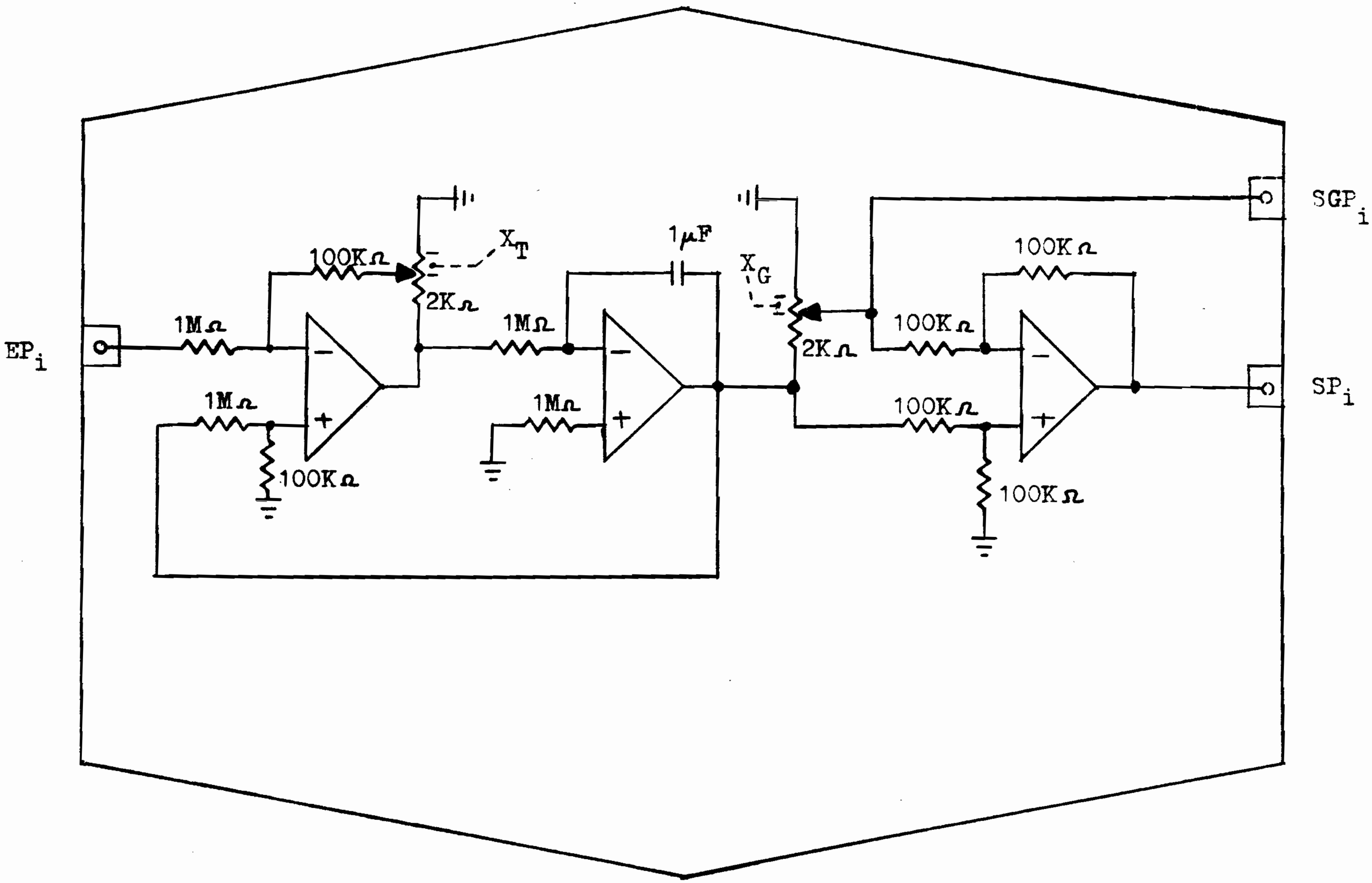

FIG. 3-9 WIRING DIAGRAM FOR A STEAM DISTRIBUTION MODULE

3.4.2 Module Inputs

The terminal on the left hand side of the diagram of fig. 3-8 is the input to the module. It is described, for the i^{th} module, as following:

Terminal EP_i : "$(1-G_{i-1})P_{i-1}$", this is the steam power received from the $i^{th}-1$ steam distribution module

3.4.3 Module Outputs

The terminals on the right hand side of the diagram of fig. 3-8 are the outputs of the module. These are described, for the i^{th} module, as following:

Terminal SGP_i : "G_iP_i", this is the amount of steam power delivered to the i^{th} turbine section

Terminal SP_i : "$(1-G_i)P_i$", this is the amount of steam power passed to the $i^{th}+1$ steam distribution module

3.4.4 Steam Distribution Power Fractioning Unit

The steam power can be further distributed with the use of a power distribution unit. This unit was introduced in section 2.3.2 . The electronic implementation is shown in fig. 3-11. The input G_iP_i is the total power derived from the reheater unit. Then, this power is fractioned to the two turbine sections as follows:

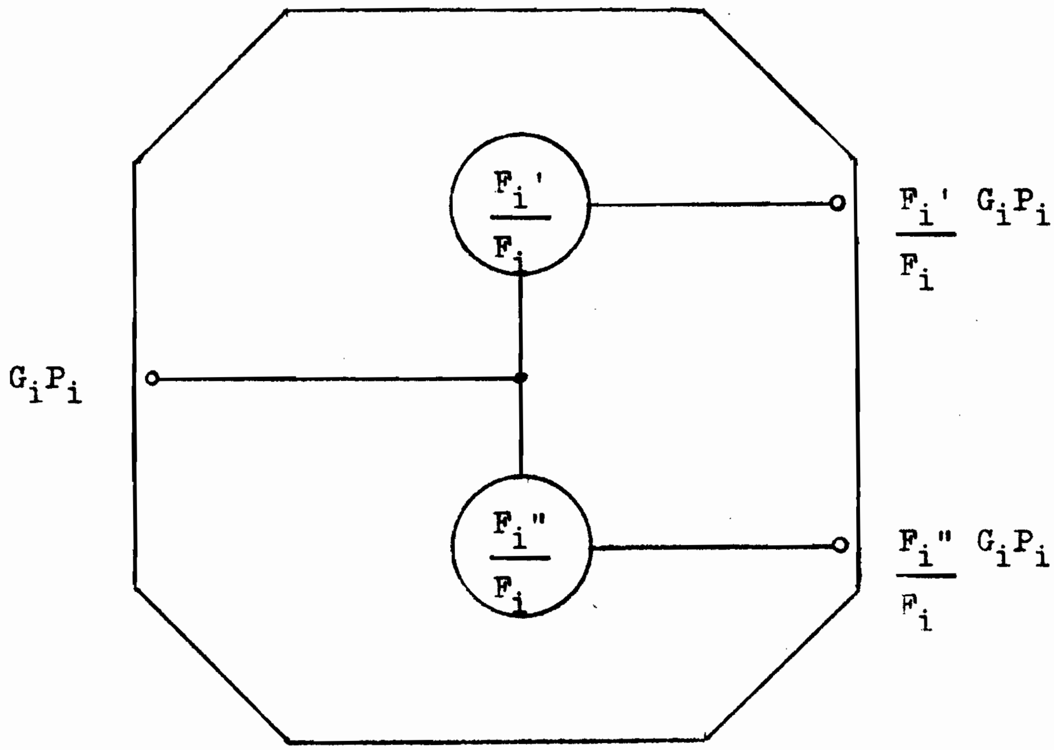

FIG. 3-10 MIMIC DIAGRAM FOR THE FRACTIONING MODULE

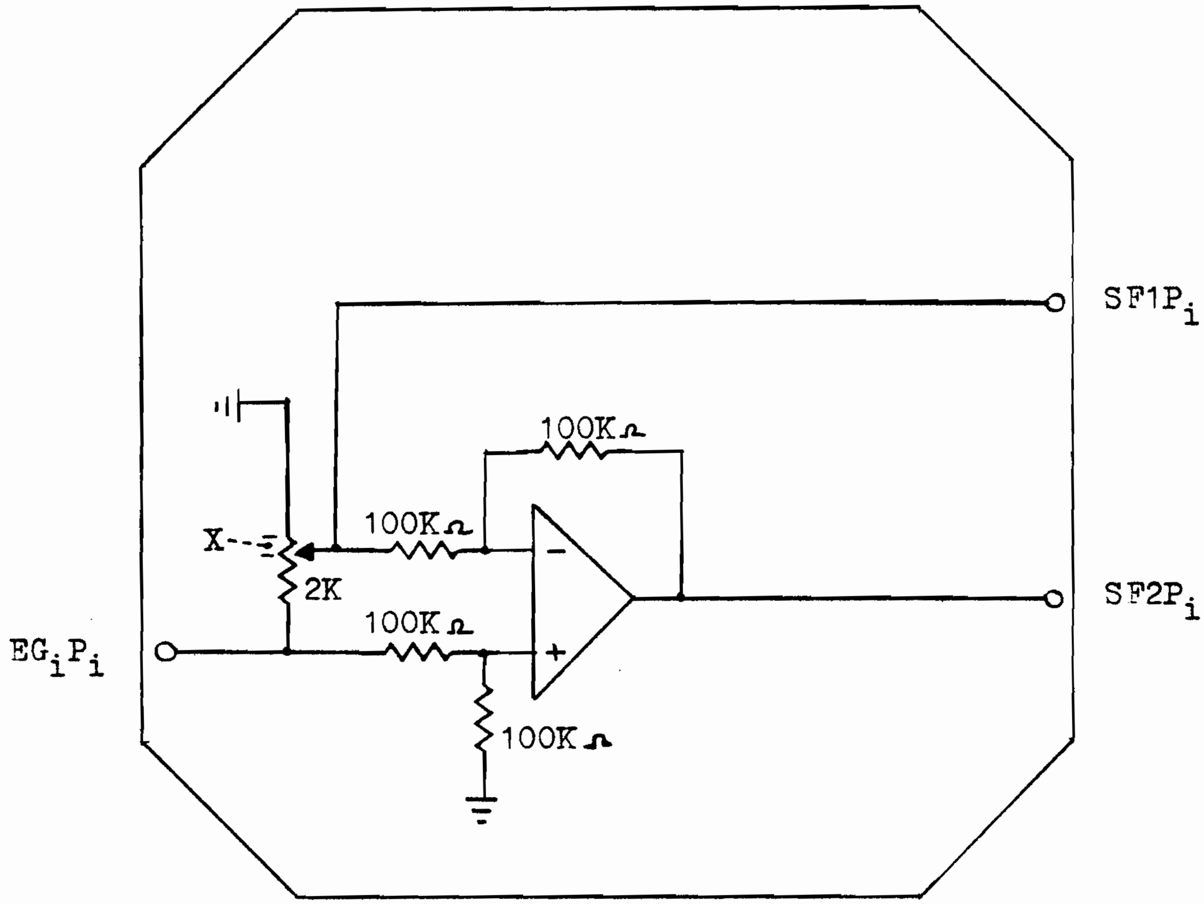

FIG. 3-11 WIRING DIAGRAM FOR THE FRACTIONING MODULE

$(F_i'/F_i)G_iP_i = XG_iP_i$ (at terminal $SF1P_i$)

$(F_i''/F_i)G_iP_i = (1-X)G_iP_i$ (at terminal $SF2P_i$)

Where X is in p.u. of the $2K\Omega$ potentiometer.

3.5 Speed-Governor Module

The general model for the speed governing system of steam turbines was developed in section 2-5. From this model, the following three equations were derived:

$$T_1 S\,\omega_{IS} = \omega_G - \omega_o - \omega_{IS} \qquad (3\text{-}5)$$

$$P_{IS} = KT_2(\omega_G - \omega_o)/T_1 + K(1-T_2/T_1)\omega_{IS} \qquad (3\text{-}6)$$

$$T_3 S P_{GV} = P_o - P_{IS} - P_{GV} \qquad (3\text{-}7)$$

The realization of equations 3-5 and 3-6 is shown in fig. 3-13. The realization of equation 3-7 is shown in fig. 3-14. The implementation of the model for the speed-governor is acheived by interconnecting the two modules shown in fig. 3-13 and fig. 3-14, as indicated in fig. 3-12. This approach to implementing the governor equations was selected so that more complex transfer functions could be easily implemented. Fig. 3-14 is a typical circuit configuration to implement the saturation functions of the speed-governor. The choice of resistances, R_1 to R_8, is to be determined experimentally.

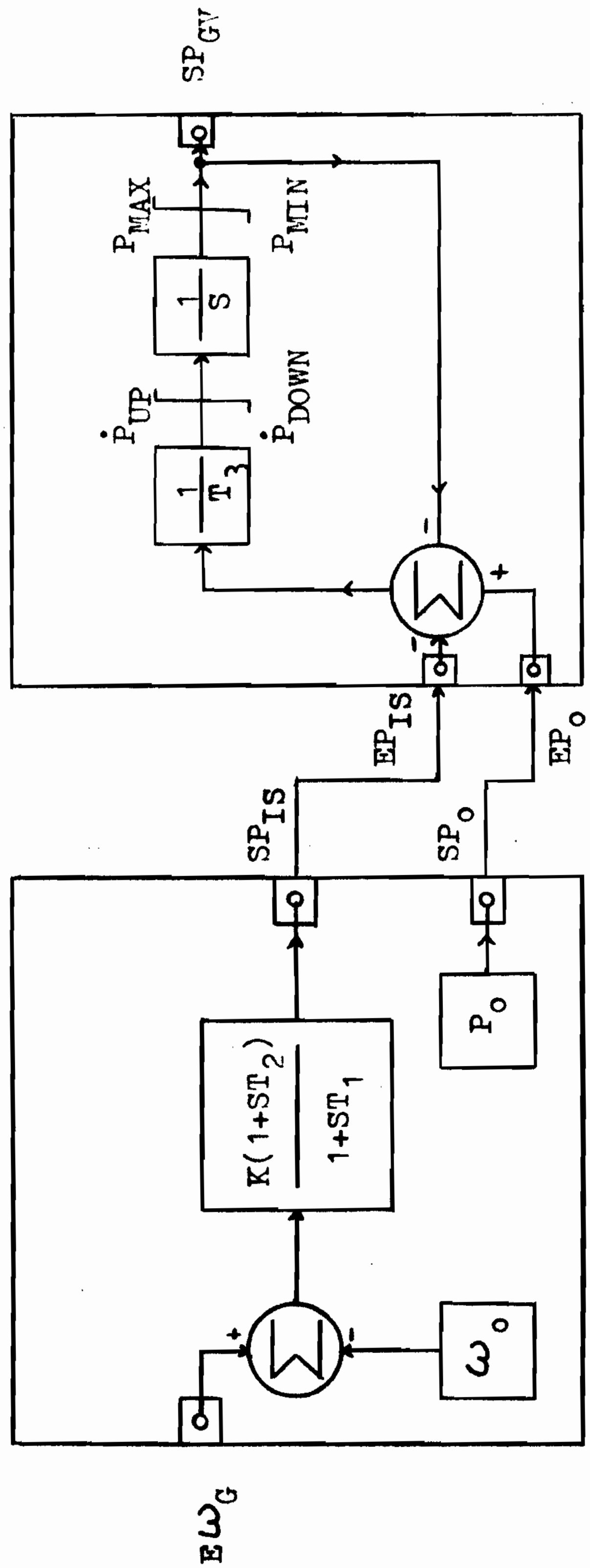

FIG. 3-12 MIMIC DIAGRAM FOR THE SPEED-GOVERNOR MODULE

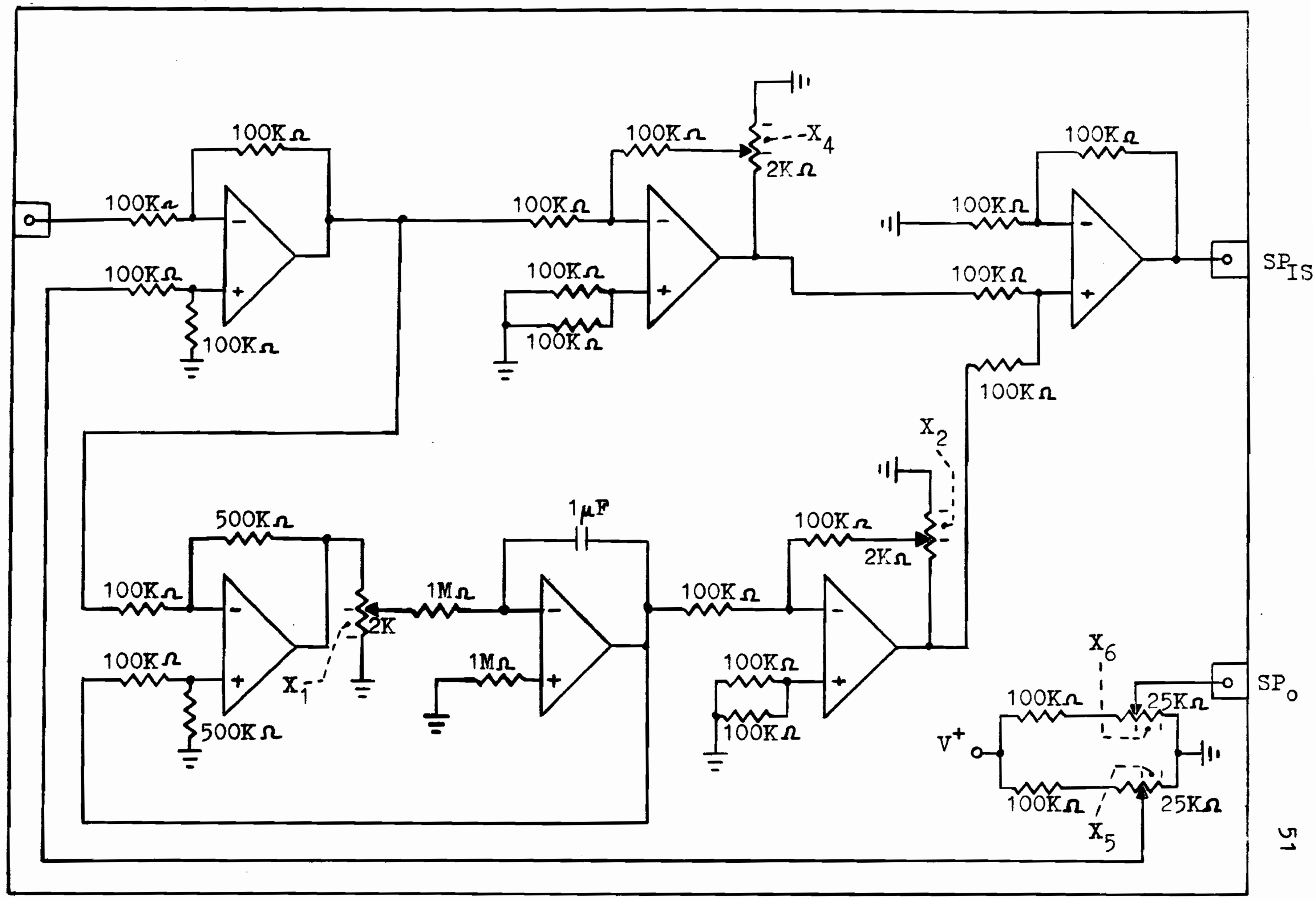

FIG. 3-13 WIRING DIAGRAM FOR THE SPEED-GOVERNOR MODULE (1)

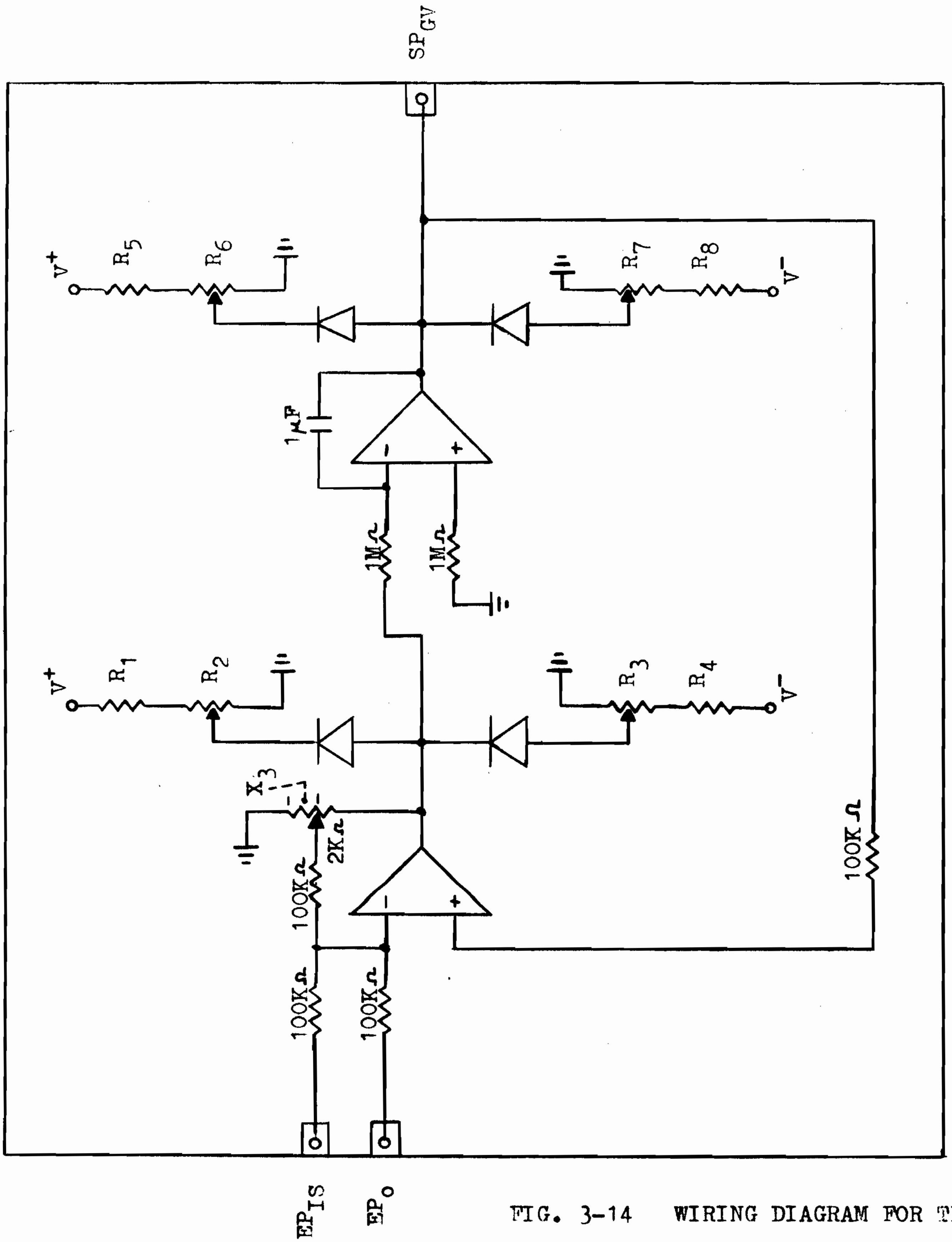

FIG. 3-14 WIRING DIAGRAM FOR THE SPEED-GOVERNOR MODULE (2

3.5.1 Module Parameters

Four potentiometers are provided for the setting of parameter values.

$T_1 = 5/X_1$, where X_1 is in p.u. of 2KΩ potentiometer

$KT_2/T_1 = 1/X_2$, where X_2 is in p.u. of 2KΩ potentiometer

$K(1-T_2/T_1) = 1/X_4$, where X_4 is in p.u. of 2KΩ potentiometer

These are shown in fig. 3-13.

$T_3 = 1/X_3$, where X_3 is in p.u. of 2KΩ potentiometer

This is shown in fig. 3-14.

3.5.2 Module Inputs

The terminals on the left hand side of the diagram of fig. 3-12 are the inputs to the module. As mentionned previously, this module was built in two sections. These inputs are described as follows:

Terminal $E\omega_G$: "ω_G", this is the angular velocity of the generator

Terminal EP_{IS} : "P_{IS}", this is a state variable introduced in section 2.5

Terminal EP_o : "P_o", this is the reference power

3.5.3 Module Outputs

The terminals on the right hand side of the diagram of fig. 3-12 are the outputs of the module. These are described as follows:

Terminal SP_{IS}: "P_{IS}", this is a state variable introduced in section 2.5 . Its output is the input signal to the EP_{IS} terminal

Terminal SP_{GV}: "P_{GV}", this is the steam power to the turbines

3.5.4 Control Setting

1) Reference Angular Velocity, ω_o

The variable resistance X_5 in the fig. 3-13 provides the adjustment of the reference angular velocity. The output of one volt corresponds to one per unit angular velocity.

2) Reference Power, P_o

The variable resistance X_6 in the fig. 3-13 provides the adjustment of the power setting. The signal is outputted through terminal SP_o. A per unit power demand is signalled by a one volt setting. Usually, the terminal SPO is linked to EP_o.

3.6 Steam System Configurations

The electronic system is composed of a number of modules described in sections 3-2 to 3-5. The electronic modules "plug-in" sytem provides the user with flexibility for the representation of different possible steam system configurations. Some of the possible steam system configurations, that can be represented, are illustrated in fig. 3-15 [14]. These are the most commonly encountered system configurations. For the purpose of illustrating how these configurations are implemented, examples of actual interconnection of modules are given in fig. 3-16 and in fig. 3-17. A two-shaft system interconnection is shown in fig. 3-18.

3-7 Fast-Valving Simulation, Boiler Dynamics Representation and Governor Dead Band

This thesis has not treated the subjects of fast-valving, boiler dynamics, and governor dead band. But provisions for their inclusions in future development of the simulation hardware have been considered.

Addition of Fast-Valving

In order to increase power system stability, especially during transients, fast valving is an option that is receiving serious considerations [37-44]. In this study, fast valving has not been implemented. A convenient way of implementing fast valving is through the output stage of a reheater unit using a multiplier and a waveform generator unit. Fig. 3-19 reproduces the reheater module except that the multiplier is inserted before the power division to $G_i P_i$ and $(1-G_i)P_i$.

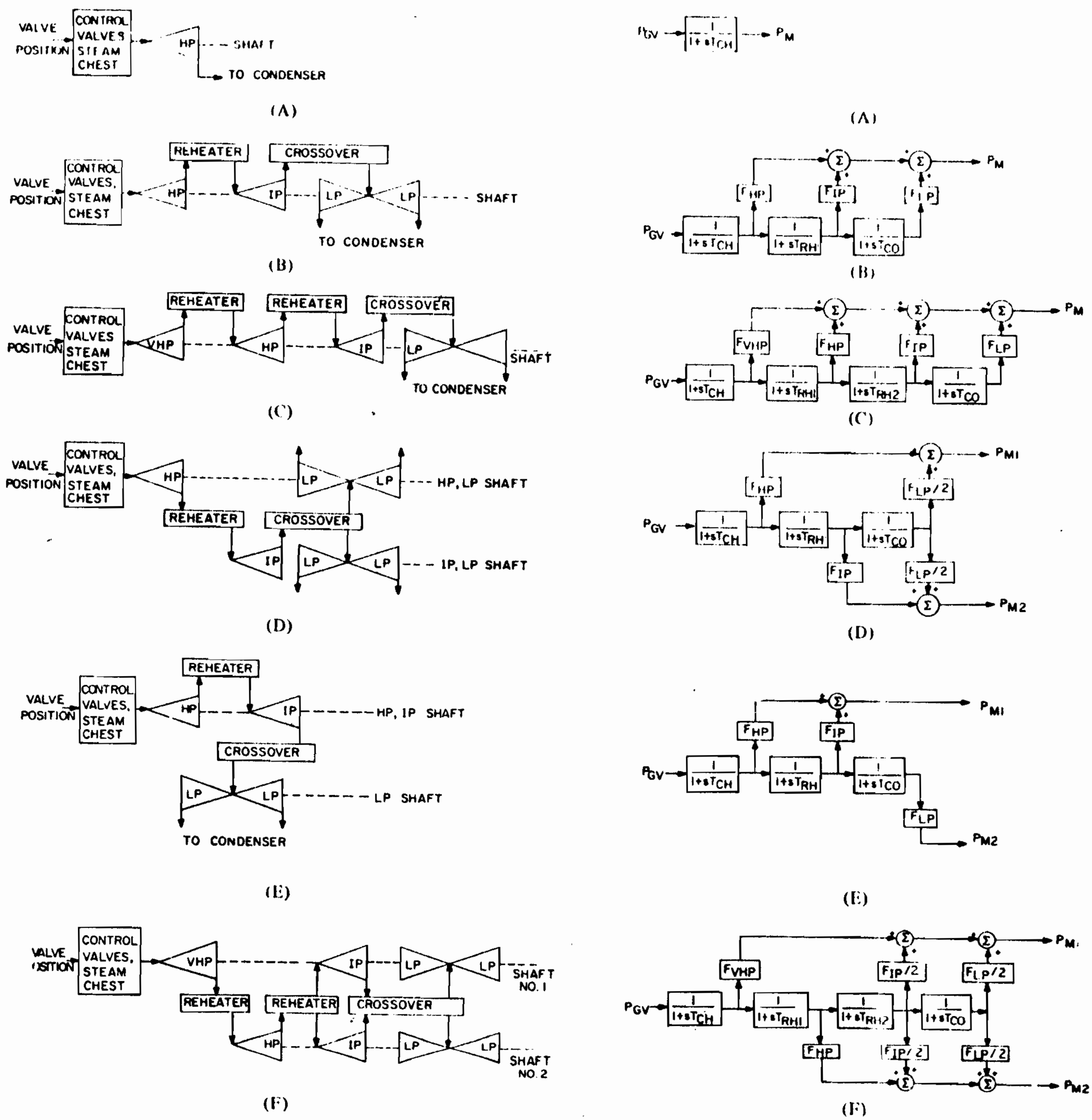

Common Steam System Configurations *Approximate Linear Models*

A) Nonreheat
B) Tandem Compound, Single Reheat
C) Tandem Compound, Double Reheat
D) Cross Compound, Single Reheat
E) Cross Compound, Single Reheat
F) Cross Compound, Double Reheat

FIG. 3-15 DIAGRAM REPRODUCED FROM IEEE COMMITTEE REPORT [14], FIG. 6 AND FIG. 7

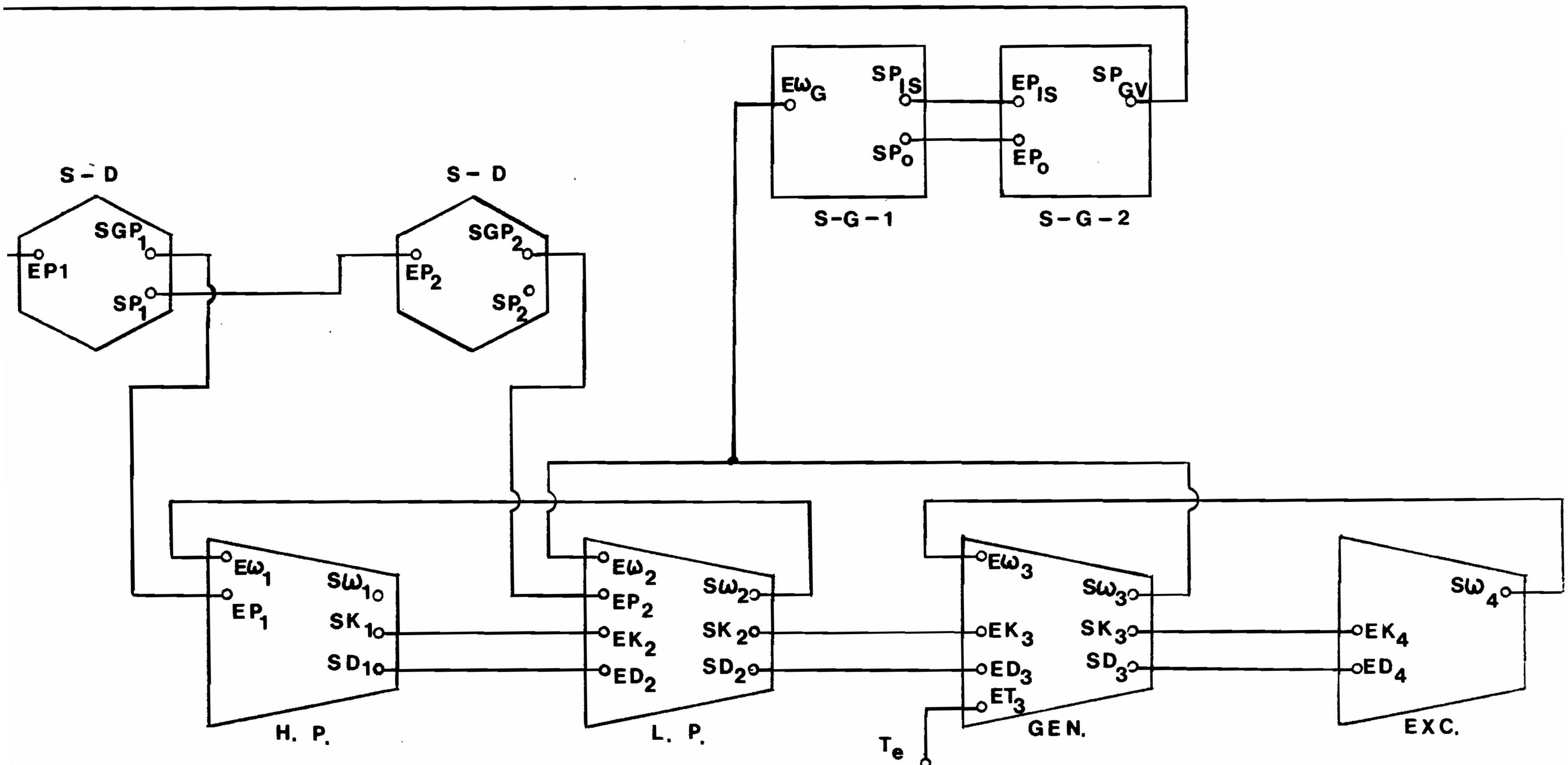

FIG. 3-16 BLOCK DIAGRAM FOR A ONE-SHAFT SYSTEM CONFIGURATION

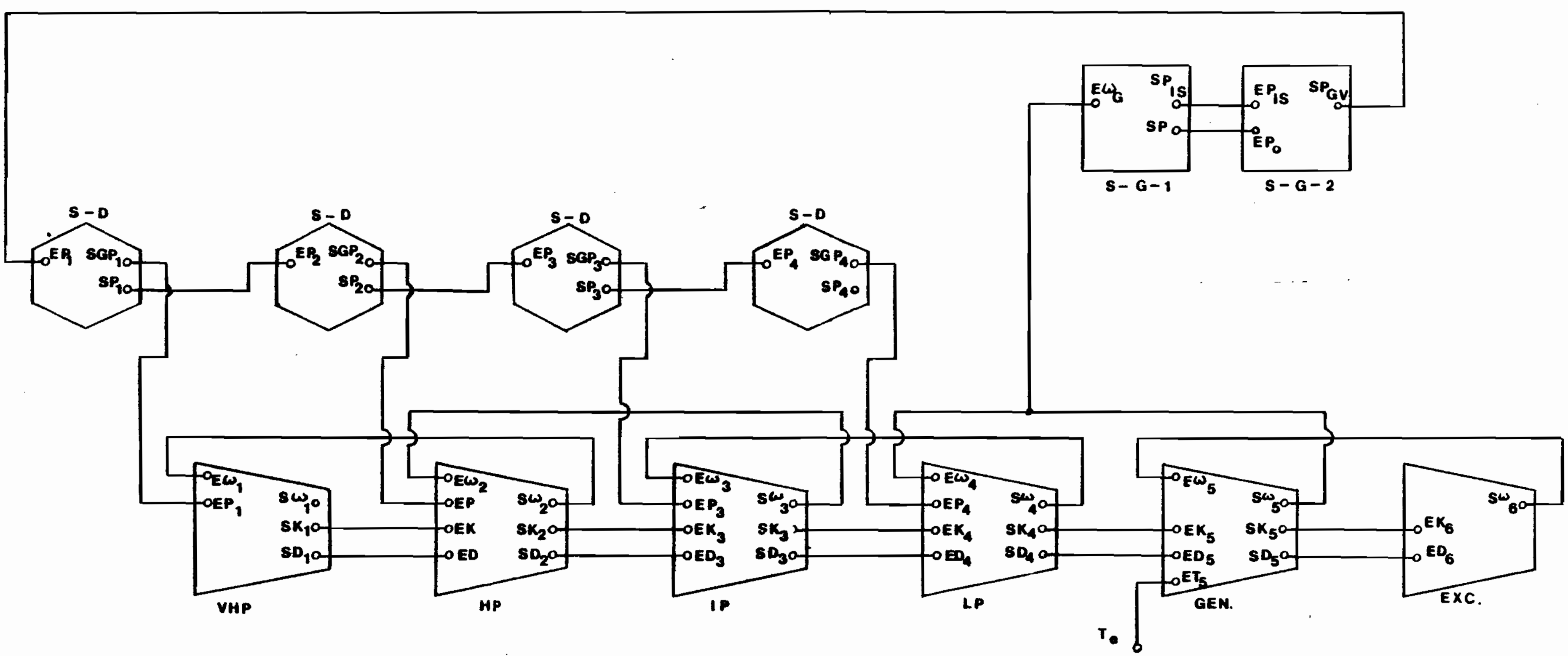

FIG. 3-17 BLOCK DIAGRAM FOR A FOUR TURBINE SECTION ONE-SHAFT SYSTEM CONFIGURATION

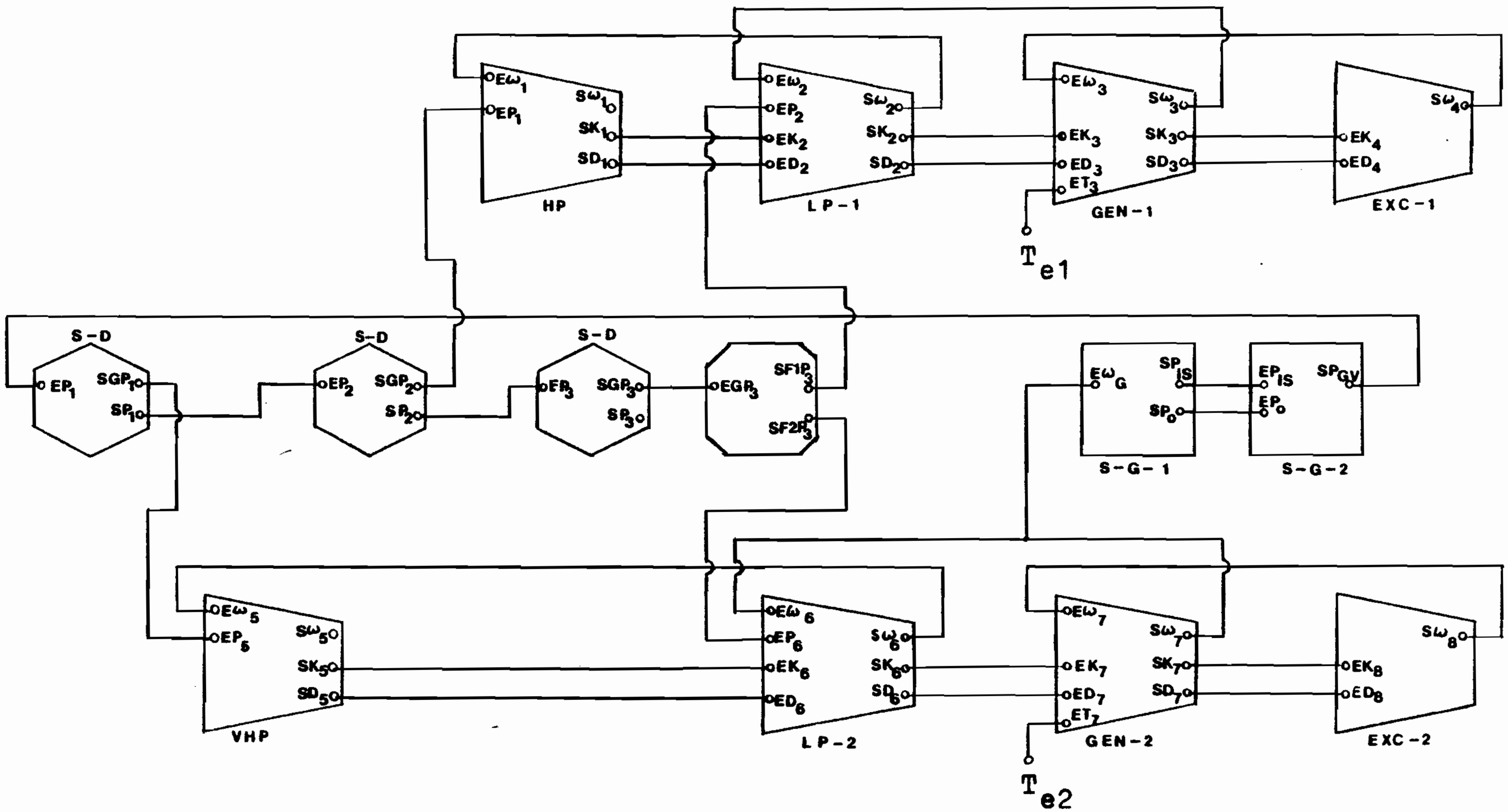

FIG. 3-18 BLOCK DIAGRAM FOR A TWO-SHAFT SYSTEM CONFIGURATION

The terminal FV is connected to a waveform generator. The waveform generator is triggered at the simulating instant when the fast valving is actuated. The waveform Y and the time delays should be such that on multiplying with the output X, the product Z=XY should approximate the test results such as shown in fig. 3-20 [39].

Addition of Boiler Dynamics

The boiler dynamics representation is considered to be beyond the scope of this thesis. Its inclusion is necessary only when the transients have durations much longer than the time constants of the reheaters (lasting tens of seconds). Some studies of boiler representation have been reported in references [45-48].

In the event that a model for the dynamics of a boiler be built, the point of integration with the work of this thesis lies in the governor valve. The governor valve controls the opening of the steam output of the boiler system. Assuming that the power outputted is linearly proportional to the valve opening, a multiplier may be used to combine the governor output and the boiler output signals.

In the existing governor model, the valve opening variable C_V is used indistinguishably as the power output P_{GV}. Of course, this amounts to saying that the boiler ouput is regulated at 1.0 p.u. always.

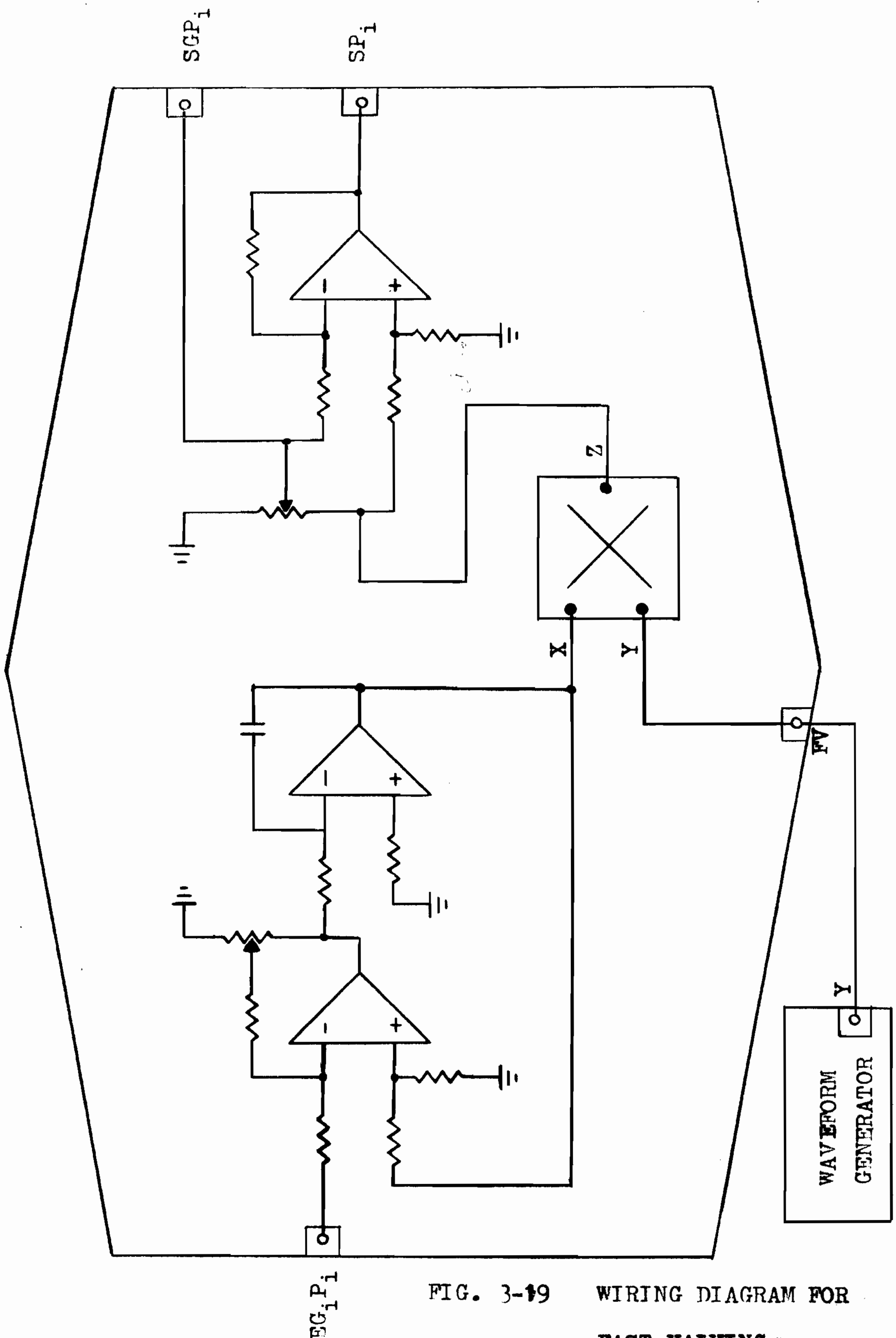

FIG. 3-19 WIRING DIAGRAM FOR FAST VALVING

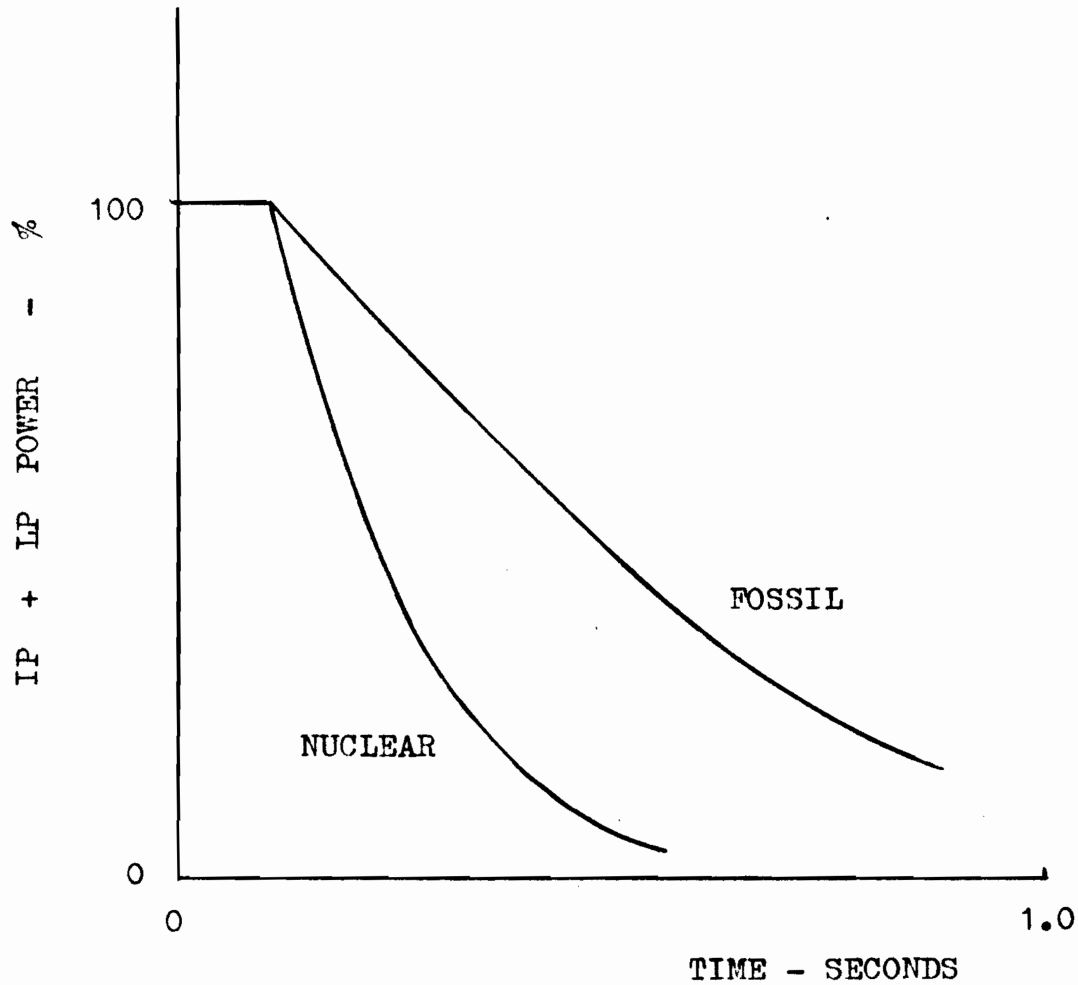

FIG. 3-20 TYPICAL TURBINE POWER DECAY CURVES

Governor Dead Band

Governor dead band has not been included in any of these modules, since it is not normally necessary for large system studies. It may be necessary to represent it when the performance of speed governor itself is of interest [14].

CHAPTER 4

PERFORMANCE OF MODULES

INTRODUCTION

Linear system behaviour can be characterized either in the real-time or in the frequency-domain. These two domains are essentially equivalent. One easily moves from the time domain to the frequency domain by way of the Fourier Transform.

In the time domain testing, one uses standard excitation input waveforms, such as the impulse or the step. One records the output response in an oscilloscope or a chart recorder.

The test which are performed on the modules and the integrated system of modules, are based on the frequency domain. The results are presented in the form of Bode diagrams showing the magnitude of the gain and the phase angle as functions of the frequency. Conceptually at least, one should be able to assess the time domain response based on the inverse Fourier transform of these results.

To ensure that the linear theory applies, the following modifications have been performed on each module during the tests;

1) The dividers in each of the inertia modules have been by-passed. The divider is a non-linear element.

2) In the governor module, the saturation limits again represent non-linear functions. In the performance of these tests, the input signal level have been chosen so that the saturation never occurs.

With these two provisions taken care of, so as to ensure system linearity, the test in the frequency-domain remain valid.

For the data in the frequency domain to be equivalent to those in the time domain, the Bode diagrams should range from 0 Hertz to infinity. In practice, the transfer function of the modules is band limited. As such, it was found that the frequency range of the output extends from 20 to 60 Hertzs. The attenuation outside this band becomes so severe that the ouput signal is indistinguisable from noise.

A prototype of the system presented in the previous chapter was built to determine at which level of accuracy it could be implemented. The results for the testing of this prototype are presented in the remainder of this chapter.

4.1 Performance Criteria

The acceptability of the module is based on the close agreement between the measured Bode diagrams and the predictions based on transfer functions. In the first instance, individual modules are tested separately and have been found to be acceptable. Then, the modules have been combined in integrated systems and again theory and measurement have been found to be close. As an external check, the torsional resonant system of Schmus [23] was simulated by modules and again the results justify a high confidence level for the modules developed in this thesis.

4.2 Module Testing and Results

Each modules were tested to ensure that their frequency response was as predicted. First, the frequency response is obtained mathematically, then these are compared to the test results through graphs. Finally, the evaluation of the results is made for each module.

Test results are given for the different modules in the following order:

1) Inertia-Shaft Modules-Turbine Section
2) Inertia-Shaft Modules-Generator Section
3) Exciter Modules
4) Steam Distribution Modules
5) Speed-Governor Module

Then finally, range tests were performed on the inertia module. The parameters varied were $2H_i$ and $K_{i,i+1}$. These were tested for specific values, and it was found that the module performed as theoretically predicted.

4.2.1 Test results for the inertia module: Turbine sections

Mathematically, the transfer function determining the frequency response for these modules is obtained as following:

$$\begin{aligned} 2H_i S\omega_i = {} & G_iP_i - D_{i-1,i}(\omega_i - \omega_{i-1}) - D_{i,i+1}(\omega_i - \omega_{i+1}) \\ & - D_{ii}\omega_i - K_{i-1,i}(\theta_i - \theta_{i-1}) \\ & - K_{i,i+1}(\theta_i - \theta_{i+1}) \end{aligned} \tag{4-1}$$

With all inputs grounded, except P_i, the equation 4-1 becomes:

$$2H_iS^2\theta_i = G_iP_i - D_{i,i+1}S\theta_i - D_{ii}S\theta_i - K_{i,i+1}\theta_i \tag{4-2}$$

$$2H_iS^2\theta_i + (D_{i,i+1} + D_{ii})S\theta_i + K_{i,i+1}\theta_i = G_iP_i \tag{4-3}$$

Therefore the transfer function relating the angular displacement of each section of the turbine to the input power is as follows:

$$\frac{\theta_i}{G_iP_i} = \frac{1}{2H_iS^2 + (D_{i,i+1} + D_{ii})S + K_{i,i+1}} \tag{4-4}$$

From this transfer function, the magnitude of the frequency response is calculated, using the following

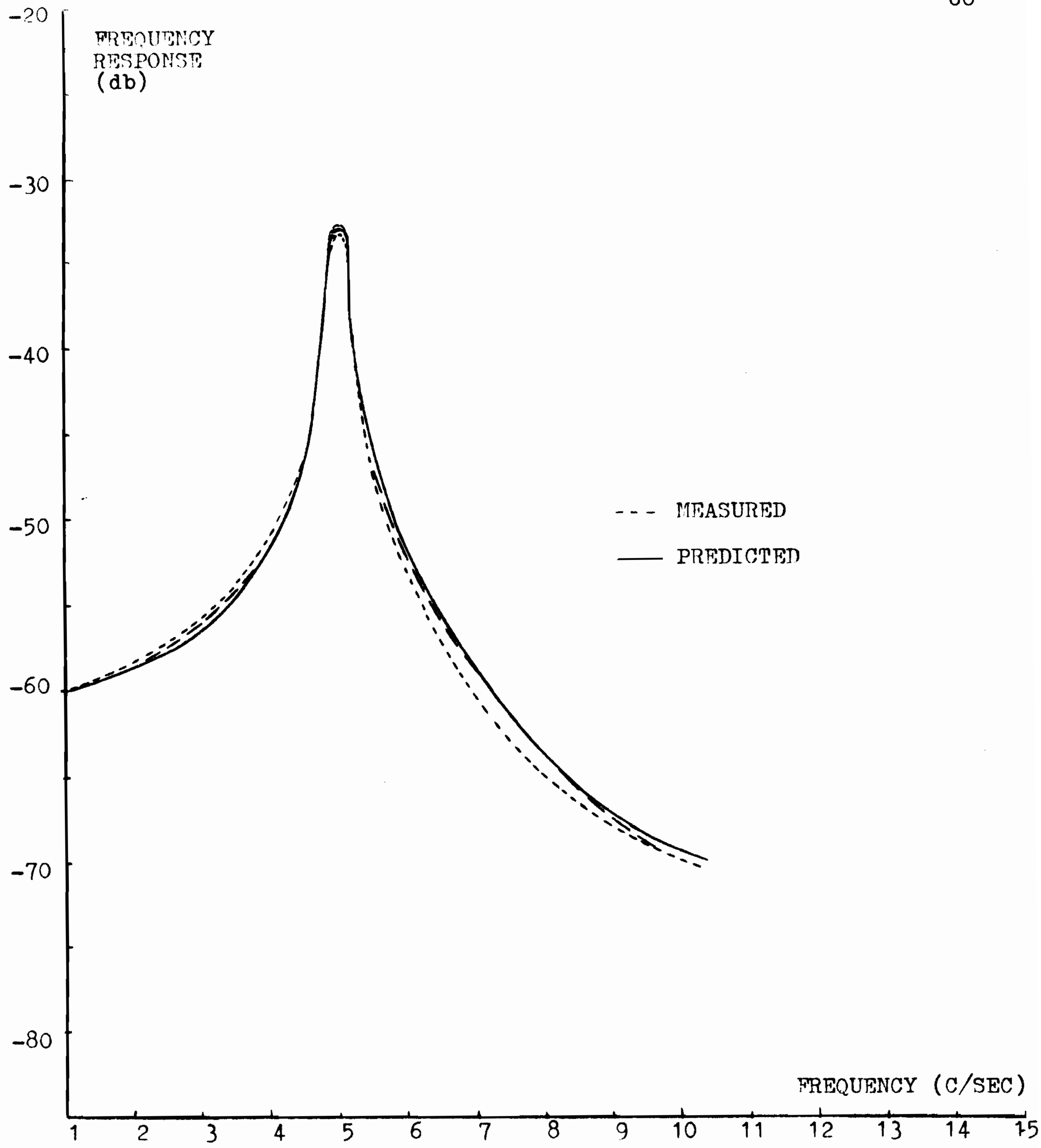

FIG. 4-1 MAGNITUDE OF THE FREQUENCY RESPONSE OF THE INERTIA MODULES: TURBINE SECTIONS

parameter constants:

$D_{ii} = 1.0$ p.u. (4-5) $\qquad K_{i,i+1} = 1000$ p.u. (4-7)

$D_{i,i+1} = 0.5$ p.u. (4-6) $\qquad 2H_i = 1.0$ p.u. (4-8)

The calculated frequency response and the test results obtained for these modules are shown in fig. 4-1 .

4.2.2 Test results for the inertia modules: Generator Unit

Mathematically, the transfer function determining the frequency response for the modules is obtained as follows:

$$2H_i S\omega_i = T_e - D_{i-1,i}(\omega_i - \omega_{i-1}) - D_{ii}\omega_i - D_{i,i+1}(\omega_i - \omega_{i+1}) - K_{i-1,i}(\theta_i - \theta_{i-1}) - K_{i,i+1}(\theta_i - \theta_{i+1}) \tag{4-9}$$

With all inputs grounded, except T_e, the equation 4-9 becomes:

$$2H_i S^2\theta_i = -T_e - D_{i,i+1}S\theta_i - K_{i,i+1}\theta_i \tag{4-10}$$

$$2H_i S^2\theta_i + (D_{ii}+D_{i,i+1})S\theta_i + K_{i,i+1}\theta_i = T_e \tag{4-11}$$

Therefore the transfer function relating the angular displacement of each generator to the input torque is as follows:

$$\frac{\theta_i}{T_e} = \frac{1}{2H_i S^2 + (D_{i,i+1} + D_{ii})S + K_{i,i+1}} \tag{4-12}$$

From this transfer function, the magnitude of the frequency response is calculated, using the following parameter constants:

$D_{ii} = 1.0$ p.u. (4-13) $\qquad 2H_i = 1.0$ p.u. (4-15)

$D_{i,i+1} = 0.5$ p.u. (4-14) $\qquad K_{i,i+1} = 1000$ p.u. (4-16)

The calculated frequency response and the test results obtained for these modules are shown in fig. 4-2.

4.2.3 Test results for the inertia modules: exciter unit

Mathematically, the transfer function determining the frequency response for the circuit of the modules is obtained as follows:

$$2H_i S\omega_i = -D_{i,i-1}(\omega_i-\omega_{i-1}) - D_{ii}\omega_i - K_{i,i-1}(\theta_i-\theta_{i-1}) \qquad (4\text{-}17)$$

$$2H_i S\omega_i + D_{ii}\omega_i = -D_{i,i-1}(\omega_i-\omega_{i-1}) - K_{i,i-1}(\theta_i-\theta_{i-1}) \qquad (4\text{-}18)$$

With the $K_{i,i-1}(\theta_i-\theta_{i-1})$ input on the right hand side of the equation 4-18 being grounded, the equation becomes:

$$2H_i S\omega_i + D_{ii}\omega_i = -D_{i,i-1}(\omega_i-\omega_{i-1}) \qquad (4\text{-}19)$$

Therefore the transfer function relating the angular velocity of each exciter to either of the inputs are as follows:

$$\frac{\omega_i}{D_{i,i-1}(\omega_i-\omega_{i-1})} = \frac{-1}{2H_i S + D_{ii}} \qquad (4\text{-}20)$$

From the transfer functions, the magnitude of the frequency response is calculated, using the following

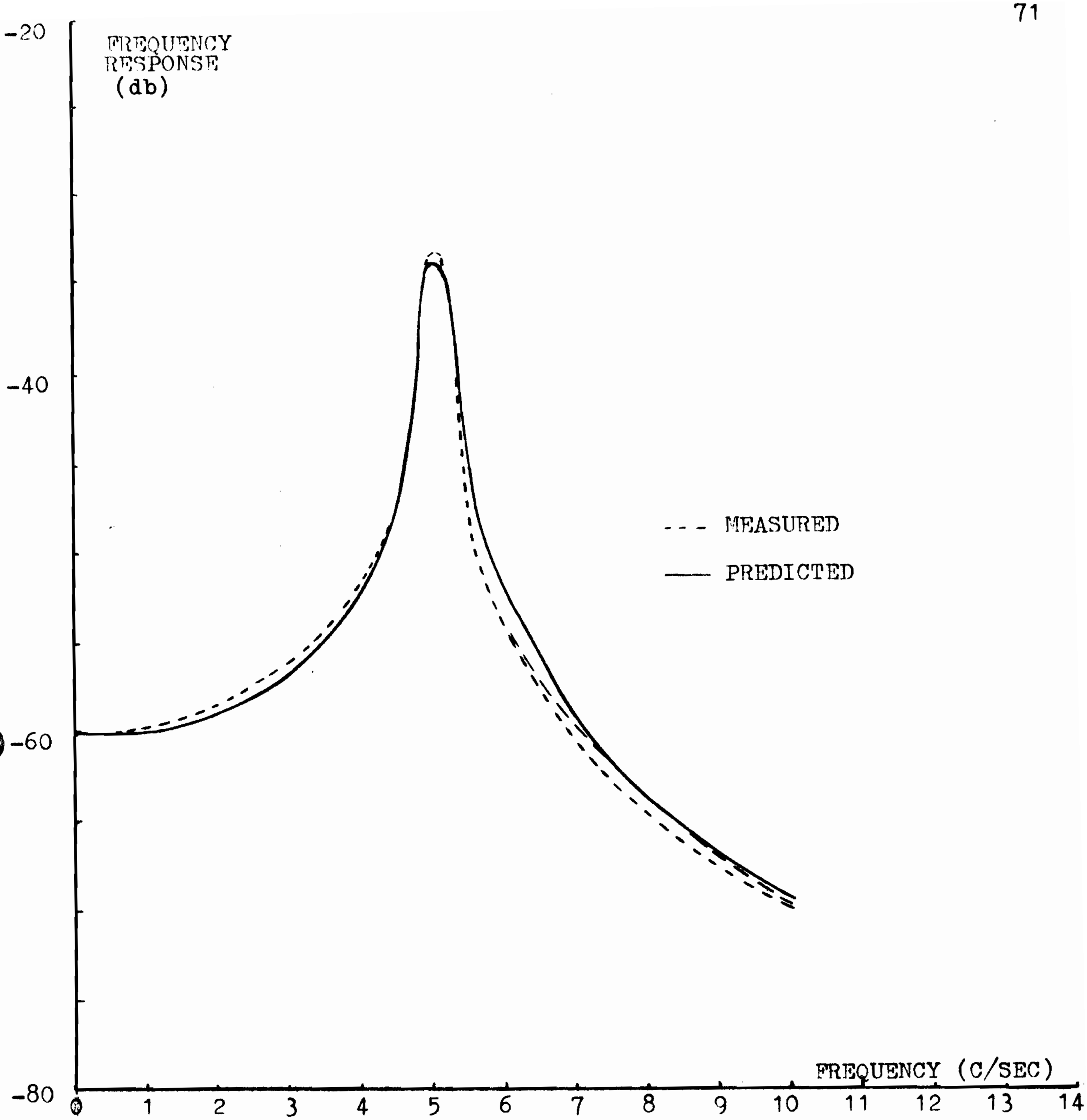

FIG. 4-2 MAGNITUDE OF THE FREQUENCY RESPONSE OF THE INERTIA MODULES: GENERATOR UNITS

parameter constants: $D_{ii} = 1.0$ p.u. and $2H_i = 1.0$ p.u. The frequency response and the test results obtained for these modules are shown in fig. 4-3.

4.2.4 Test results for the steam distribution modules

Mathematically, the transfer function determining the frequency response for these modules is obtained as following:

$$T_i S P_i = -P_i + F_{i-1} P_{i-1} \tag{4-21}$$

$$T_i S P_i + P_i = F_{i-1} P_{i-1} \tag{4-22}$$

Therefore the transfer equation relating the output power of a steam distribution unit to its input power is as follows:

$$\frac{P_i}{F_{i-1} P_{i-1}} = \frac{1}{1+ S T_i} \tag{4-23}$$

From this transfer function, the magnitude of the frequency response is calculated, using the following parameter constant: $T_i = 1.0$ p.u.

The frequency response and the test results obtained for these modules are shown in fig. 4-4.

4.2.5 Test results for the speed-governor module.

The speed-governor unit consist of two modules Therefore, the mathematical transfer functions determining the frequency response for these modules are obtained as follows:

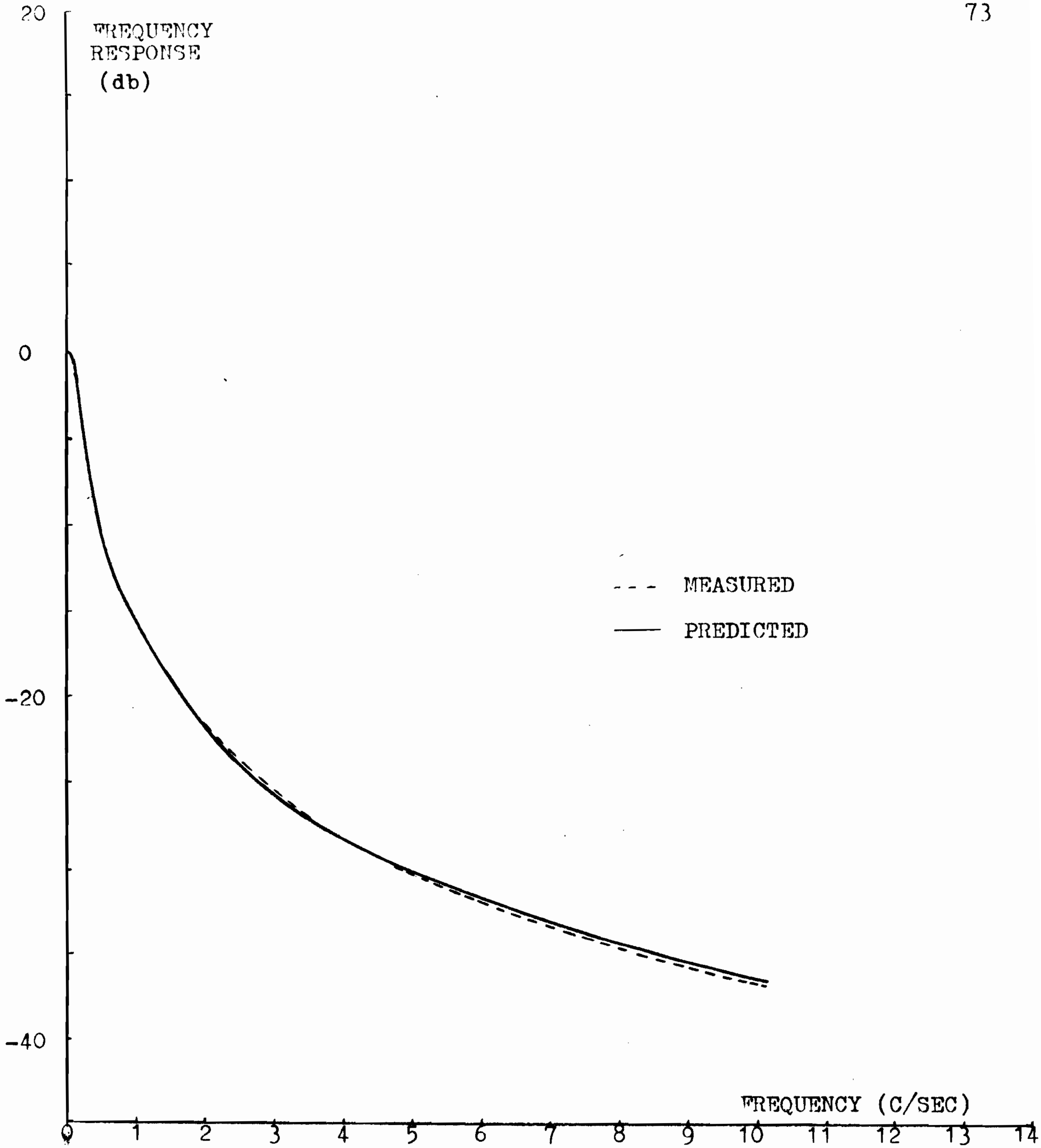

FIG. 4-3 MAGNITUDE OF THE FREQUENCY RESPONSE OF THE EXCITER MODULES

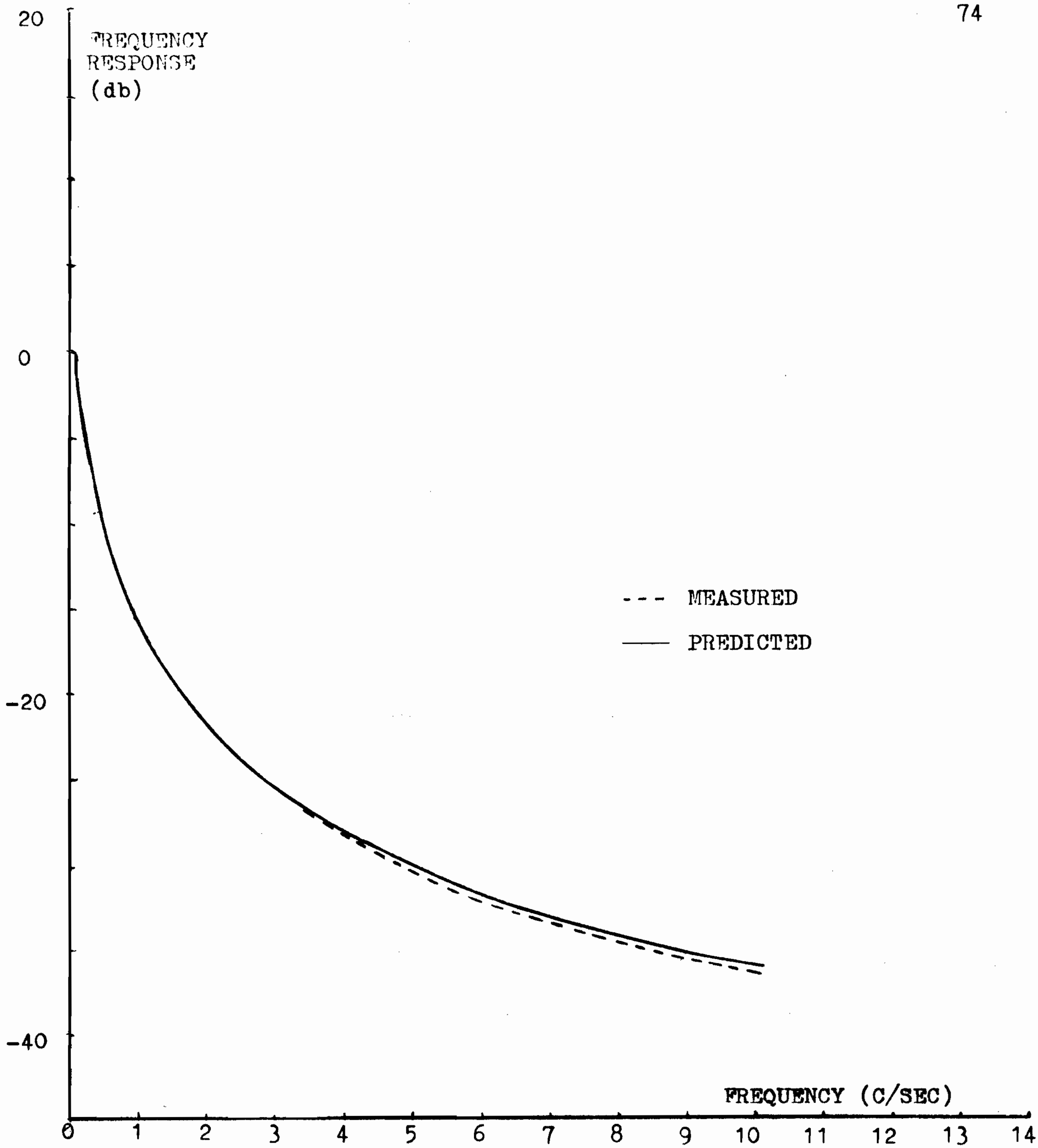

FIG. 4-4 MAGNITUDE OF THE FREQUENCY RESPONSE OF THE STEAM DISTRIBUTION MODULES

1) first module implements

$$P_{IS} = [\ KT2/T1 + K(1-T2/T1)/(1+ST1)]\times(\omega_G - \omega_o) \qquad (4\text{-}24)$$

2) Second module implements:

$$(1+ST3)\ P_{GV} = P_o - P_{IS} \qquad (4\text{-}25)$$

With inputs ω_o and P_o grounded in the respective equations, the equations 4-24 and 4-25 become:

$$P_{IS} = \omega_G\ [KT2/T1 + K(1-T2/T1)/(1+ST1)] \qquad (4\text{-}26)$$

$$P_{GV} = -P_{IS}/\ (1+ST3) \qquad (4\text{-}27)$$

Therefore the transfer functions relating the output variables (ie. P_{IS}, P_{GV}) to the input (ie. ω_G, P_{IS} respectively; in 4-29, the KT2/T1 term from eq. 4-27 has been neglected) are:

$$\frac{P_{IS}}{\omega_G} = \frac{K(1-T2/T1)}{1 + ST1} \qquad (4\text{-}28)$$

$$\frac{P_{GV}}{P_{IS}} = \frac{1}{1 + ST3} \qquad (4\text{-}29)$$

From these transfer function, the magnitude of the frequency response is calculated, using the following parameter: T1 = 5 p.u., T3 = 1 p.u. KT2/T1 = 1.0 p.u. The frequency response and the test results obtained for the transfer functions of equations 4-28 and 4-29 are shown in fig. 4-5 and 4-6, respectively.

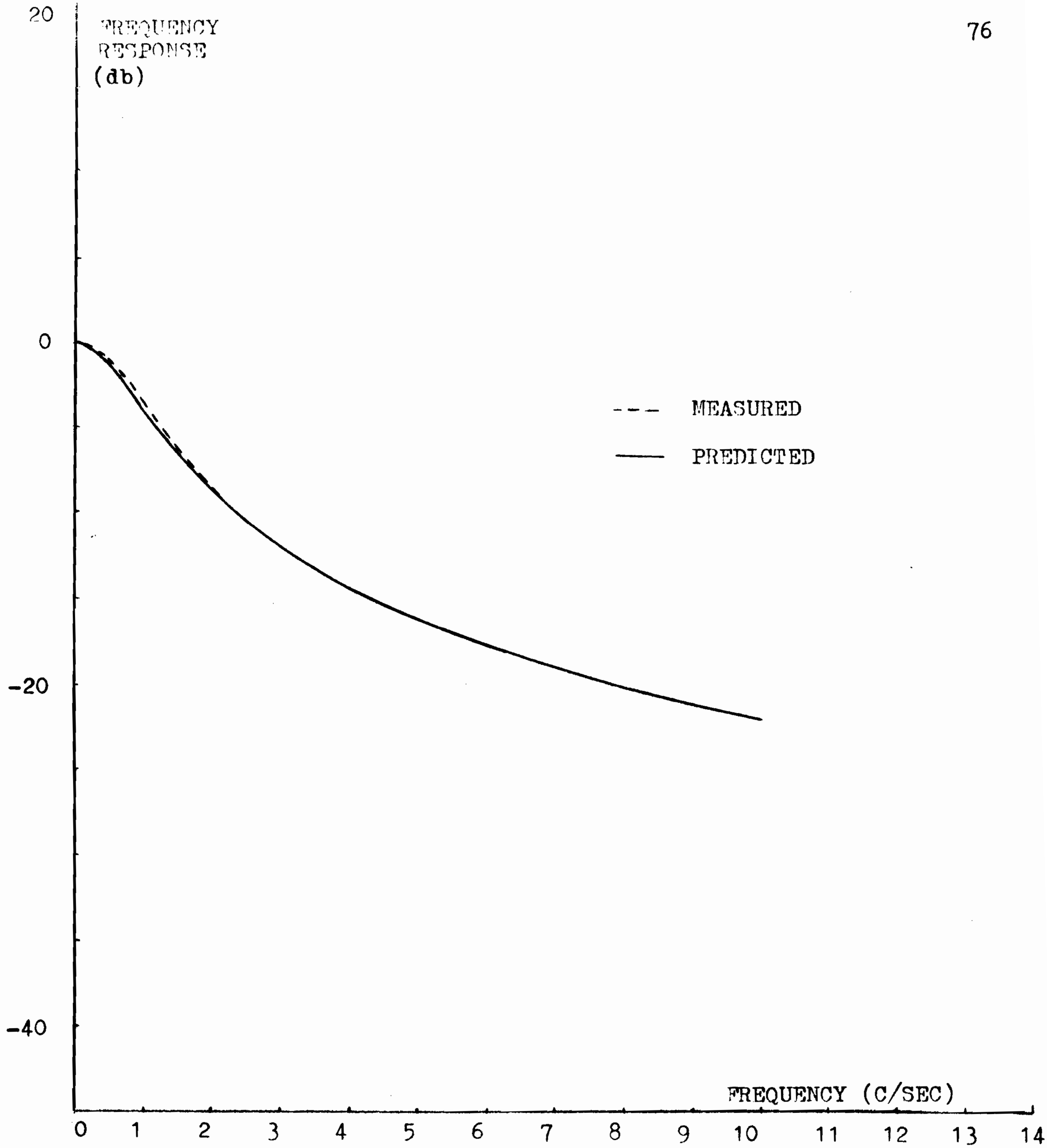

FIG. 4-5 MAGNITUDE OF THE FREQUENCY RESPONSE OF THE SPEED-GOVERNOR MODULES: MODULE # 1

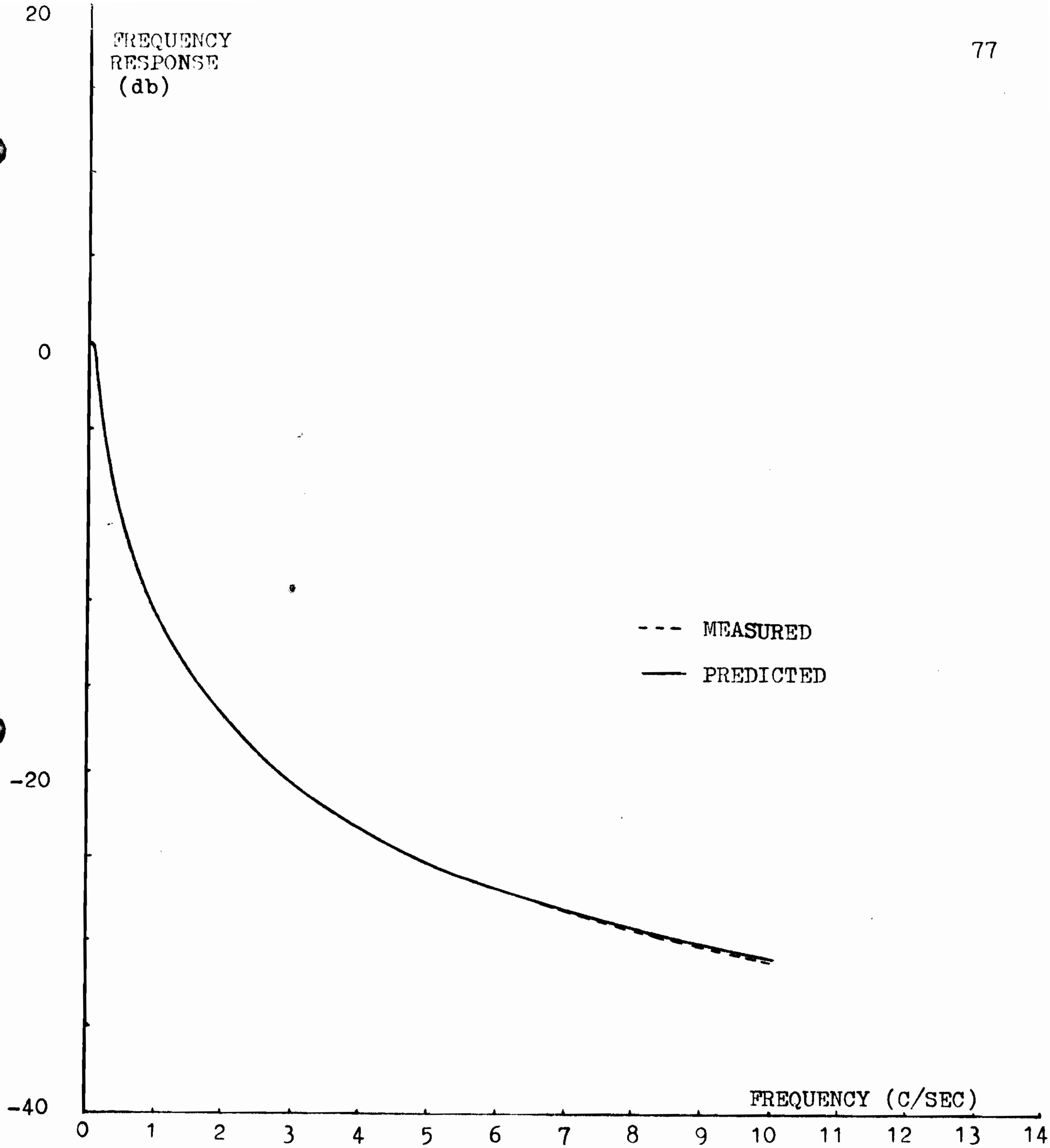

FIG. 4-6 MAGNITUDE OF THE FREQUENCY RESPONSE OF THE SPEED-GOVERNOR MODULES: MODULE # 2

4.2.6 Test results on range of operation of given variables

Three variables were tested to determine the precision of operation of the circuit as these are varied over a given range. The module used to perform these test was for a turbine section of the shaft assembly. The transfer function for this module was obtained in section 4.2.1 equation 4-4, and it is as follows:

$$\frac{\theta_i}{F_i P_i} = \frac{1}{2H_i S^2 + (D_{i,i+1} + D_{ii})\,S + K_{i,i+1}} \qquad (4\text{-}30)$$

The variables tested are $2H_i$ and $K_{i,i+1}$. In the fig. 4-7 and fig. 4-8 , calculated frequency response and test results are given for $2H_i$ and $K_{i,i+1}$, in this respective order.

4.3 Inertia Shaft Assembly System

The system configuration that was tested is shown in fig. 4-9. The frequency response (amplitude) are obtained mathematically in section 4.3.1, and the results are listed in section 4.3.2. Then, these results are compared to those obtained by Goldberg and Schmus [23]. The parameter constants used in the system shown in fig. 4-10 are the following (in p.u.)

$K = 10.0$ (4-33) $H_1 = 0.2$ (4-43)

$K_{1,2} = 17900.$ (4-34) $H_2 = 0.35$ (4-44)

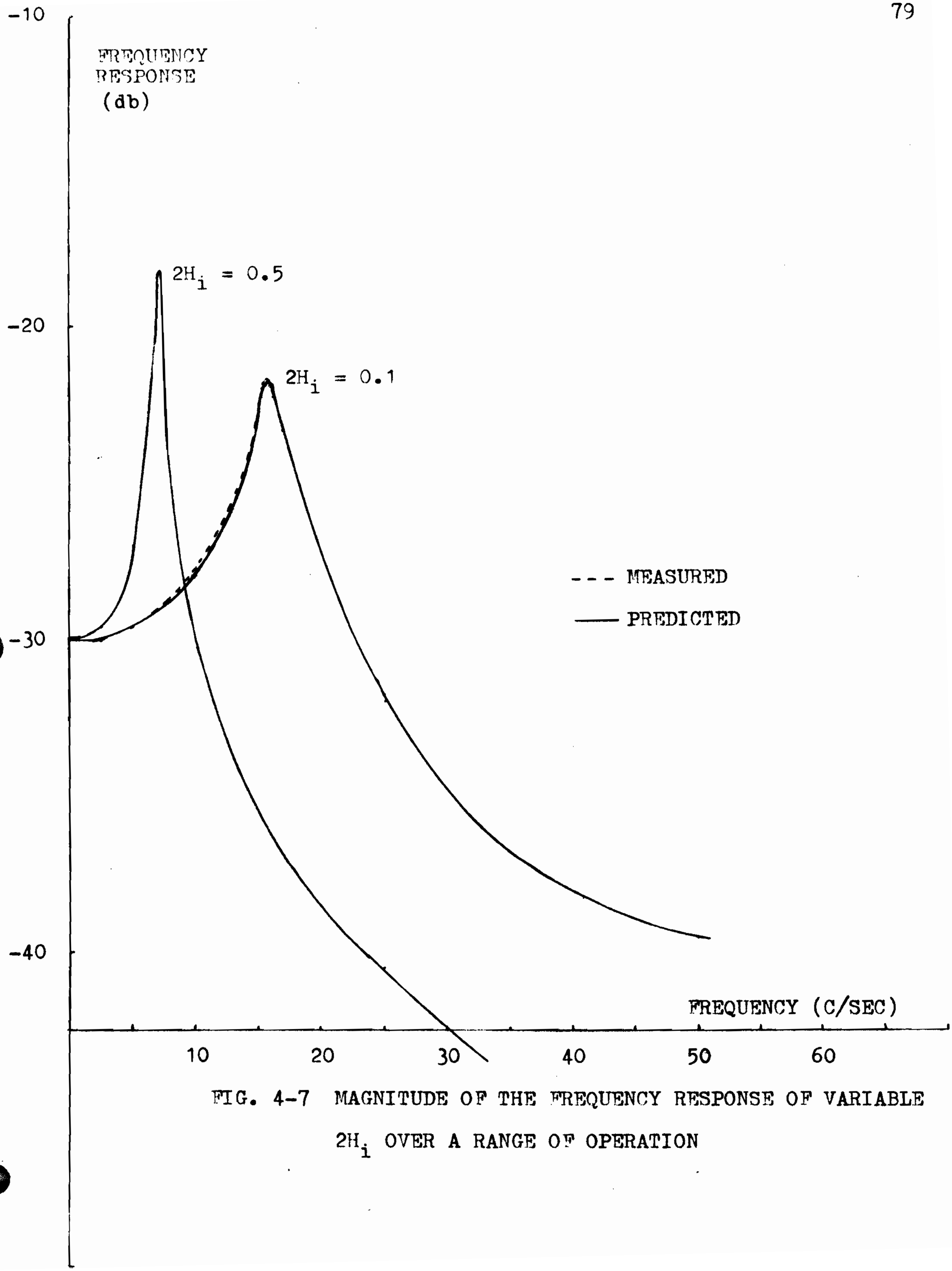

FIG. 4-7 MAGNITUDE OF THE FREQUENCY RESPONSE OF VARIABLE $2H_i$ OVER A RANGE OF OPERATION

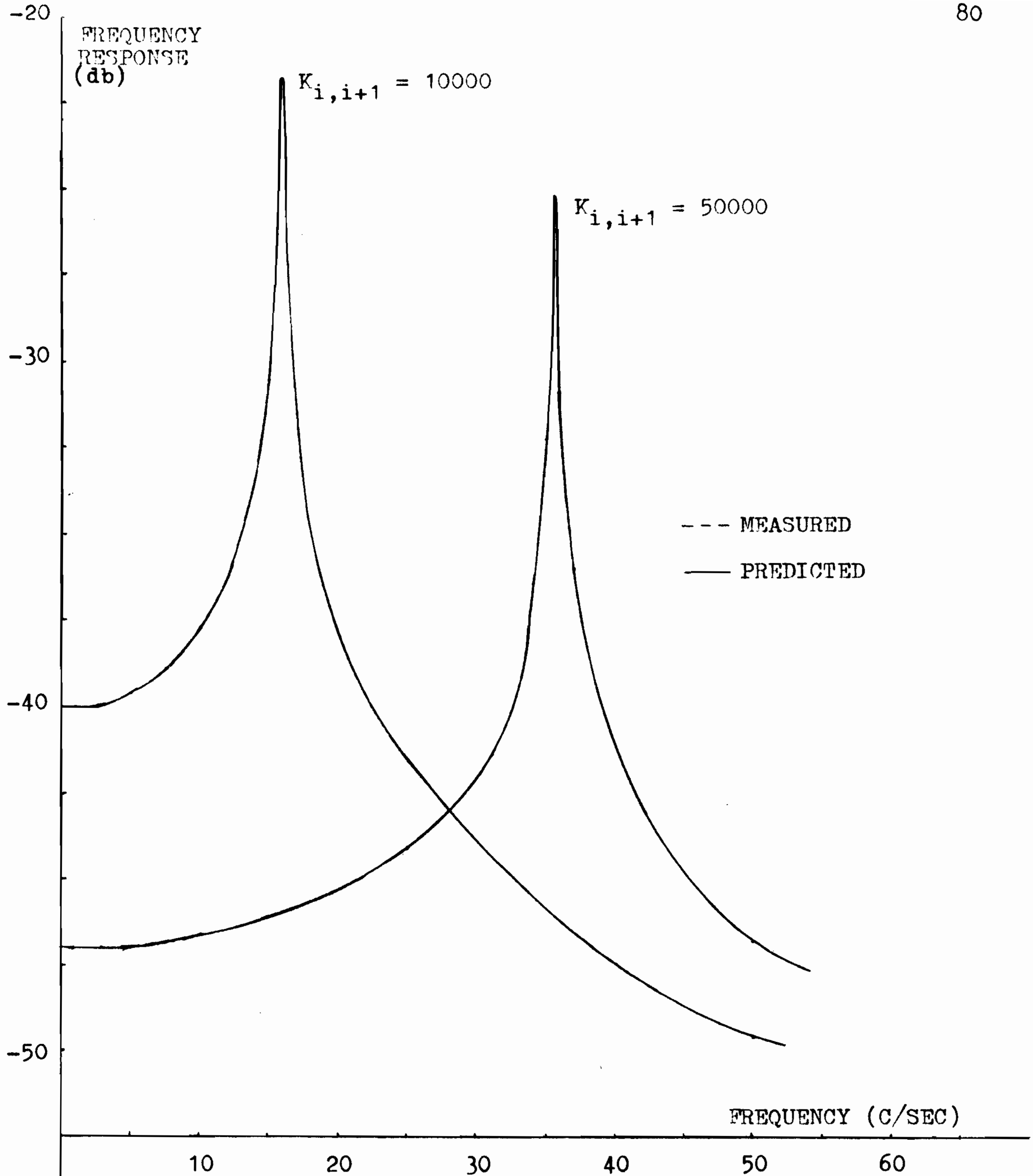

FIG. 4-8 MAGNITUDE OF THE FREQUENCY RESPONSE OF THE VARIABLE $K_{i,i+1}$ OVER A RANGE OF OPERATION

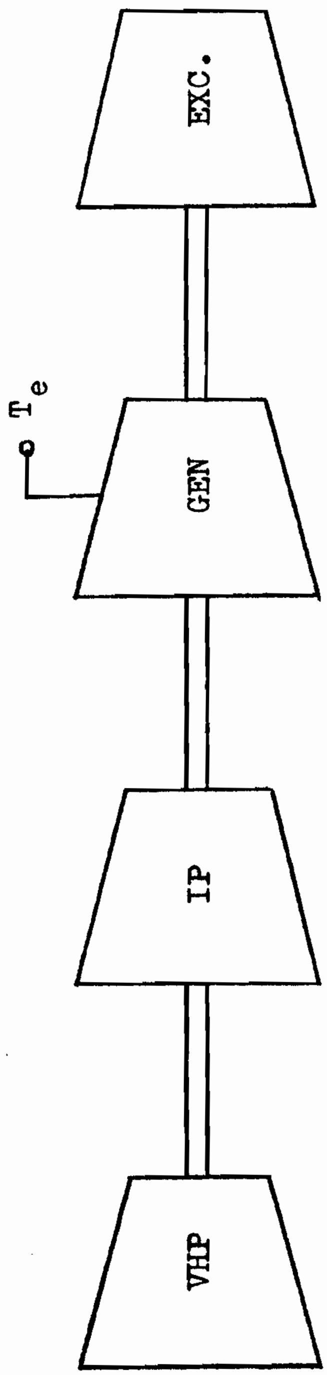

FIG. 4-9 BLOCK DIAGRAM FOR INERTIA SHAFT ASSEMBLY SYSTEM

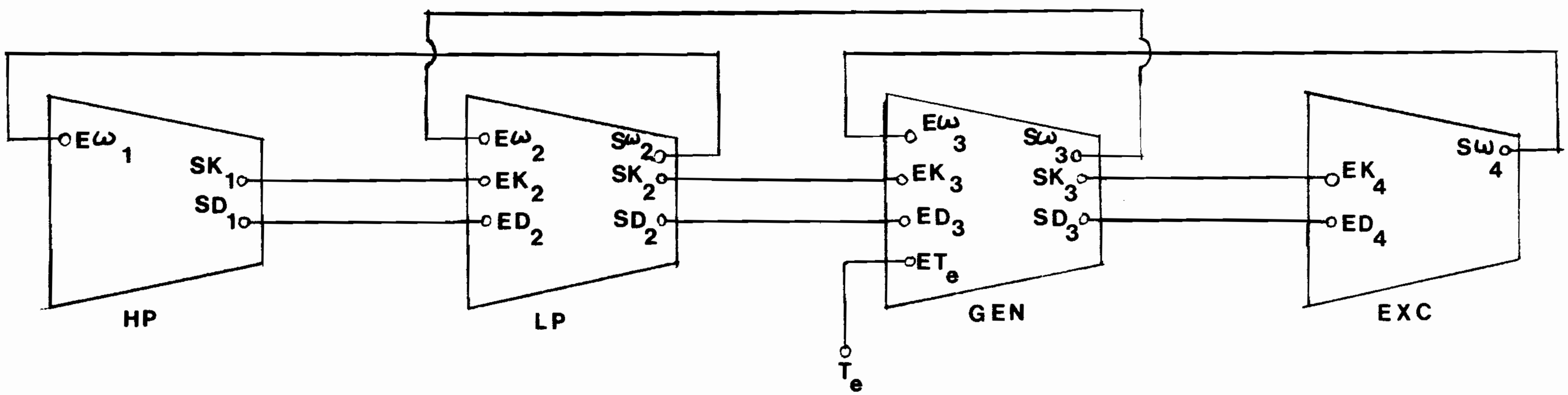

FIG. 4-10 MODULES INTERCONNECTION FOR IMPLEMENTATION OF INERTIA-SHAFT ASSEMBLY SYSTEM

$K_{2,3} = 23300.0$ (4-35) $H_3 = 0.75$ (4-45)

$K_{3,4} = 1700.0$ (4-36) $H_4 = 0.035$ (4-46)

$D_{11} = 0.55$ (4-37) $D_{33} = 0.0$ (4-47)

$D_{1,2} = 0.6$ (4-38) $D_{3,4} = 0.05$ (4-48)

$D_{22} = 0.45$ (4-39) $D_{44} = 0.0$ (4-49)

$D_{2,3} = 0.6$ (4-40)

4.3.1 Mathematical Predictions

The equations describing the system are the following:

$$2H_1S\omega_1 = -D_{1,2}(\omega_1-\omega_2) - D_{11}\omega_1 - K_{1,2}(\theta_1-\theta_2) \qquad (4\text{-}50)$$

$$2H_2S\omega_2 = -D_{1,2}(\omega_2-\omega_1) - D_{22}\omega_2 - D_{2,3}(\omega_2-\omega_3) - K_{1,2}(\theta_2-\theta_1) - K_{2,3}(\theta_2-\theta_3) \qquad (4\text{-}51)$$

$$2H_3S\omega_3 = -T_e - D_{2,3}(\omega_3-\omega_2) - D_{33}\omega_3 - D_{3,4}(\omega_3-\omega_4) - K_{2,3}(\theta_3-\theta_2) - K_{3,4}(\theta_3-\theta_4) \qquad (4\text{-}52)$$

$$2H_4S\ \ _4 = -D_{3,4}(\omega_4-\omega_3) - D_{44}\omega_4 - K_{3,4}(\theta_4-\theta_3) \qquad (4\text{-}53)$$

From these equations, the transfer functions relating the angular displacement, ie θ_i (i=1,2,3,4), to the input torque, T_e, are obtained. Then the following torque response are calculated:

$$K_{1,2}(\theta_1-\theta_2)/T_e$$

$$K_{2,3}(\theta_2-\theta_3)/T_e$$

$$K_{3,4}(\theta_3-\theta_4)/T_e$$

The results are then compared to the measurements, as discussed in section 4.3.2 .

4.3.2 Test Results

In this section, the test results, shown through graphs, describe the magnitude of the frequency response of the shaft torque for a given electrical torque input. On the graphs, the calculated response is the solid curve, and the measured response is the dotted curve. The results are presented in the following order (in the respective fig.)

i) $K_{1,2}(\theta_1-\theta_2)/T_e$ (fig. 4-11)

ii) $K_{2,3}(\theta_2-\theta_3)/T_e$ (fig. 4-12)

iii) $K_{3,4}(\theta_3-\theta_4)/T_e$ (fig. 4-13)

By comparing these results with the ones predicted by S. Goldberg and W. R. Schmus, the measured resonance frequency is practically the same as their predicted resonance frequency.

4.4 Complete System Testing and Results

The final series of tests performed were on a complete system. The system configuration that was tested is shown in fig. 4-14 .

The frequency response are obtained mathematically in section 4.4.1, and the test results are listed in section 4.4.2 . The parameter constants used in the system configuration shown in fig. 4-14 are as follows (in p.u.):

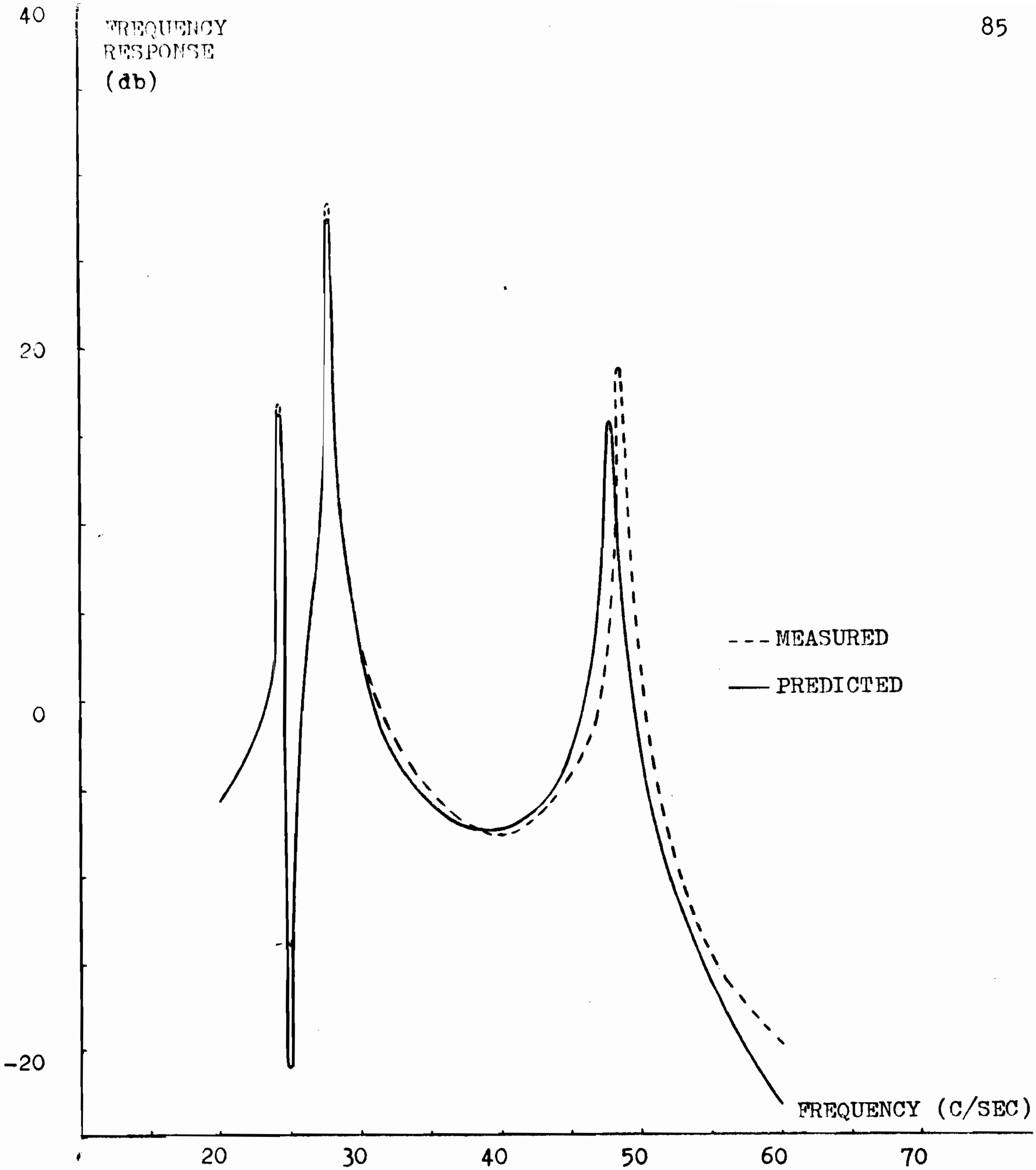

FIG. 4-11 MAGNITUDE OF THE FREQUENCY RESPONSE OF THE TORQUE $[K_{1,2}(\theta_1-\theta_2)/T_e]$ BETWEEN THE VHP-IP SECTIONS OF THE INERTIA SHAFT ASSEMBLY

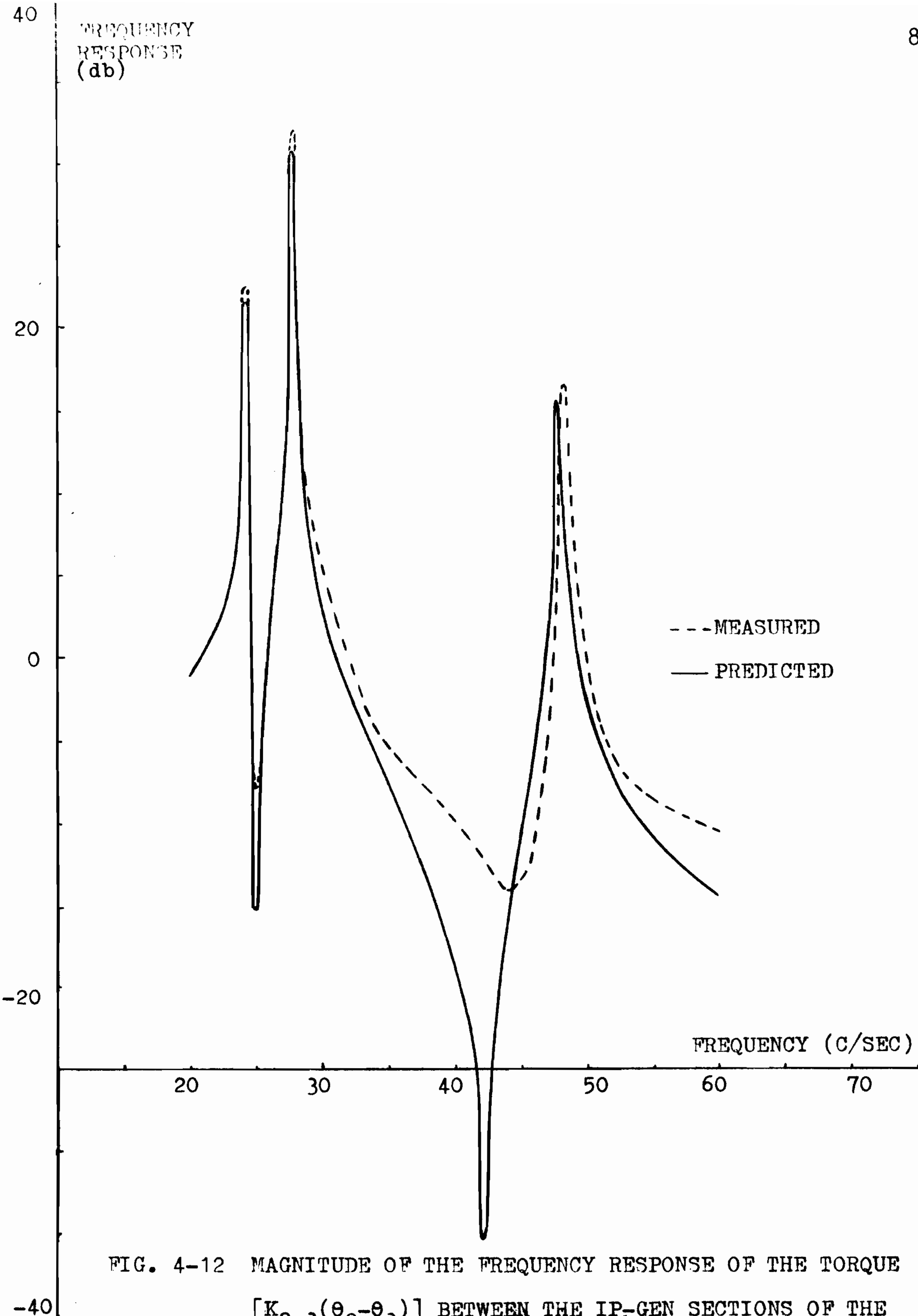

FIG. 4-12 MAGNITUDE OF THE FREQUENCY RESPONSE OF THE TORQUE $[K_{2,3}(\theta_2-\theta_3)]$ BETWEEN THE IP-GEN SECTIONS OF THE INERTIA SHAFT ASSEMBLY

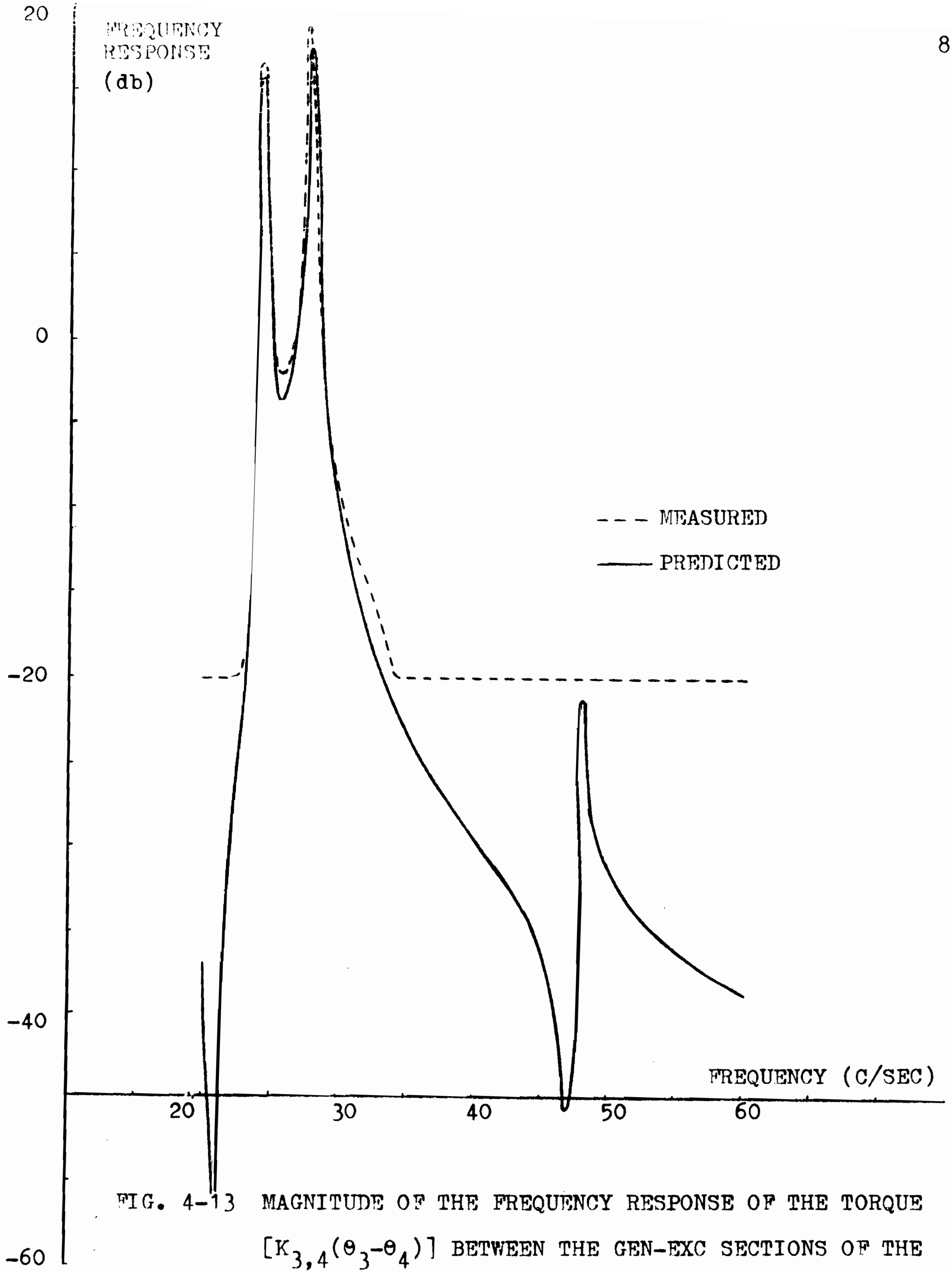

FIG. 4-13 MAGNITUDE OF THE FREQUENCY RESPONSE OF THE TORQUE $[K_{3,4}(\theta_3-\theta_4)]$ BETWEEN THE GEN-EXC SECTIONS OF THE INERTIA SHAFT ASSEMBLY

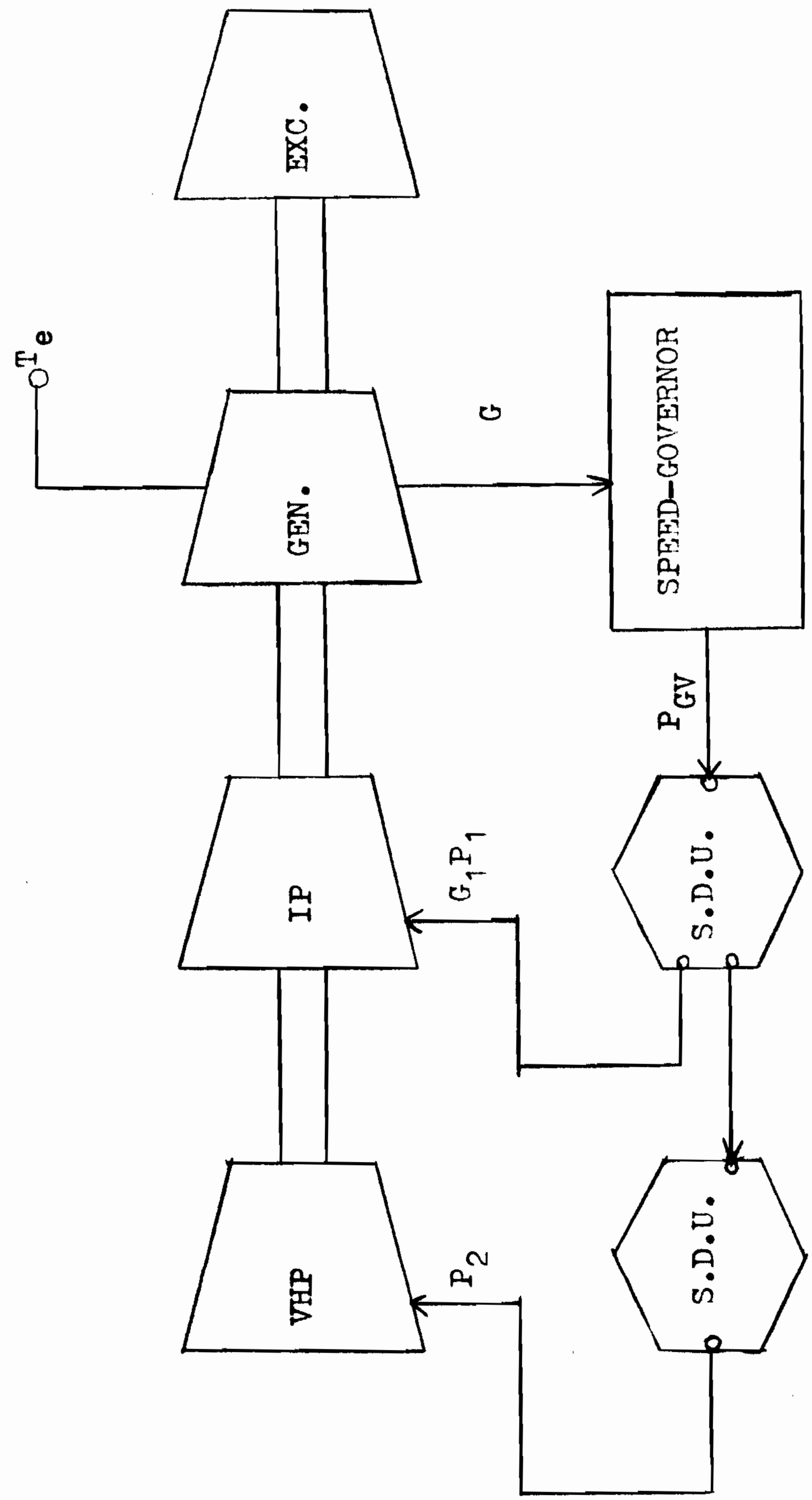

FIG. 4-14 BLOCK DIAGRAM OF A COMPLETE TURBINE-GENERATOR SYSTEM, WITH STEAM DISTRIBUTION SYSTEM AND SPEED-GOVERNOR SYSTEM

$$F_{VHP} = 0.5 \qquad (4\text{-}75)$$
$$F_{IP} = 0.5 \qquad (4\text{-}76)$$
$$T_{CH} = 0.25 \qquad (4\text{-}77)$$
$$T_{RH} = 5.0 \qquad (4\text{-}78)$$
$$T_1 = 2.8 \qquad (4\text{-}79)$$
$$T_2 = 1.0 \qquad (4\text{-}80)$$
$$T_3 = 0.15 \qquad (4\text{-}81)$$
$$K = 10.0 \qquad (4\text{-}82)$$
$$H_1 = 0.2 \qquad (4\text{-}83)$$
$$H_2 = 0.35 \qquad (4\text{-}84)$$
$$D_{34} = 0.05\text{p.u.} \qquad (4\text{-}85)$$
$$D_{44} = 0.0 \text{ p.u.} \qquad (4\text{-}86)$$
$$H_3 = 0.75 \qquad (4\text{-}87)$$
$$H_4 = 0.035 \qquad (4\text{-}88)$$
$$K_{1,2} = 17900.0 \qquad (4\text{-}89)$$
$$K_{2,3} = 23300.0 \qquad (4\text{-}90)$$
$$K_{3,4} = 1700.0 \qquad (4\text{-}91)$$
$$D_{11} = 0.55 \qquad (4\text{-}92)$$
$$D_{12} = 0.6 \qquad (4\text{-}93)$$
$$D_{22} = 0.45 \qquad (4\text{-}94)$$
$$D_{23} = 0.6 \qquad (4\text{-}95)$$
$$D_{33} = 0.0 \qquad (4\text{-}96)$$
$$T_e = 1.0+50.0 \text{ p.u.} \qquad (4\text{-}97)$$

4.4.1 Mathematical Predictions

The equations describing the system are as follows:

$$T_1 \omega_{IS} = U - \omega_{IS} = \omega_G - \omega_0 - \omega_{IS} \qquad (4\text{-}98)$$

$$T_3 P_{GV} = P_o + \frac{KT_2}{T_1}(\omega_o - \omega_G) - K\left(1 - \frac{T_2}{T_1}\right)\omega_{IS} - P_{GV} \qquad (4\text{-}99)$$

$$T_{CH} P_{VHP} = P_{GV} - P_{VHP} \qquad (4\text{-}100)$$

$$T_{RH} P_{IP} = -P_{IP} + (1 - F_{VHP}) P_{VHP} \qquad (4\text{-}101)$$

$$2H_1 \omega_1 = F_{VHP} P_{VHP} - D_{12} S(\theta_1 - \theta_2) - D_{11} S\theta_1 - K_{12}(\theta_1 - \theta_2) \qquad (4\text{-}102)$$

$$2H_2\omega_2 = \left(\frac{F_{IP}}{1-F_{VHP}}\right) P_{IP} - D_{12}\, S(\theta_2-\theta_1) - D_{23}\, S(\theta_2-\theta_3)$$
$$-D_{22}\, S\theta_2 - K_{23}(\theta_2-\theta_3) - K_{12}(\theta_2-\theta_1) \qquad (4\text{-}103)$$
$$2H_3\omega_3 = -T_e - D_{23}S(\theta_3-\theta_2) - D_{34}S(\theta_3-\theta_4)$$
$$-D_{33}\, S\theta_3 - K_{23}\,(\theta_3-\theta_2) - K_{34}(\theta_3-\theta_4) \qquad (4\text{-}104)$$
$$2H_4\omega_4 = -D_{34}S(\theta_4-\theta_3) - D_{44}S\theta_4 - K_{34}(\theta_4-\theta_3) \qquad (4\text{-}105)$$

From these equations, the transfer functions relating the angular displacement, ie. θ_i (i=1,2,3,4) to the input torque, T_e , are obtained. Then the following torques response are calculated.

$K_{1,2}\,(\theta_1-\theta_2)/T_e$

$K_{2,3}\,(\theta_2-\theta_3)/T_e$

$K_{3,4}\,(\theta_3-\theta_4)/T_e$

4.4.2 Test Results

In this section, the frequency response obtained by calculation and by testing is illustrated in fig. 4-15 to 4-19.

The results are presented in the following order:

i) $K_{1,2}(\theta_1-\theta_2)/T_e$ (4-148)

- Magnitude Fig. 4-15
- Phase Fig. 4-16

ii) $K_{2,3}(\theta_2-\theta_3)/T_e$ (4-149)

- Magnitude Fig. 4-17
- Phase Fig. 4-18

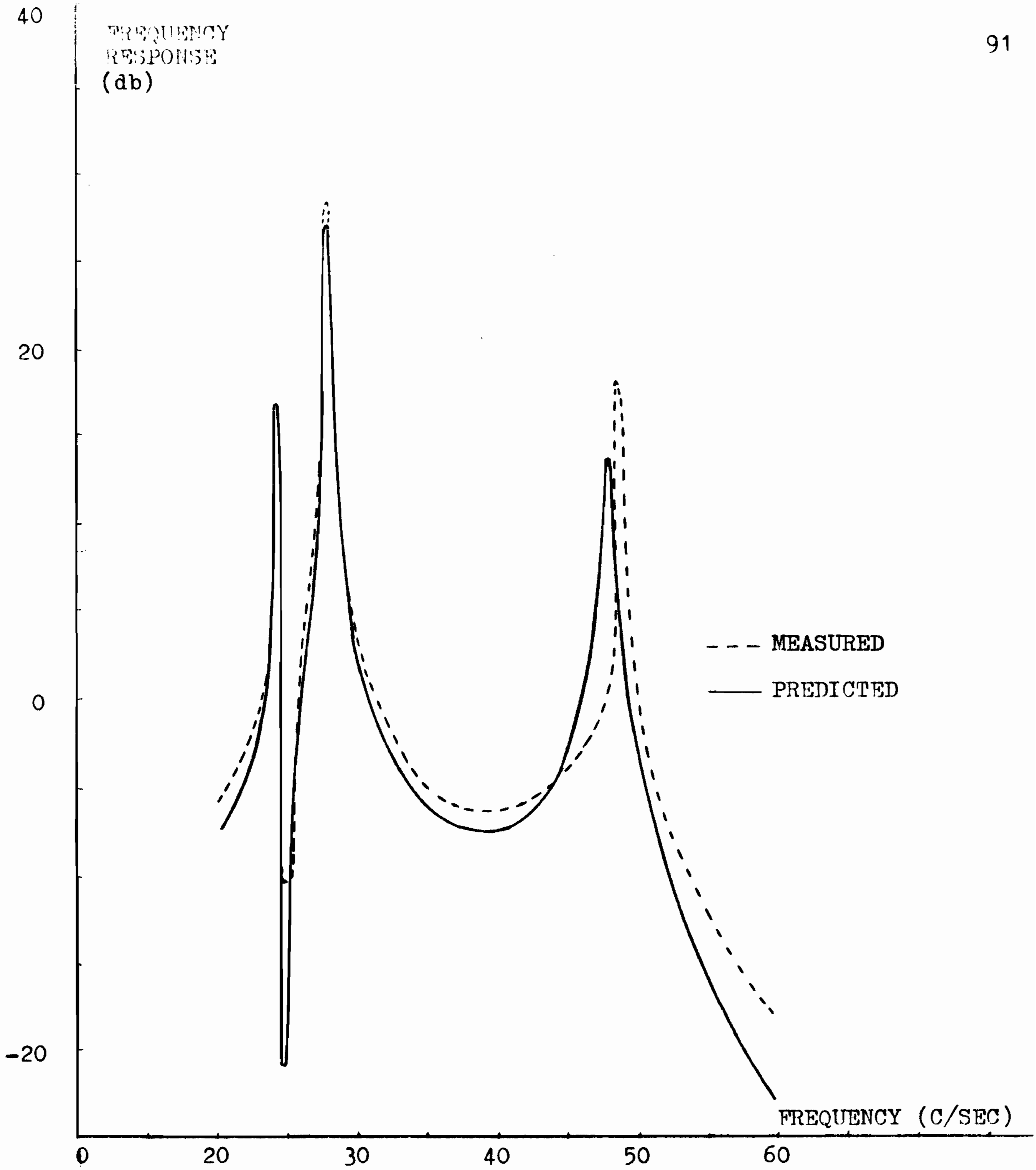

FIG. 4-15 MAGNITUDE OF THE FREQUENCY RESPONSE OF THE TORQUE $[K_{1,2}(\theta_1-\theta_2)]$ BETWEEN THE VHP-IP INERTIA SHAFT SECTIONS OF THE COMPLETE SYSTEM

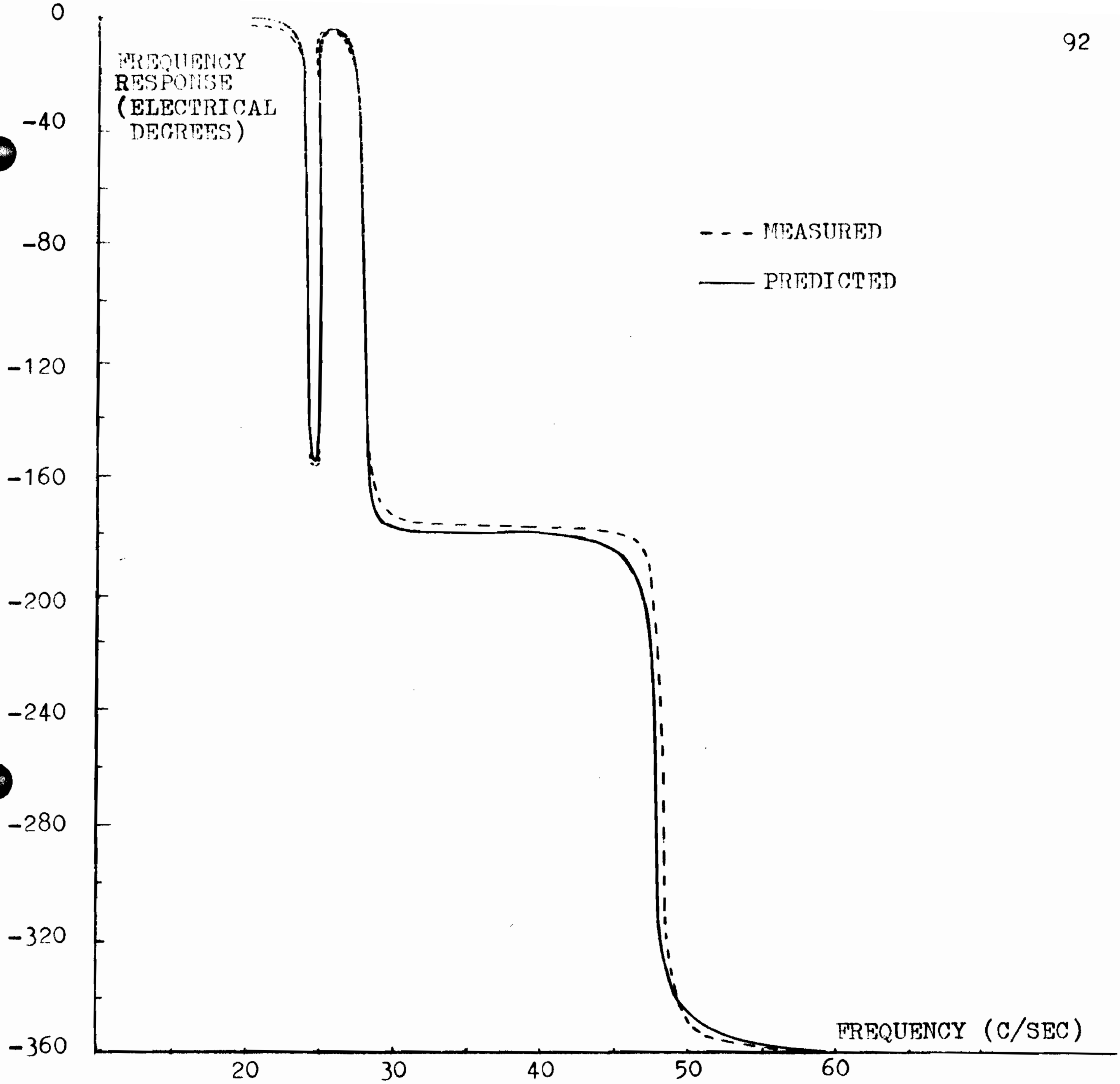

FIG. 4-16 PHASE OF THE FREQUENCY RESPONSE OF THE TORQUE $[K_{1,2}(\theta_1-\theta_2)]$ BETWEEN THE VHP-IP INERTIA SHAFT SECTIONS OF THE COMPLETE SYSTEM

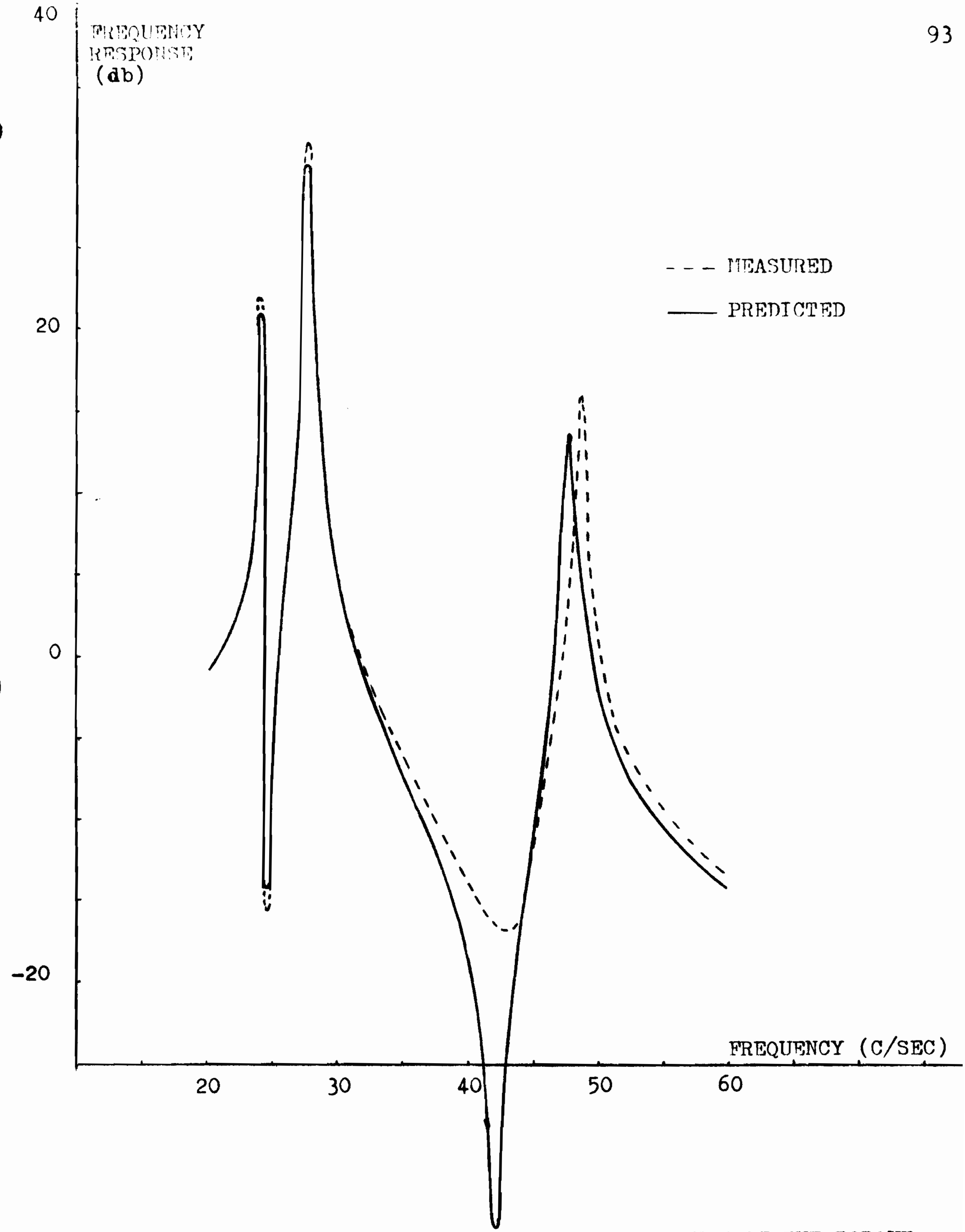

FIG. 4-17 MAGNITUDE OF THE FREQUENCY RESPONSE OF THE TORQUE $[K_{2,3}(\theta_2-\theta_3)]$ BETWEEN THE IP-GEN INERTIA SHAFT SECTIONS OF THE COMPLETE SYSTEM

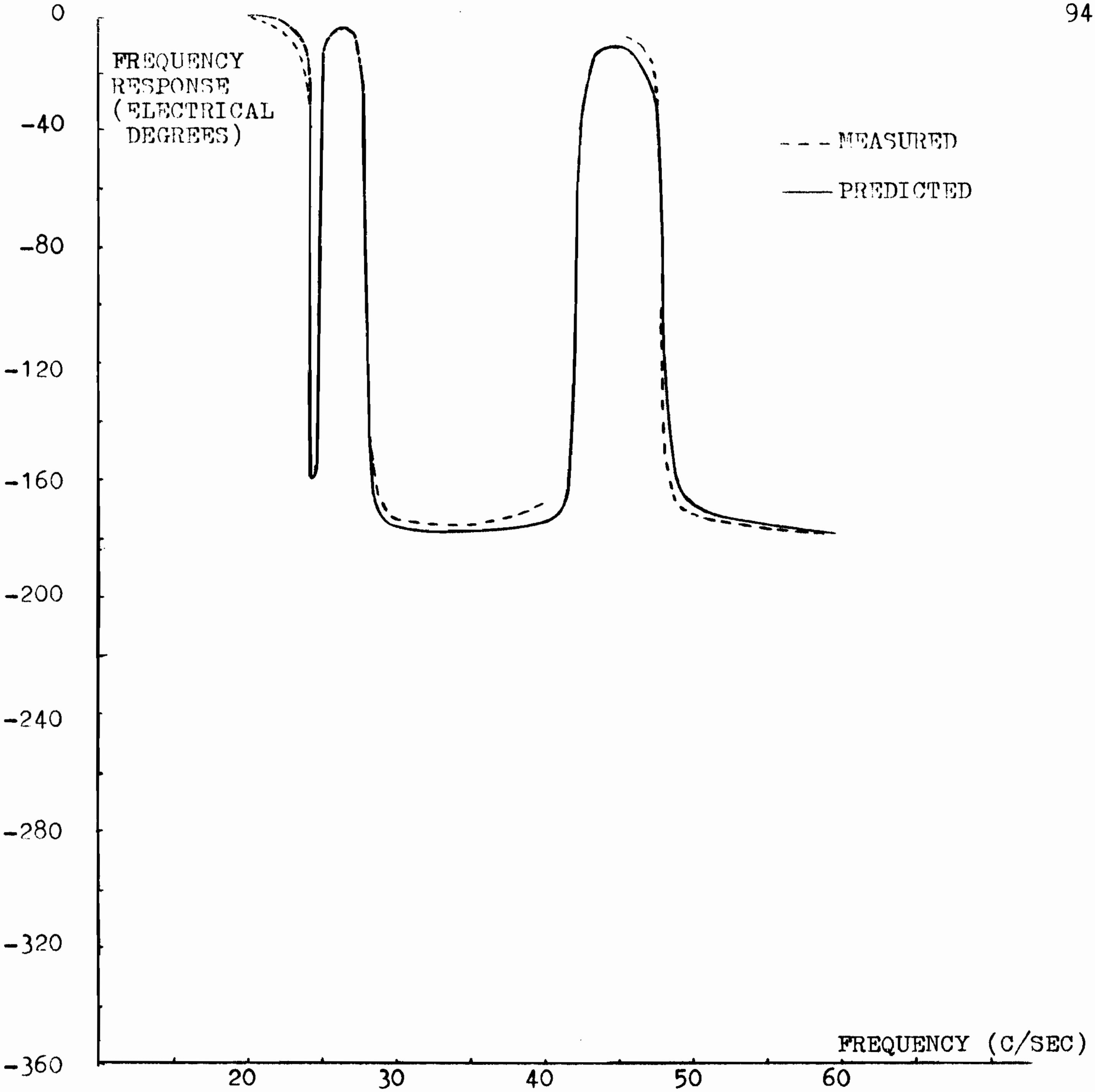

FIG. 4-18 PHASE OF THE FREQUENCY RESPONSE OF THE TORQUE $[K_{2,3}(\theta_2-\theta_3)]$ BETWEEN THE IP-GEN INERTIA SHAFT SECTIONS OF THE COMPLETE SYSTEM

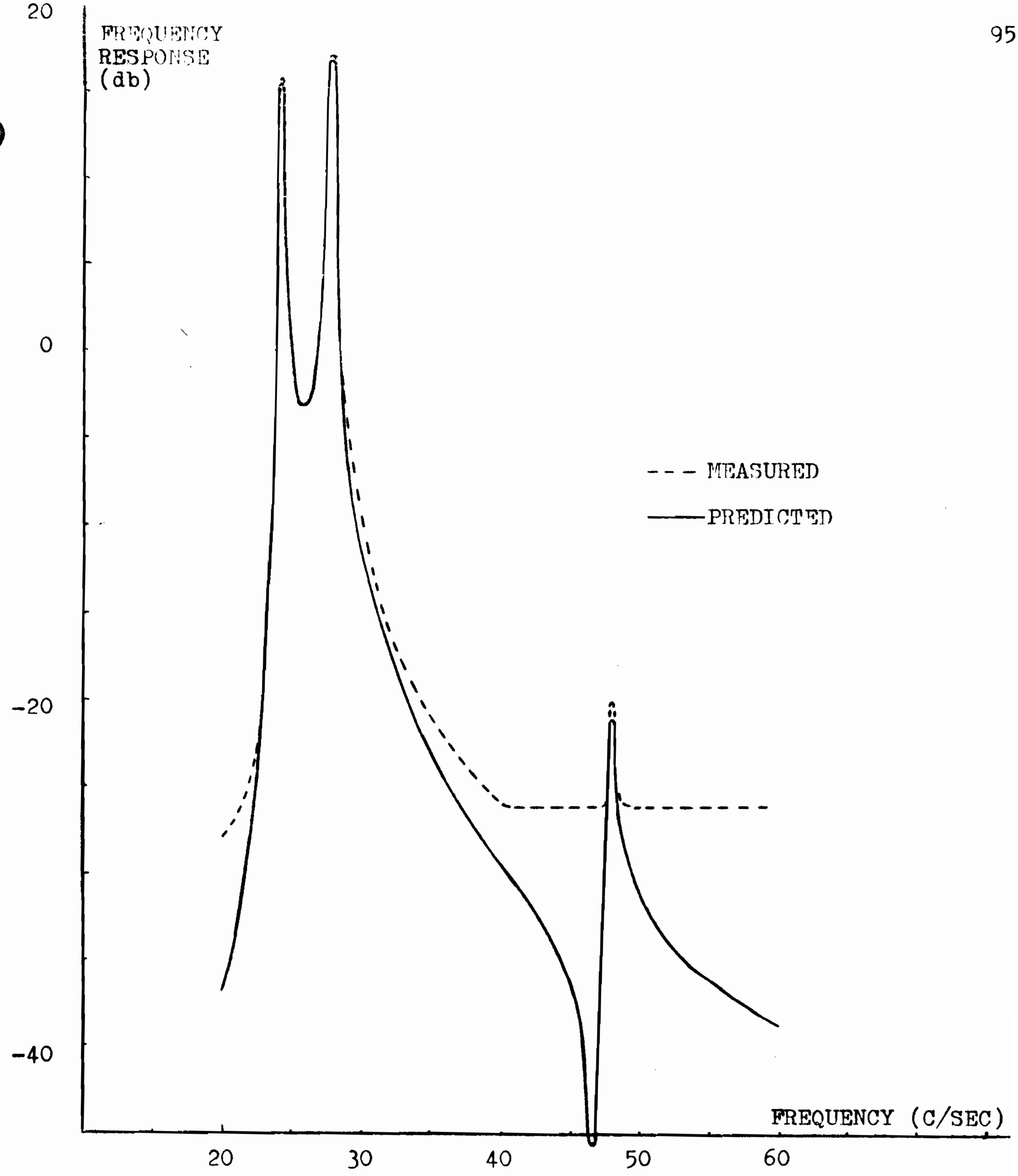

FIG. 4-19 MAGNITUDE OF THE FREQUENCY RESPONSE OF THE TORQUE $[K_{3,4}(\theta_3-\theta_4)]$ BETWEEN THE GEN-EXC INERTIA SHAFT SECTIONS OF THE COMPLETE SYSTEM

iii) $K_{3,4}(\theta_3-\theta_4)/T_e$ (4-150)

- Magnitude Fig. 4-19

For the last one, the phase could not be obtained due to the small amplitude of the signal, (which could not be distinguished from the noise).

4.5 Evaluation of System Performance

Tests on the electronic simulator have demonstrated good agreement with the mathematical predictions. This can be seen in this chapter. By examining fig.s 4-1 to 4-19, it is seen that there exist only minor discrepencies. The discrepencies have arisen mainly from the difficulty of finding electronic components which are sufficiently close to the required values. This is especially critical in the construction of integrators. In making the RC ratios equal to one, care has been exercised in selecting resistances and capacitances of fine tolerances to match the product. Because of their unavailability in stock, and being pressed for time, a few of the integrators have been built with components of one percent accuracy. This explains in part the slight shift in resonance frequency of fig. 4-11 to 4-19.

CHAPTER 5

CONCLUSION

The objective of this thesis has been to develop an electronic analog simulator of the steam turbine-generator system. There are a number of ground rules to this exercise:

1) The simulator must dovetail with the existing simulator of the Institute de Recherche de Hydro-Quebec (IREQ).
2) The simulator must be able to reproduce torsional resonance phenomena in the turbo-generator shaft.
3) The simulator must be capable of been configured into a variety of reheats and turbines topologies.

The first stage of the development has consisted of deciding on the mathematical models of the system. The two papers: 1) Subsynchronous Resonance and Torsional Stresses in Turbine-Generator Shafts, by S. Goldberg and W.R. Schmus [23], and 2) Dynamic Models for Steam and Hydro turbines in Power System Studies, by IEEE Committee Report [14], were adopted for the purpose of this study. The integration of the steam turbine dynamics with the elastic shaft inertia dynamics has been accomplished in section 2-6.

The second stage has consisted of deciding on the minimum set of modules which on interconnection offer the maximum flexibility in the implementing of all conceivable turbine-reheat configurations.

The module sets are:

1) Inertia-Shaft Modules (Sect.3-2)

   1) Turbine Section

   2) Generator Unit

2) Exciter Module (Sect.3-3)

3) Steam Distribution Modules (Sect.3-4)

   (Reheaters, crossover and steam chest are represented with this module).

4) Speed-Governor Module (Sect.3-5)

The third part of this thesis consisted of building each of these modules. The schematic diagram and the wiring diagram of each are shown in the corresponding sections given with the previous list of modules.

The electronic modules have been tested individually, then as an inertia-shaft assembly system and finally as part of an integrated governor, turbine, reheat and shaft-inertia system. The test consisted of frequency domain measurements and the results are presented in the form of Bode diagrams in chapter 4. Close agreement between measurements and predictions has been observed. This gives a high level of confidence in the design of the modules and in their capabilities to perform as part of the simulator.

It is recommended from this study that the modules based on the designs be constructed as adjunct to the simulating facilities of IREQ.

REFERENCES

[1] M. H. Kent, W. R. Schmus, F. A. McCraken, and L. M. Wheeler, " Dynamic Modelling of Loads in the Stability Studies ", Stability of Large Electric Power Systems, Edited by R. T. Byerly and E. W. Kimbark, IEEE Press, 1974, pp. 139-146.

[2] F. Iliceto, A. Ceyhan, and G. Ruckstuhl, " Behavior of Loads During Voltage Dips Encountered in Stability Studies - Field and Laboratory Tests ", Stability of Large Electric Power Systems, Edited by R. T. Byerly and E. W. Kimbark, 1974 IEEE Press, pp. 154-163.

[3] IEEE Committee Report, " System Load Dynamics - Simulation Effects and Determination of Load Constant ", Stability of Large Electric Power Systems, Edited by R. T. Byerly and E. W. Kimbark, 1974 IEEE Press, pp. 164-173.

[4] R. B. Adler and C. C. Mosher, " Steady-State Voltage Power Characteristic for Power System Loads ", Stability of Large Electric Power Systems, Edited by R. T. Byerly and E. W. Kimbark, 1974 IEEE Press, pp. 147-153.

[5] D. W. Olive, " Digital Simulation of Synchronous Machine Transients ", Stability of Large Electric Power Systems, Edited by R. T. Byerly and E. W. Kimbark, 1974 IEEE Press, pp. 13-19.

[6] R. P. Schulz, W. D. Jones, and D. N. Ewart, " Dynamic Models of Turbine Generators Derived from Solid Rotor Equivalent Circuits ", IEEE Transaction on Power Apparatus and System, vol. PAS-92, NO.3, May/June 1973, pp. 926-933.

[7] P. L. Dandeno, R. L. Hauth, and R. P. Schulz, " Effects of Synchronous Machine Modelling in Large Scale System Studies ", Stability of Large Electric Power Systems, Edited by R. T. Byerly and E. W. Kimbark, 1974 IEEE Press, pp. 28-36.

[8] G. Manchur, D. C. Lee, M. E. Coultes, J. D. A. Griffin, and W. Watson, " Generators Models Established by Frequency Response Tests on a 555 MVA Machine ", Stability of Large Electric Power Systems, Edited by R. T. Byerly and E. W. Kimbark, 1974 IEEE Press, pp. 37-44.

[9] Y. Yu and H. A. M. Mousa, " Experimental Determination of Exact Equivalent Circuit Parameters of Synchronous Machines ", Stability of Large Electric Power Systems, Edited by R. T. Byerly and E. W. Kimbark, 1974 IEEE Press, pp. 45-49.

[10] IEEE Committee Report, " Computer Representation of Excitation Systems ", Stability of Large Electric Power Systems, Edited by R. T. Byerly and E. W. Kimbark, 1974 IEEE Press, pp. 50-54.

[11] IEEE Committee Report, " Excitation System Dynamic Characteristics ", Stability of Large Electric Power Systems, Edited by R. T. Byerly and E. W. Kimbark, 1974 IEEE Press, pp. 55-66.

[12] M. A. Eggenberger, " A simplified Analysis of the No-Load Stability of Mechanical-Hydraulic Speed Control Systems for Steam Turbines ", Stability of Large Electric Power Systems, Edited by R. T. Byerly and E. W. Kimbark, 1974 IEEE Press, pp.103-120.

[13] D. G. Ramey and J. W. Skooglund, " Detailed Hydro-governor Representation for System Stability Studies ", Stability of Large Electric Power Systems, Edited by R. T. Byerly and E. W. Kimbark, 1974 IEEE Press, pp. 121-127.

[14] IEEE Committee Report, " Dynamic Models for Steam and Hydro Turbines in Power System Studies ", Stability of Large Electric Power Systems, Edited by R. T. Byerly and E. W. Kimbark, 1974 IEEE Press, pp. 128-138.

[15] R. G. Farmer, A. L. Schwalb and Eli Katz. " Navajo Project Report on Subsynchronous Resonance Analysis and Solutions ", IEEE Transaction on Power Apparatus and Systems, vol. PAS-96, NO.4, July/Aug. 1977, pp. 1226-1232.

[16] H. W. Dommel and N. Sato, " Fast Transient Stability Solutions ", Stability ofLarge Electric Power Systems, Edited by R. T. Byerly and E. W. Kimbark, 1974 IEEE Press, pp. 253-260.

[17] K. Prabhashankar and Wasyl Janischewsyj, " Digital Simulation of Multimachine Power Systems for Stability Studies ", IEEE Transaction on Power Apparatus and Systems, vol. PAS-87, NO.1, January 1968, pp. 73-79.

[18] T. A. Nondahl and T. A. Lipo, " Transient Analysis of a Linear Induction Machine Using d,q Pole-By-Pole Model ", IEEE Transaction on Power Apparatus and Systems, vol. PAS-98, NO.4, Julu/Aug. 1979, pp. 1366-1374

[19] T. L. Skvarenina and P. C. Krause, " Accuracy of Reduced Order Model of Induction Machines in Dynamic Stability Studies " IEEE Transaction on Power Apparatus and Systems, vol. PAS-98, NO.4, July/Aug. 1979, pp. 1192-1197.

[20] D. R. Brown and P. C. Krause, " Modelling of Transient Electrical Torques in Solid Rotor Turbogenerators ", IEEE Transients on Power Apparatus and Systems, vol. PAS-98, NO.5, Sept./Oct. 1979, pp. 1502-1508

[21] G. Jasmin, J. P. Bowles, A. Leraux and D. Mukhedkar, " Electronic Simulation of a Hydro-Generator with Static Excitation ", IEEE Transaction on Power Apparatus and Systems, vol. PAS-100, NO.9, September 1981, pp. 4207-4215.

[22] G. Jasmin and D. Mukhedkar, " Electronic Micro Machine Simulation ", International Conference on Electrical Machines, Sept. 15-17, 1980, Athens, Greece, Proceeding p. 6/8.

[23] S. Goldberg and W. R. Schmus, " Subsynchronous Resonance and Torsional Stresses in Turbine-Generator Shafts ", IEEE Transaction on Power Apparatus and Systems, vol. PAS-98, NO.4, July/Aug. 1979, pp. 1233-1237.

[24] C. C. Young, " Equipment and System Modelling for Large-Scale Stability Studies ", IEEE Transaction on Power Apparatus and Systems, vol. PAS-91, NO.1, Jan./Feb. 1972, pp. 99-109.

[25] J. M. Undrill, J. A. Casazza, E. M. Gulachenski and L. K. Kerchmayer, " Electromechanical Equivalents for use in Power System Stability Studies ", IEEE Transaction on Power Apparatus and Systems, vol. PAS-90, NO.5, Sept./Oct. 1971, pp.2060-2071.

[26] A. Kuppurajulu and S. Elangovan, " Simplified Power System Models for Dynamic Stability Studies ", IEEE Transaction on Power Apparatus and Systems, vol. PAS-90, NO.1, Jan./Feb. 1971, pp. 11-23.

[27] IEEE Subsynchronous Resonance Task Force of the Dynamic System Performance Working Group Power System Engineering Committee, " First Benchmark Model for Computer Simulation of Subsynchronous Resonance ", IEEE Transaction on Power Apparatus and Systems, vol. PAS-96, NO.5, Sept./Oct. 1971, pp. 1565-1572.

[28] A. A. Fouad and K. T. Khu, " Subsynchronous Resonance Zones in the IEEE " Benchmark " Power System ", IEEE Transaction on Power Apparatus and System, vol. PAS-97, NO.3, May/June 1978, pp. 754-762.

[29] L. A. Kilgore, D. G. Ramey and M. C. Hall, " Simplified Transmission and Generation System Analysis Procedures for Subsynchronous Resonance Problems ", IEEE Transaction on Power Apparatus and Systems, vol. PAS-96, NO.6, Nov./Dec. 1977, pp. 1840-1846.

[30] G. J. Bowler, D. N. Ewart and C. Concordia, "Self-Excited Torsional Frequency Oscillations with Series Capacitors ", IEEE Transactions on Power Apparatus and Systems, vol. PAS-92, NO.5, Sept./Oct. 1973, pp. 1688-1695.

[31] R. G. Farmer, A. L. Schwalb and E. Katz, " Navajo Project Report on Subsynchronous Resonance Analysis and Solutions ", IEEE Transactions on Power Apparatus Systems, vol. PAS-96, NO.4, July/Aug. 1977, pp. 1226-1232.

[32] B. T. Ooi, " Phase Modulation Theory of Electromechanical Damping in Subsynchronous Generators ", IEEE Transactions on Power Apparatus and Systems, vol. PAS-100, NO.5, May 1981, pp. 2211-2218.

[33] B. T. Ooi and M. M. Sartawi, " Concepts and Field Excitation Control of Subsynchronous Resonance in ynchronous Machines ", IEEE Transactions, vol. PAS-97, NO.5, Sept./Oct. 1978, pp. 1637-1645.

[34] H. Nicholson, " Integrated Control of a Non-Linear Turboalternator Model under Fault Conditions ", Proceeding IEE (London), Vol. 114, June 1967, pp.834.

[35] H. Nicholson, " Dynamic Optimisation of a Boiler-Turboalternator Model ", Proceeding IEE (London), Vol. 113, February 1966, pp. 385.

[36] IEEE Committee Report, " Switching Surges III - Field and Analyzer Results for Transmission Lines-Past, Present, and Future Trends ", IEEE Transactions on Power Apparatus and Systems, vol. PAS-92, NO.2, February 1970, pp. 173-189.

[37] R. H. Park, " Fast Turbine Valving ", IEEE Transactions on Power Apparatus and Systems, vol. PAS-92 NO.3, May/June 1973, pp. 1065-1073.

[38] J. P. Bayne and P. Kundar, " A Study of Early Valve Actuation Using Detailed Prime Mover and Power System Simulation ", IEEE Transaction on Power Apparatus and Systems, vol. PAS-94, NO.4, July/Aug. 1975, pp. 1275-1287.

[39] E. W. Cushing Jr., G. E. Drechsler, W. P. Killgoar, and H. G. Marshall, " Fast Valving as an aid to Power System Transient Stability and Prompt Resynchronization and Rapid Reload after full Load Rejection ", IEEE Transaction on Power Apparatus and Systems, vol. PAS-91, NO.4, July/Aug. 1972, pp. 1624-1636.

[40] J. P. Bayne, D. C. Leene and W. Watson, " A Power System Stabilizer for Thermal Units Based on Derivations of Accelerating Power ", IEEE Transactions on Power Apparatus and Systems, vol. PAS-96, NO.6, Nov./Dec. 1977, pp.1777-1783.

[41] N. G. Balu, " Fast Turbine Valving and Independent Pole Tripping Breakness Applications for Plant Stability ", IEEE Transactions on Power Apparatus and Systems, vol. PAS-99, NO.4, July/Aug. 1980, pp. 1330-1342.

[42] T. J. Hammons, " Shaft Torsional Phenomena in Governing Large Turbine-Generators with Non-Linear Steam Valve Stroking Constraints ", IEEE PES Winter Meeting, New York, NY , February 3-8, 1980, Paper A80 024-0.

[43] J. L. Dineley and S. E. Mikhail, " The Dynamic Stability of a Steam Turbine Driven Synchronous Generator under leading Power Factor Load Conditions ", IEEE PES Summer Meeting and Energy Resources Conf., Anaheim, Cal., July 14-19, 1974, Paper T. 74 307-5.

[44] M. E. Martin, D. M. Triezenberg, P. C. Krause, " A Study of Fast Turbine Valving". IEEE Conference Paper C73080-9. Presented at the IEEE PES Winter Power Meeting, New York. January 28 to February 2, 1973.

[45] G. H. Herget and C. U. Park, " Parameter Identification and Verification of Low Order Boiler Models ", IEEE Transaction on Power Apparatus and Systems, vol. PAS-95 NO.4, July/Aug. 1976, pp. 1153-1157.

[46] H. Nicholson, " Dynamic Optimization of a Boiler ", Proceeding IEE, vol. NO.111, August 1964, pp.1479-1499.

[47] Dr. Ing. Günther Klefenz, " La regulation dans les centrales thermiques ", Hartmann and Brown Ag. Minden, Edition Eyrolles.

[48] J. Adams, D. Clark, J. Louis and J. Spanbauer, " Mathematical Modelling of Once-Through Boiler Dynamics ", IEEE Transaction on Power Apparatus and Systems, vol. PAS- 84 , No. 2 , February 1965, pp.146-156.

APPENDIX I

PER UNIT SYSTEM OF EQUATIONS

The mathematical models used in this thesis to develop the electronic modules are in the per unit form. In this appendix, the equations are per-unitized in terms of the machine constants. The inertia is expressed in terms of the inertia constant "H" based on the rated KVA. The base torque is that required at synchronous speed to deliver the machanical power in kilowatts equal to the rated KVA value. The spring constant is defined as the base torque divided by the base angle. The different constants, with their corresponding units, are as follows:

Power (P)	1 Watt = 1 Kg-m^2-rad^2/sec^3
Torque (T)	1 N-m = 1 Kg-m^2-rad/sec^2
Spring Constant (K)	N-m/rad
Damping Constant (D)	N-m-sec/rad
Inertia Constant (J)	1 Kg-m^2 = 1 N-m-sec^2

<u>Base Quantities:</u>

Base Electrical Angular Displacement (θ_{eb})	= 120	radians
Base Electrical Angular Velocity (ω_{eb})	= 120	radians/second

Base Mechanical Angular Displacement (θ_b) $= 2\theta_{eb}/p$ (p=number of poles of generator)

Base Mechanical Angular Velocity $= 2\omega_{eb}/p$

Base Torque (T_{eb}) $=$ rated KVA$/\omega_b$

Base Power (P_{eb}) $= \omega_b T_{eb}$

Base Time $=$ 1 second

$2H = J\omega_b/T_{eb}$

The per-unitization of the system's equations is given in sections I.1 to I.4.

I.1 Inertia Shaft Equations: Turbine Section

The equation for the i^{th} inertia (turbine section) is as follows:

$$J_i S\omega_i - G_i P_i/\omega_i + D_{i-1,i}(\omega_i - \omega_{i-1}) + D_{ii}\omega_i$$
$$+ D_{i,i+1}(\omega_i - \omega_{i-1}) + K_{i-1,i}(\theta_i - \theta_{i-1})$$
$$+ K_{i,i+1}(\theta_i - \theta_{i+1}) = 0 \qquad \text{(I-1)}$$

The per unit terms are obtained by dividing equation I-1 by the base torque. Equation I-1 the becomes:

$$\frac{J_i\omega_b\, S\omega_i}{T_{eb}\quad \omega_b} - \frac{G_i P_i \omega_b}{\omega_i T_{eb}\omega_b} + \frac{D_{i-1,i}(\omega_i - \omega_{i-1})\omega_b}{T_{eb}\omega_b} +$$
$$\frac{D_{ii}\omega_i\omega_b}{T_{eb}\omega_b} + \frac{D_{i,i+1}(\omega_i - \omega_{i+1})\omega_b}{T_{eb}\omega_b} +$$
$$\frac{K_{i-1,i}(\theta_i - \theta_{i-1})\theta_b}{T_{eb}\theta_b} + \frac{K_{i,i+1}(\theta_i - \theta_{i+1})\theta_b}{T_{eb}\theta_b} = 0 \qquad \text{(I-2)}$$

The per unit terms are now the following:

$$2H_i = \frac{J_i\omega_b}{T_{eb}} \frac{(Kg\text{-}m^2)(rad/sec)}{(Kg\text{-}m^2\text{-}rad/sec^2)} = \frac{J_i\omega_b}{T_{eb}} \text{ sec}$$

$$\bar{P}_i = \frac{P_i}{\omega_b T_{eb}} \frac{(Kg\text{-}m^2\text{-}rad^2/sec^3)}{(rad/sec)(Kg\text{-}m^2\text{-}rad/sec^2)} = \frac{P_i}{\omega_b T_{eb}}$$

$$\bar{D}_{i,j} = \frac{D_{i,j}\omega_b}{T_{eb}} \frac{(N\text{-}m\text{-}sec)(rad/sec)}{(N\text{-}m)} = \frac{D_{i,j}\omega_b}{T_{eb}}$$

$$\bar{K}_{i,j} = \frac{K_{i,j}\theta_b}{T_{eb}} \frac{(N\text{-}m/rad)(rad)}{(N\text{-}m)} = \frac{K_{i,j}\theta_b}{T_{eb}}$$

$$\bar{\theta}_i = \frac{\theta_i \ (rad)}{\theta_b \ (rad)} = \frac{\theta_i}{\theta_b}$$

$$\bar{\omega}_i = \frac{\omega_i \ (rad/sec)}{\omega_b \ (rad/sec)} = \frac{\omega_i}{\omega_b}$$

The per unit equation is then as follows:

$$\begin{aligned} &2H_i\omega_i - G_i\bar{P}_i/\bar{\omega}_i + \bar{D}_{i-1,i}(\bar{\omega}_i - \bar{\omega}_{i-1}) + \bar{D}_{ii}\bar{\omega}_i \\ &+ \bar{D}_{i,i+1}(\bar{\omega}_i - \bar{\omega}_{i+1}) + \bar{K}_{i-1,i}(\bar{\theta}_i - \bar{\theta}_{i-1}) \\ &+ \bar{K}_{i,i+1}(\bar{\theta}_i - \bar{\theta}_{i+1}) = 0 \end{aligned} \qquad \text{(I-3)}$$

I-2 Inertia Shaft Equations: Generator Unit

The equation for the i^{th} inertia, generator unit, is as follows:

$$\begin{aligned} &J_i S\omega_i + T_e + D_{i-1,i}(\omega_i - \omega_{i-1}) + D_{ii}\omega_i \\ &+ D_{i,i+1}(\omega_i - \omega_{i+1}) + K_{i-1,i}(\theta_i - \theta_{i-1}) \\ &+ K_{i,i+1}(\theta_i - \theta_{i+1}) = 0 \end{aligned} \qquad \text{(I-4)}$$

As in section I.1, the equation I-4 is divided by the base torque. The obtained equation is same except for the input torque term, i.e. T_e instead of $G_i P_i/\omega_i$. The per unit torque terms are the same as in the section I.1, except the per unit input electrical torque to the generator, which is as follows: $\overline{T}_e = T_e/T_{eb}(N-m)/(N-m)$. The per-unit equation for the generator unit inertia is as follows:

$$2H_i S\overline{\omega}_i + \overline{T}_e + \overline{D}_{i-1,i}(\overline{\omega}_i-\overline{\omega}_{i-1}) + \overline{D}_{ii}\overline{\omega}_i$$
$$+ \overline{D}_{i,i+1}(\overline{\omega}_i-\overline{\omega}_{i+1}) + \overline{K}_{i-1,i}(\overline{\theta}_i-\overline{\theta}_{i-1})$$
$$+ \overline{K}_{i,i+1}(\overline{\theta}_i-\overline{\theta}_{i+1}) = 0 \qquad \text{(I-5)}$$

I.3 Steam Power Distribution Equations

The equation for the i^{th} steam power distribution module is as follows:

$$(1+ST_i)\ P_i = (1-G_{i-1})\ P_{i-1} \qquad \text{(I-6)}$$

The per unit terms are obtained by dividing equation I-6 by the base power. Equation I-6 then becomes:

$$\frac{(1+ST_i)\ P_i}{\omega_b T_{eb}} = \frac{(1-G_{i-1})\ P_{i-1}}{\omega_b T_{eb}} \qquad \text{(I-7)}$$

The per unit power terms are of the following form:

$$\overline{P}_i = \frac{P_i \qquad (Kg\text{-}m^2\text{-}rad^2/sec^3)}{\omega_b T_{eb}\ (rad/sec)(kg\text{-}m^2\text{-}rad/sec^2)} = \frac{P_i}{\omega_b T_{eb}}$$

The per unit equation is then as follows:

$$(1+S\overline{T}_i)\ \overline{P}_i = (1-G_{i-1})\ \overline{P}_i \qquad \text{(I-8)}$$

I.4 Speed-Governor Equations

The per-unitization of the speed-governor equations was performed in the reference 14.

APPENDIX II

BASIC ELECTRONIC COMPONENTS AND CONFIGURATIONS

The electronic components used in the construction of this electronic model are quality off-the-shelf integrated circuits (operational amplifiers and dividers) and passive elements (resistance, capacitors, and potentiometers).

The operational amplifier and the divider are represented in the circuit diagrams by the symbols shown in fig. II-1 and fig. II-8 respectively. With the use of operational amplifier, the basic operation of addition, substraction, integration and variable constant are implemented, as shown in fig.s II-3 to II-7 respectively. Division is implemented by the integrated circuit shown in fig. II-10. The symbol for a multiplier is shown in fig. II-11.

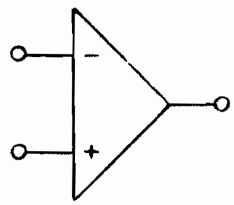

FIG. II-1 OPERATIONAL AMPLIFIER SYMBOL

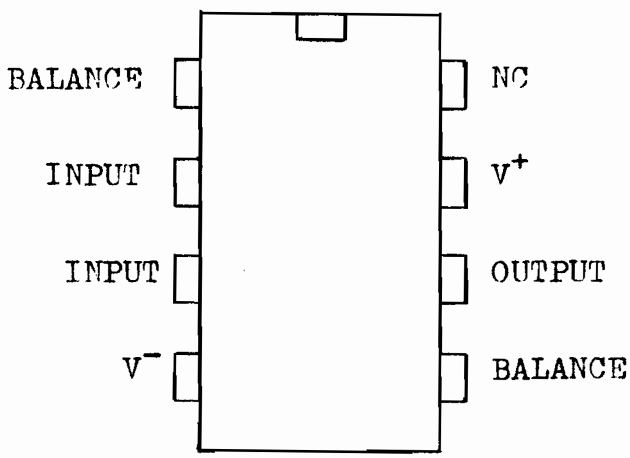

NATIONAL
SEMICONDUCTOR
8041 LF356N

FIG. II-2 OPERATIONAL AMPLIFIER PIN CONNECTION DIAGRAM

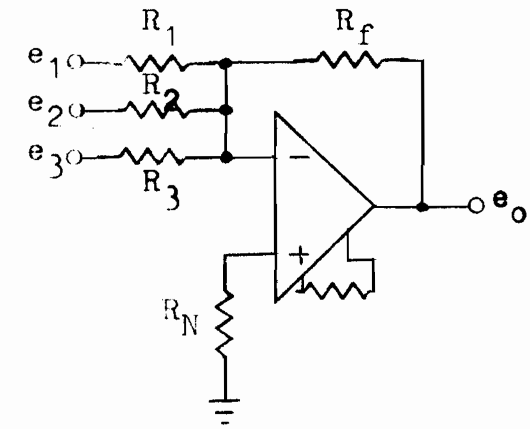

$$e_o = -\left(\frac{R_f}{R_1} e_1 + \frac{R_f}{R_2} e_2 + \frac{R_f}{R_3} e_3\right)$$

$$\frac{1}{R_N} = \frac{1}{R_1} + \frac{1}{R_2} + \frac{1}{R_3} + \frac{1}{R_f}$$

FIG. II-3 WIRING DIAGRAM FOR ADDITION OPERATION

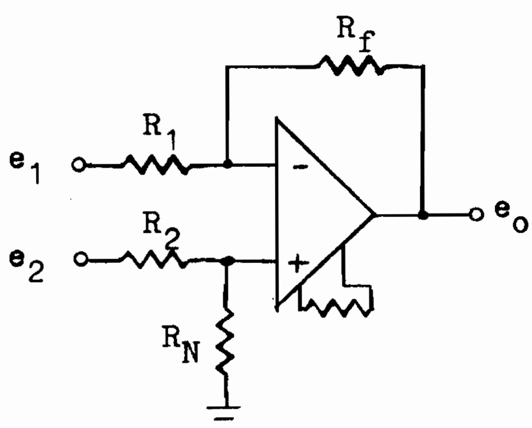

$$e_o = -\frac{R_f}{R_1} e_1 + \frac{R_f}{R_2} e_2$$

$$\frac{1}{R_N} + \frac{1}{R_2} = \frac{1}{R_1} + \frac{1}{R_f}$$

FIG. II-4 WIRING DIAGRAM FOR SUBSTRACTION OPERATION

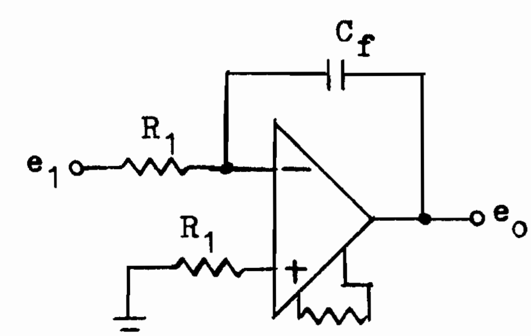

$$e_o = -\frac{e_1}{R_1 C_f S}$$

FIG. II-5 WIRING DIAGRAM FOR INTEGRATION OPERATION

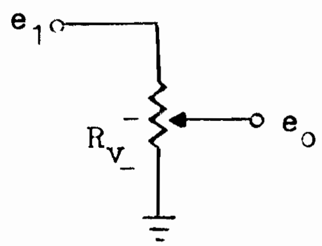

$$e_o = e_1(R_v/R)$$
$$R_v \leq 1.0$$

FIG. II-6 WIRING DIAGRAM FOR VARIABLE CONSTANT

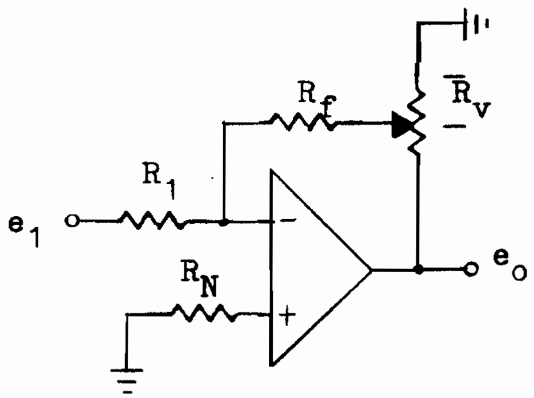

$$R_v \ll R_f$$
$$e_o = - \frac{R_f e_1}{R_1 R_v}$$
$$\frac{1}{R_N} = \frac{1}{R_1} + \frac{1}{R_N}$$

FIG. II-7 WIRING DIAGRAM FOR VARIABLE CONSTANT OPERATION

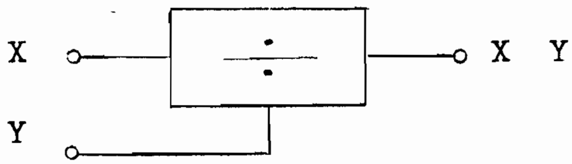

FIG. II-8 DIVIDER SYMBOL

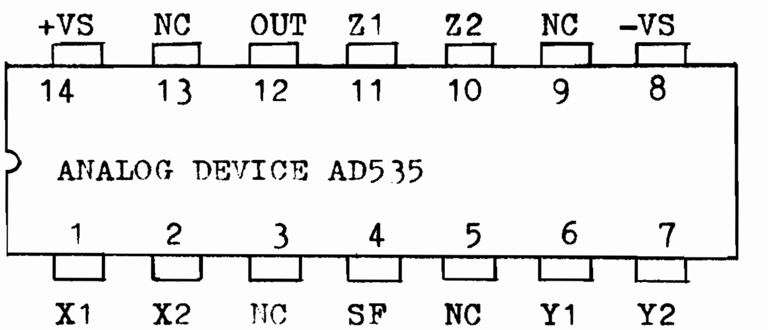

FIG. II-9 DIVIDER PIN CONNECTION DIAGRAM

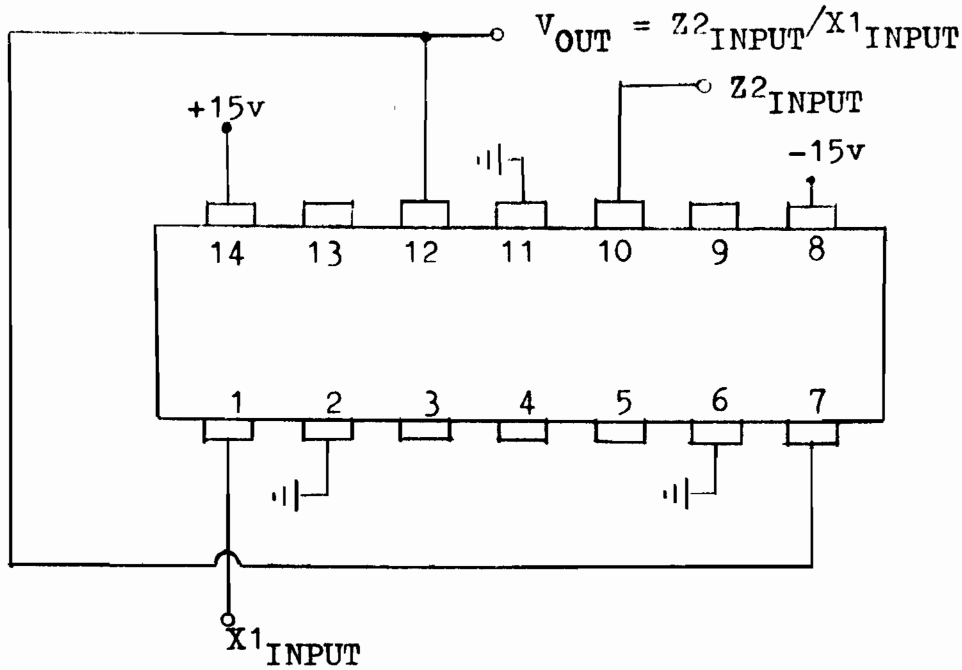

FIG. II-10 DIVIDER CIRCUIT IMPLEMENTATION

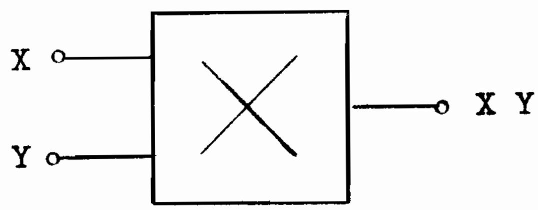

FIG. II-11 MULTIPLIER SYMBOL

APPENDIX III

SPEED-GOVERNING SYSTEM: MATHEMATICAL MODEL

The model for the speed-governor is shown in fig. 2-9. It is a model recommended in the IEEE Committee Report [14]. This model is described mathematically in the following equations.

$$SP_{GV} = (1/T_3)(P_o - P_{IS} - P_{GV}) \tag{III-1}$$

$$\frac{P_{IS}}{(\omega_G - \omega_o)} = \frac{(K/T_1)(1+ST_2)}{S+1/T_1} = \frac{KT_2}{T_1} + \frac{K(1-T_2/T_1)}{1+ST_1} \tag{III-2}$$

Let $\dfrac{\omega_{IS}}{(\omega_G - \omega_o)} = \dfrac{1}{1+ST_1}$ (III-3)

Then

$$P_{IS} = KT_2(\omega_G - \omega_o)/T_1 + K(1-T_2/T_1)\omega_{IS} \tag{III-4}$$

The breakdown of equation II-2 into equation II-4 simplifies the electronic implementation of the speed-governor system model.